Mechanistic studies on a peptide-based self-replicating system

Mathieu Colomb-Delsuc

The work described in this thesis was executed at the Stratingh Institute for Chemistry, University of Groningen, The Netherlands.

The author of this thesis wishes to thank the University of Groningen for financial support.

Cover design by Mathieu Colomb-Delsuc
Printed by GrafiMedia

ISBN: 978-90-367-8471-9 (printed version)

ISBN: 978-90-367-8470-2 (digital version)

university of groningen

Mechanistic studies on a peptide-based self-replicating system

PhD thesis

to obtain the degree of PhD at the
University of Groningen
on the authority of the
Rector Magnificus Prof. E. Sterken
and in accordance with
the decision by the College of Deans.

This thesis will be defended in public on

Friday 18 December 2015 at 09.00 hours

by

Mathieu Colomb-Delsuc

born on 8 November 1985
in Saint Céré, France

Supervisor
Prof. S. Otto

Assessment Committee
Prof. J.G. Roelfes
Prof. G. Ashkenasy
Prof. J. van der Gucht

Table of Contents

Chapter I

Advances towards a synthetic living system

This Chapter introduces the latest achievements towards reaching a living system made synthetically, by describing a theoretical model of an artificial cell and introducing the research that has been performed on the individual elements composing that model, getting inspiration from our prebiotic world, modern biological organisms, but also from synthetic systems.

I.1. Introduction

Creating life is unquestionably one of the most challenging and ambitious goals of mankind, and has been inspiring human beliefs and imagination through the ages, in Arts and in Science.
Nowadays, Science reached a point where making life *de-novo* is not unrealistic,[1] and many groups are actively working on different approaches in order to get a better understanding of the pathways that may one day lead to it.[2,3]
The first legitimate point to address before trying to make life is to define it. Up to date, the only sources of life available to base such definition on are the different forms of life on Earth, so our definition of life has to come from this. Among the broad biodiversity found in our planet, some elements are shared by all living systems, and may be a starting point for scientists to work-on.[4,5]
Those "ingredients" necessary for a system to be considered alive have been widely discussed in the scientific community, and among the different essential elements needed, some are agreed by everyone.[6,7]
For example, all the living systems are contained in an envelope, in which all the metabolism, metabolites, and information of that living system are contained. The simplest form of container for a living system is the membrane of a cell, delimiting it. All living systems are compartmentalised. Any synthetic system that is claimed to be alive should therefore respect this first prerequisite.
Another essential element is metabolism: indeed all living systems known on earth are capable to sustain themselves by staying out of thermodynamic equilibrium, through a series of reactions occurring within the cell. Metabolism is accompanied by consumption of energy, and renewal of the metabolites present in the living system.
Finally, any living system should be able to replicate itself to sustain the species, by passing information on its own nature to a next generation sharing therefore the same characteristics, and which will, in turn, be able to replicate giving rise to a next generation of living systems keeping in that way the species alive.

These essential elements were implemented in a model, introduced by its author as the "minimal cell model" [8,9] (Scheme I.1). The model describes the necessary elements and mechanisms for the creation of a *de-novo* autonomously living system.

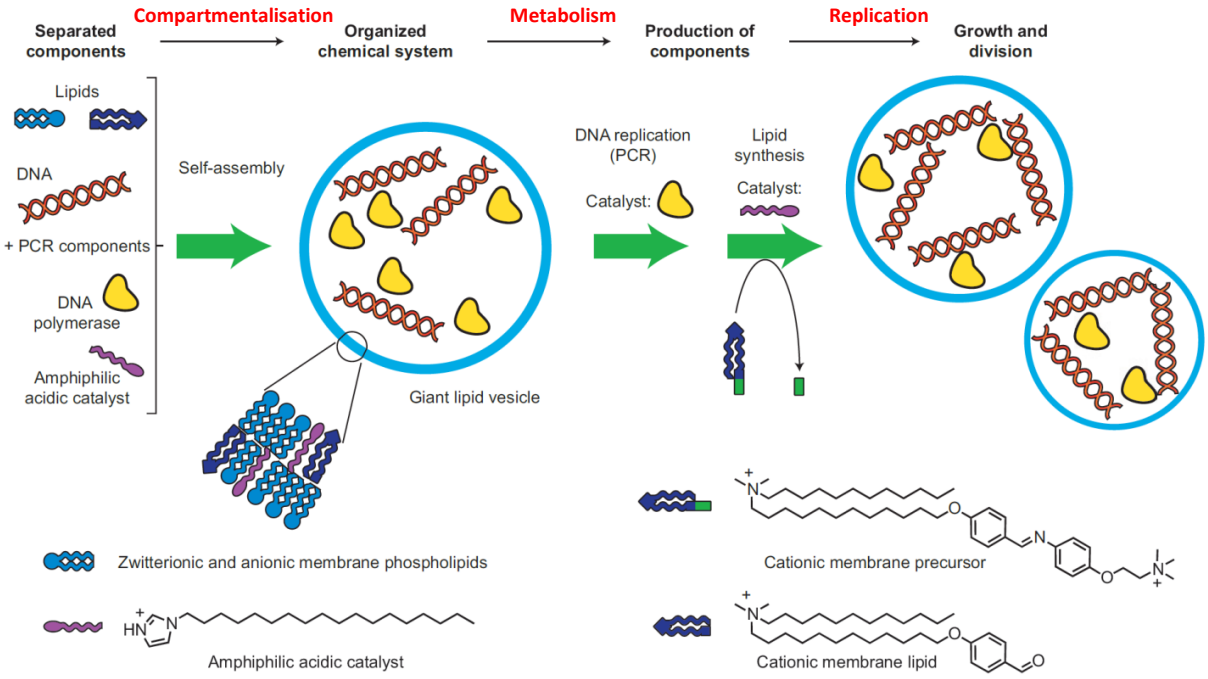

Scheme I.1. *Representation of the minimal cell model proposed by Luisi, describing the necessary elements and mechanisms for the creation of a de-novo autonomously living system. Adapted from reference 8.*

Any system which would display those three essential elements could therefore in principle be considered as alive. However, and although the topic has been studied for several decades, making life *de-novo* is still out of reach. A rational way of approaching the problem is to follow a bottom-up strategy, starting from simple molecules and trying to make them mimic some features of a living system. For this reason, most of the studies done up to date are not trying to display the three ingredients of life in a single system, but are rather focusing on the individual parameters of life.
The bottom-up approach is an interesting methodology, in that it allows exploring different pathways to reach a particular goal, and although Nature remains the main source of inspiration, molecules not present in the biological world can be envisaged, therefore broadening the range of possibilities and in consequence the understanding of life.

The following paragraphs will be discussing the different research performed to understand and develop systems individually featuring one of the characteristics of living systems mentioned above, with a particular focus on replication, representing the base for the work described in this thesis.

I.2. Compartmentalisation

Compartmentalisation represents a fundamental feature of life, as it defines in space each individual of a species. All the elements composing a living system are comprised within defined boundaries, and the vicinity induced by this closed environments allows efficient reactions, as the concentration is higher than it would be in a dispersed media. For those reasons, the development of a stable artificial compartment is of prime importance for the development of synthetic life.[10]

Although contemporary living cells are composed of heterogeneous lipid bilayers including transmembrane proteins that facilitate metabolite transport, it is likely that the membranes of the first living organisms were simpler. For this reason, small molecules have been envisaged and observed to form synthetic cell membranes.[11,12] These include fatty acids and fatty alcohols, alkyl sulfates and alkyl glycols, as well as acylglycerols. All those molecules share some features, as they are amphiphilic, *i.e.* composed of a hydrophobic tail and a hydrophilic head, and can assemble in aqueous media, leading to the formation of micelles, rod-like structures or vesicles.

Of those assemblies, vesicles represent potentially the most interesting structures to study and create a protocell when working in aqueous media, as they can play the role of a compartment by encapsulating water soluble molecules.

Among the different amphiphile molecules, fatty acids are most widely studied and reveal the formation of possible cell compartments,[13,14,15,16] due to their simple structure, and their capacity to easily form vesicles stable to different environmental changes (temperature and pH),[17] with an easily tuneable size.[18] When growing, the assemblies undergo morphological changes, and can in some cases divide when reaching a critical size.[19] This latter feature is of particular interest, as it parallels cell division in biology, although the present system is much simpler, since division originates from environmental and physical constraints, and not from genetic control as in biology.
Interestingly, kinetic studies on the growth of fatty acid vesicles developed by Luisi et al. have proven their ability to undergo a self-reproducing behaviour by growing following an autocatalytic pathway,[20] through hydrolysis of fatty acid anhydrides under basic conditions. The hydrolysis of the anhydride is promoted by the presence of vesicles in the media, explaining the observed autocatalysis. Later work proved that the same methodology can also be applied to phospholipids anhydrides, which also lead to the formation of vesicles in an autocatalytic manner under basic conditions.[21]

Since then, more complex classes of self-reproducing vesicles have been developed, including new sets of chemistries and molecules, as illustrated by the system developed by Sugawara *et al.*, in which the incorporation of a phosphate lipid equipped with an imine into a vesicle is facilitated by an autocatalytic imine hydrolysis process, occurring on the membrane of the vesicle.[22]

I.3. Metabolism

As described in the model of the minimal cell (Scheme I.1), metabolism plays a central role and is one of the parameters necessary for sustaining a living system, and has most certainly played a role in the origins of life.[23] In order to implement a metabolic system in an artificial living system, one should study it, and as often for synthetic chemists, the main source of inspiration comes from the biological world. In modern biological organisms, however metabolism is of an extreme complexity, as illustrated for example by the Krebs cycle, involving highly evolved mechanisms and a broad variety of well-defined large biological structures, such as enzymes. Reproducing synthetically such complexity is simply out of reach for the chemists. For this reason, a rational way of studying metabolism by taking inspiration from Nature is to follow a bottom-up approach, starting by describing the essential features of metabolism, and studying non-enzymatic systems displaying key features, such as autocatalysis and the ability to be self-sustaining.

Up to date, the formose reaction is one of the few systems featuring an autocatalytic cycle that is self-sustaining that has been able to give insights on possible protometabolic pathways. Observed first in the 19th century,[24] this reaction has been since then widely studied and described.[25] This autocatalytic cycle consists of the condensation of formaldehyde giving rise to a complex mixture of sugars. This system can be seen as a protometabolic system. A simplified illustration of this system is shown in Figure 1.I.a.

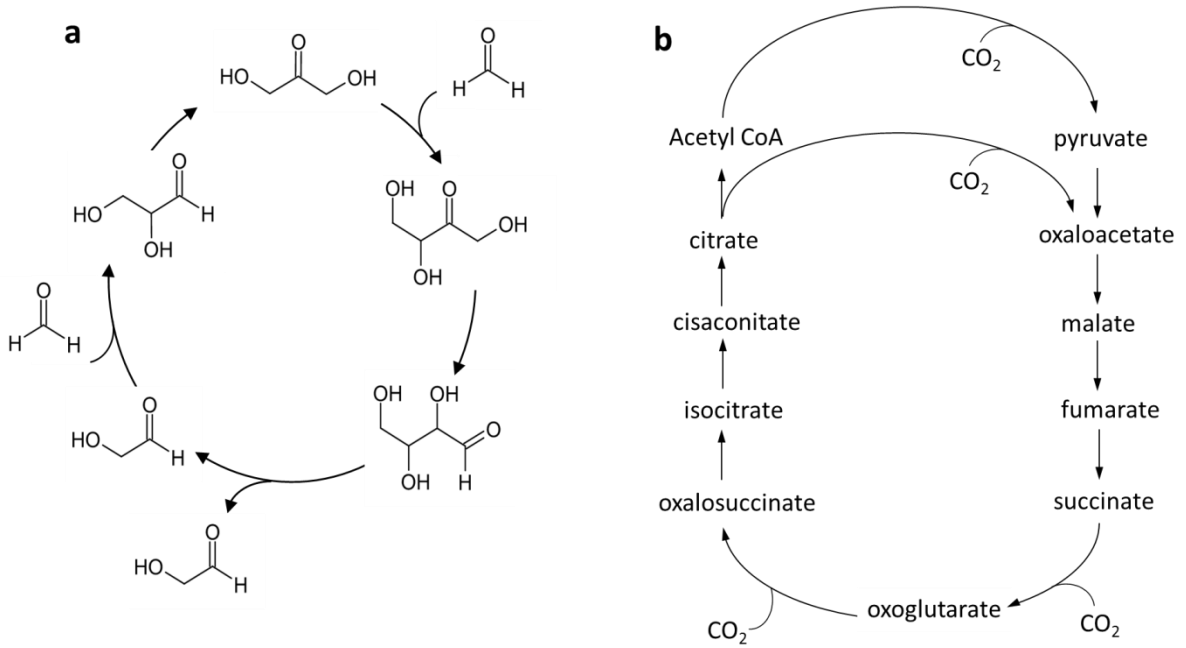

Figure I.1. *Two examples of autocatalytic cycles. a. Simplified autocatalytic cycle of the formose reaction. b. Citric acid cycle.*

In 2000, Morowitz et al.[26] proposed another naturally occurring cycle as a possible pathway towards the synthesis of more complex biomolecules. This system, the citric acid cycle, illustrated in Figure I.1.b, however, necessitates the use of enzymes in some steps of the catalytic cycle.

An interesting model sharing some protometabolic characteristics was introduced by Commeyras et al. in 2002 (Figure I.2).[27] This model, composed of a dry phase and an aqueous phase, defined by its

authors as the “primary pump”, describes the formation of peptides using N-carboxyamino acid anhydrides (NCAs), a well-described class of peptide precursors, [28,29] themselves formed by the nitrosation in dried conditions of N-carbamoylamino acids (CAAs). The dry phase allows a high concentration of material and prevents side reactions usually occurring in aqueous media, such as hydrolysis and epimerisation. In the aqueous phase, a part of the NCAs condenses into peptides, while another part is hydrolysed, forming amino acids that will form CAAs upon N-carbamoylation. Despite its environmental limitations, as a dry step would be a hurdle for development of an artificial cell, this system represents an interesting model of protometabolism.

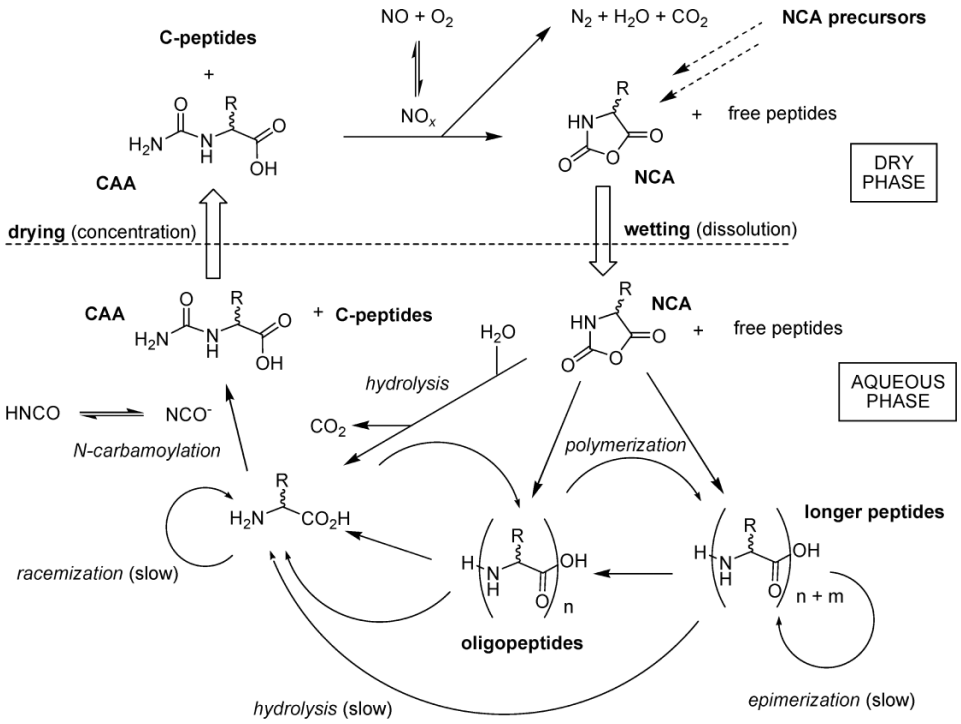

Figure I.2. *The primary pump model (reproduced from reference 6).*

Those examples of systems displaying some primitive metabolic characteristics give therefore some information on what may be expected from a synthetic metabolic system that could be implemented in an artificial living system, but despite the possibility of maintaining a system out of thermodynamic equilibrium (as long as food and energy are provided), those systems do not carry much information.

I.4. Self-Replication

The last element of the minimal cell model that will be discussed here is self-replication. In order to sustain a species, each individual needs to undergo replication, passing its information to a new generation, together with the capacity to further transmit this information, which will be ready to repeat the same process. This feature therefore played a primordial role in the emergence of life,[7,30] and for this reason has been widely studied.

A theoretical description of self-replicating systems was described in the late 1980’s by Szathsmary.[31] This study sets the basic theoretical concepts for a whole new branch of chemistry, from which chemists worked on achieving self-replicating systems, using a bottom-up approach to understand

and possibly reach simple forms of life, leading to a broad range of studies over the past decades, using a whole set of chemistries, most of them being inspired by living systems, featuring oligonucleotides, lipids, peptides, or other structures trying to uncover new classes of molecules capable of self-replication by using fully synthetic systems.

A general scheme of self-replication, involves a template that brings two precursors together thereby enhancing their ligation speed, is presented in Scheme I.2.

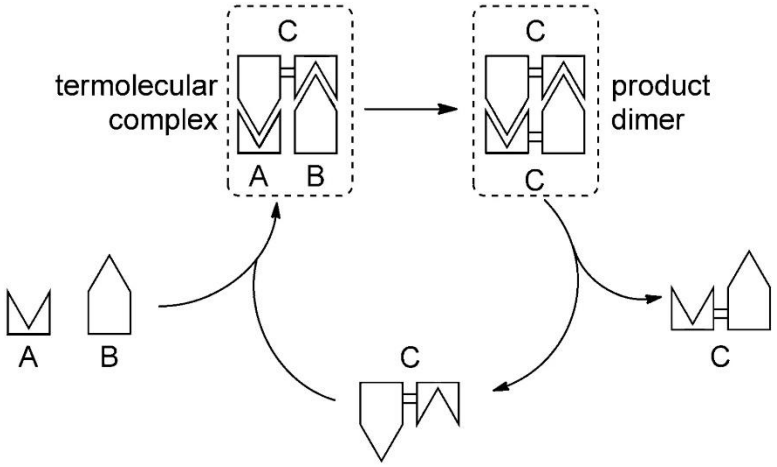

Scheme I.2. *General representation of a templated self-replicating system. Molecular recognition between building blocks A and B with C leads to the formation of a termolecular complex [A.B.C.]. A and B being in the vicinity of each other, a ligation between both is possible, forming C. The product dimer dissociates, and two molecules of C are released. The dissociation step is usually the limiting step, which may be at the origin of a low replicating efficiency. Reproduced from reference 7.*

The efficiency of the self-replication process, and more specifically the dimer dissociation, will affect the kinetics of replication of the system. A limited dissociation will lead to a parabolic growth of the replicating species in the system, while an efficient dissociation will push the system towards exponential growth.[32] In a scenario where several species are in competition, the kinetics of replication plays an essential role. The following discussion will present self-replicating systems without focusing on their kinetics of growth. The importance and relevance of exponentially self-replicating systems will be further discussed and developed in Chapter II of this thesis.

I.4.a. Nucleic acid based self-replicating systems

One of the most popular theories describing primitive aspects of life on earth is the RNA world hypothesis.[33,34] Many scientists focused on studying oligonucleotides as a way to explore and understand self-replication. The first model was introduced in the late 1980's by Von Kiedrowski, where he demonstrated the first synthetic self-replicating system, using DNA recognition with short DNA sequences (Figure I.3). The ligation of a codon CCG with a codon CGG gives a CCGCGG hexanucleotide, able to promote its own formation by ligation of the free codons CCG and CGG through a recognition step.[35]

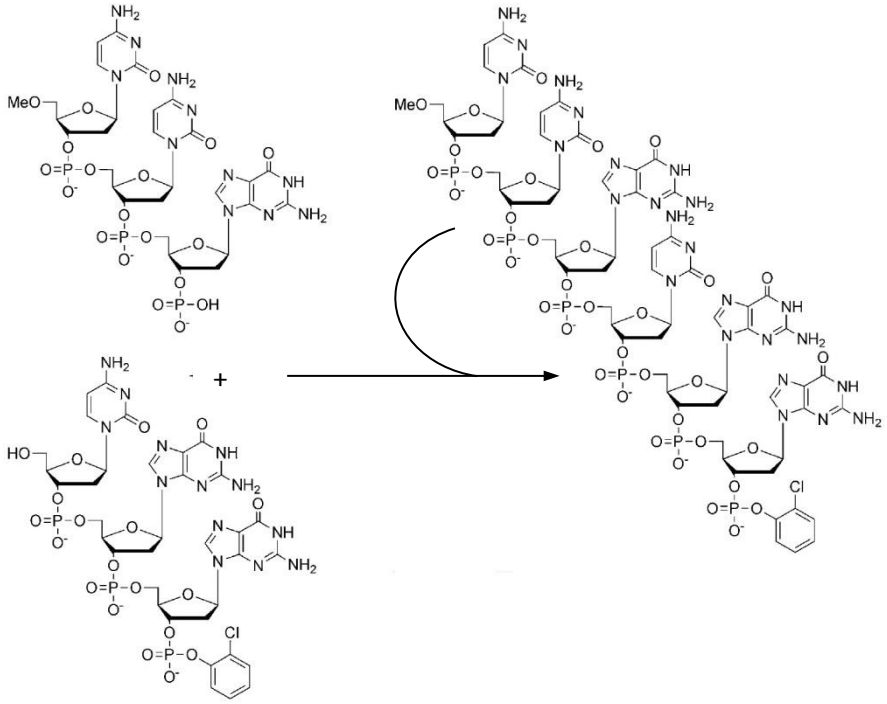

Figure I.3. *Von Kiedrowski's DNA self replicating system.*

The main limitation is the system comes from the hampered dimer dissociation resulting from the strong binding within the DNA duplex. However, this system has been improved since its introduction, and ways to overcome this limitation have been introduced (c.f. section II.1 of this thesis). Other DNA based self-replicating systems and methodologies have been proposed,[36,37] showing more complex self-replication processes, such as cross catalytic systems,[38,39] duplex DNA templated systems[40], or using biological oligomers with long nucleotide sequences.[41]

I.4.b. Abiotic Self-replicating systems

Rather than being directly inspired by Nature, chemists have also been studying the possibility of self-replicating systems using either biomolecule derivatives, or molecular systems not occurring in Nature.

A first example of a self-replicating system where an adenine derivative was used for the design of a replicator[42,43] was reported by Rebek *et al.* in 1990. This first system, represented in Figure I.4, was then developed further, and new generations of replicators, more efficient, were synthetized by developing new molecules, eventually keeping only from the original structure the nucleobase, involved in the recognition process.[44]

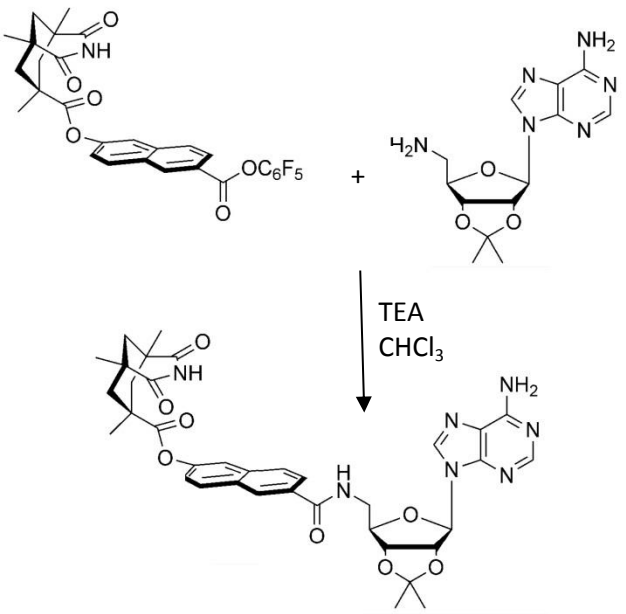

Figure I.4. *The first abiotic self-replicating system designed by Rebek and coworkers. The product of the reaction acts as a template to ligate remaining building blocks in solution.*

However, the example above is not totally unrelated to biomolecules, as a nucleobase moiety is still part of the replicating molecule.

A self-replicating system involving completely abiotic molecules was introduced in 2008 by Philp *et al.*,[45] in which a model was proposed for the autocatalytic formation of rotaxanes. In this model, a cycloaddition was proposed as the ligation reaction between the two building blocks composing the threat of the rotaxane. This cycloaddition reaction was later on used in another system based on a different class of molecules, leading insightful results.[46] This system consists of a previously described dynamic combinatorial library based on nitrone-imine exchange,[47] whose equilibrium is perturbed by the addition of a maleimide, reacting by cycloaddition with the nitrones present in the media. One of resulting cycloadducts is capable of autocatalytic amplification, driving the system towards its own formation. A representation of this system is shown in Figure I.5.

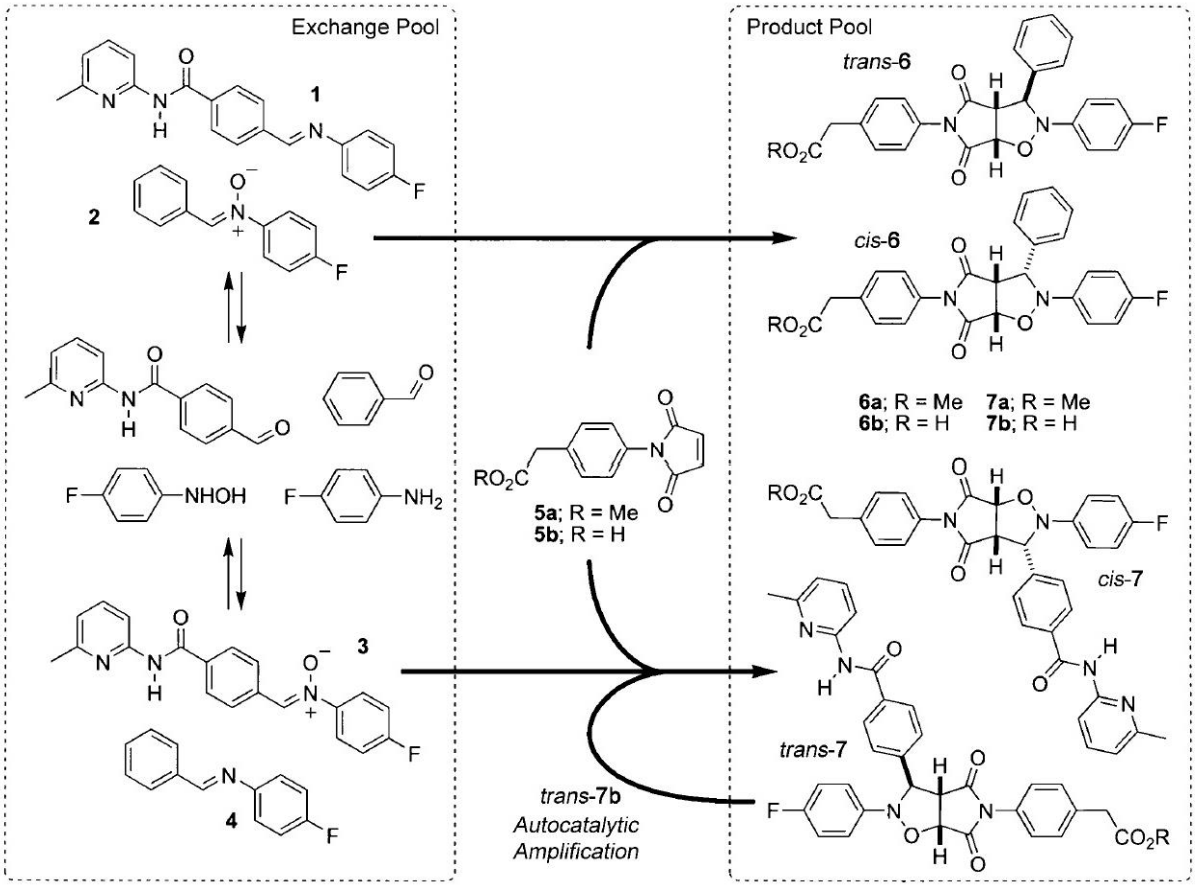

Figure I.5. *The material from a Dynamic Combinatorial Library containing imines **1** and **3** and nitrones **2** and **4** can be transferred irreversibly to a pool of products, present in the same solution, through reaction of nitrones **2** or **3** with a maleimide molecule (**5a** or **5b**). When maleimide **5b** is used as the dipolarophile, replicator trans-**7b** is formed in the product pool and this species can act as a catalyst for its own formation. Reproduced from reference 46.*

This study represents a clear example of how one species can emerge from a pool of molecules, and demonstrates the role that can be played by dynamic covalent chemistry in the field of self-replicating systems.

Other abiotic self-replicating systems have been developed, using fully synthetic molecules and reactions originating from organic chemistry, such as Diels-Alder cycloadditions. Such systems were introduced by Sutherland et al., and have been since then widely developed.[48,49,50] With time, the efficiency of these replicators has been increasing, and some are today really efficient, getting close to exponential growth.[51]

I.4.c. Peptide replicating systems

In the prebiotic world, peptides may have played an important role[52,53] in the appearance of life, since amino acids were likely one of the most abundant prebiotic ingredients, as suggested by the Miller-Urey experiment,[54,55] and their condensation into peptides has been long proven and widely studied.[56,57,58] Moreover, peptides represent a truly versatile class of molecules, as the pool of available amino acids that can be used for peptide synthesis is virtually limitless, although natural

amino acids are most commonly used, and the amount of possible combinations is vast, even for small peptides.

Furthermore, peptides are capable of intermolecular non covalent interactions, which make them a suitable class of molecules to study self-replicating systems, in which molecular recognition represents the first step of the replication cycle. Finally, peptide interactions are usually weak, such as in α-helixes or β-sheet structures, which may facilitate the dissociation of the dimer resulting from the ligation process and as a consequence enhance the speed of replication.

Considering all those characteristics, it is clear that peptides are a promising class of molecules to investigate when studying self-replicating systems. A first report of such systems was published by Ghadiri et al., where a 32 residue helical peptide was found to be able to template its own formation[59]. This system is represented in Figure I.6.

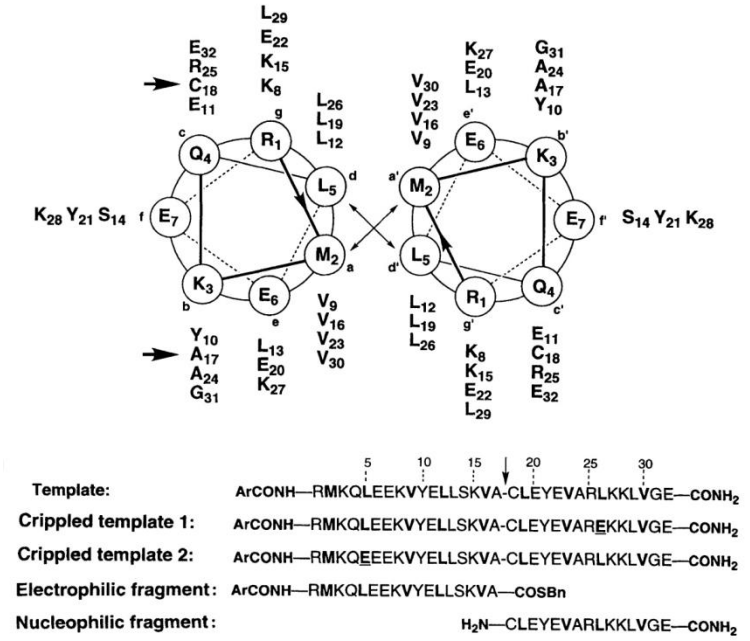

Figure I.6. *Self-replicating helical peptide system introduced by Ghadiri (reproduced from reference 59). The recognition is driven by hydrophobic packing interactions at positions a and d of the alpha-helix, together with electrostatic interactions at the positions e and g.*

The replication process occurs when the electrophilic fragment and the nucleophilic fragment present in solution links to the first part of the template, before linking to each other through a reaction between the thioester present on the electrophilic residue and the amine group of the nucleophilic residue, leading to the formation of a cysteine thioester, which then rearranges to the thermodynamically favoured native amide bond.

This peptide system opened new perspectives and inspired by it, other studies arose on self-replicating systems based on α-helical assembling peptides, such as the ones reported by Chmielewski[60] and Ashkenasy.[61] Later on, new systems using cross catalytic reactions,[62] or heteochiral peptides,[63] demonstrated the feasibility of self-replication using more complex systems.

Self-replicating peptides using β-sheet interactions have also been reported. They have been studied by Ashkenasy *et al*., where, based on a similar ligation chemistry to the one introduced by Ghadiri, a self-replicating peptide system was proposed,[64] templating its own formation by placing two building blocks in vicinity of each other, but using this time beta sheet interactions rather than coiled-coil alpha helixes. This new system proved to have remarkably efficient replication efficiency (cf Scheme II.1 of this thesis).

In our group, a new class of peptide self-replicating system was discovered[65,66] and studied extensively since then. The peptide building blocks used in this system consist of pentapeptide chains equipped with an aromatic dithiol. (Scheme I.3).

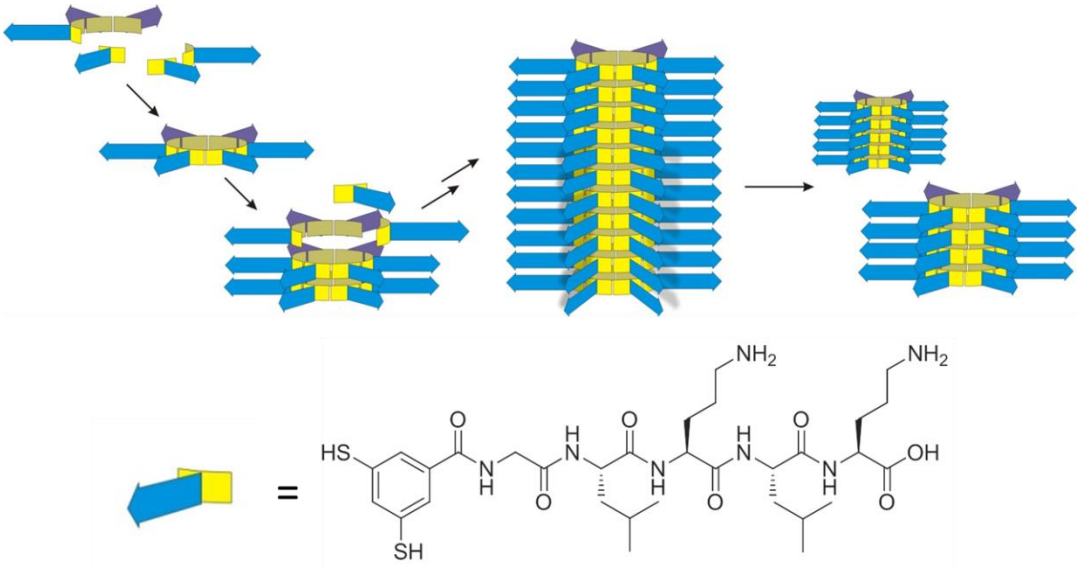

Scheme I.3. *Schematic representation of the peptide system developed in our group. The peptide building block assembles into macrocycles, which stack on top of each other thanks to* β*-sheet interactions between the peptide chains, leading to the formation of fibres that can break apart upon mechanical input.*

The aromatic dithiol group reacts at pH 8 in aqueous media to form intermolecular disulfide bonds, which results in the emergence of macrocyclic species, varying in size and dynamically exchanging with each other due to the reversible nature of the disulfide bond. The reaction results in a thermodynamically controlled product mixture when this building block is not equipped with a peptide chain. The peptide moiety, which alternates hydrophilic and hydrophobic amino acids in order to facilitate β-sheet interactions, is used to stabilise the macrocyclic species large enough to make the β-sheet formation possible between the pendant peptides, resulting in a recognition mechanism that will favour the formation of that particular species, therefore creating a kinetic trap and leading the system to form more of that species. Interestingly, the peptide used in the first study of this system has proven to be mechanosensitive, as different modes of agitation results in the emergence of different replicators.[65] Further investigations on this class of peptide replicators are discussed in the following thesis. For a more complete description of the system, see section II.2.

I.5. Conclusions and contents of this thesis

This thesis focuses on the exploration of the self-replicating peptide system developed in our group, on which a whole set of studies has been performed.

Chapter II describes the set of experiments performed in order to proof that replication is exponential, and describes the mechanism of replication. This demonstration is of primary importance since up to date few fully synthetic self-replicating system have proven to display exponential replication. Yet, this feature is a prerequisite for Darwinian evolution at a molecular level, making our peptide system a good candidate to advance towards this tantalizing goal.

It has been shown that the length of the peptide assemblies plays a central role in the self-replication cycle. Short peptide fibres are obtained upon strong shearing. As a consequence, shear stress appears to be an essential parameter for exponential replication in our system. Chapter III focuses on the study of a set of peptide libraries, in which the shear stress applied to the system was varied. The kinetics of growth of the different peptide species in the libraries was studied as a function of the shear rate.

However, those results are solely qualitative, as the experiments performed did not allow any accurate measurement of the mechanical forces occurring in solution. In order to overcome this limitation, a rheological device was designed, making experiments possible in which the shear stress applied to the system is more homogeneous, being controlled and monitored during the whole experiment. Chapter IV describes the design of this device and presents a first set of experiments performed.

During the course of this thesis, transmission electron microscopy (TEM) has been widely used to observe and study the fibres resulting from the self-assembly of our peptide system, but was also a means of collaboration with other universities. Chapter V describes three examples where TEM was used to serve a broad scope of research, including peptide self-assembly, micelle aggregation, and silk-like fibre self-assembly.

I.6. References

[1] P A. Pross, R. Pascal, *Open biol.*, **2013**, 3, 12190.

[2] P. L. Luisi, The Emergence of Life – From Chemical Origins to Synthetic Biology, *Cambridge University Press*, **2010**.

[3] F. J. Dyson, Origins of Life, *Cambridge University Press, 2nd Ed.*, **1999**.

[4] A. Pross, What is Life?: How Chemistry becomes Biology, *Oxford University Press*, **2014**.

[5] S. A. Kauffman, *Life*, **2011**, 1(1), 34-48

[6] K. Ruiz-Mirazo, C. Briones, A. de la Escosura, *Chem. rev.*, **2014**, 114, 285-366.

[7] A. J. Bisette, S. P. Fletcher, *Angew. Chem. Int. Ed.*, **2013**, 52, 12800-12826.

[8] P.L. Luisi, P. Stano, *Nature Chemistry,* **2011**, 3, 755-756.

[9] P.L. Luisi, P. Stano, *The minimal cell, Springer*, **2011**.

[10] Pier Luigi Luisi, Peter Walde and Thomas Oberholzer Current Opinion in Colloid & Interface Science 1999, 4, 33-39

[11] D.W. Deamer, *The Molecular Origins of Life, Cambridge University Press: Cambridge, U.K.,* **1998**.

[12] J.A. Thomas, F.R. Rana, *Origins Life Evol. Biospheres*, **2007**, 37, 267-285.

[13] D.W. Deamer, J.P. Dworkin, *Topics in Current Chemistry*, **2005**, 259, 1-27.

[14] J.M. Gebicki, M. Hicks*, Nature*, **1973**, 243, 232-234.

[15] W.R. Hargreaves, D.W. Deamer, *Biochemistry*, **1978**, 17, 3759-3768.

[16] G. Pozzi, V. Birault, B. Werner, O. Dannenmuller, Y. Nakatani, G. Ourisson, S. Terakawa, *Angew. Chem., Int. Ed.*, **1996**, 35, 177-180.

[17] S.S. Mansy, J.W. Szostak, *Proc. Natl. Acad. Sci. U.S.A.,* **2008**, 105, 13351-13355.

[18] Berclaz, N.; Muller, M.; Walde, P.; Luisi, P. L. J. Phys. Chem. B, 2001, 105, 1056-1064.

[19] B. Bozic, S. Svetina, *Eur. Biophys. J*., **2004**, 33, 565-571

[20] P. Walde, R. Wick, M. Fresta, A. Mangone, P. L. Luisi, *J. Am. Chem. Soc*., **1994**, 116, 11649-11654.

[21] A. Veronese, P. L. Luisi, *J. Am. Chem. Soc.*, **1998**, 120, 2662-2663.

[22] H. Takahashi, Y. Kageyama, K. Kurihara, K. Takakura, S. Murata, T. Sugawara, *Chem. Commun.*, **2010**, 46, 8791-8793.

[23] G. Wächtershäuser, *Microbiol. Rev.*, **1988**, 52, 452-484.

[24] A. Boutlerow, *Comptes rendus des séances de l'Académie des sciences*, **1861**, 53, 145-147.

[25] L.E. Orgel, *Proc. Natl. Acad. Sci. U.S.A.*, **2000**, 97, 12503-12507.

[26] H. J. Morovitz, J. D. Kostelnik, J. Yang, G. D. Cody, *Proc. Natl. Acad. Sci. U.S.A.*, **2000**, 97(14), 7704-7708.

[27] A. Commeyras, H. Collet, L. Boiteau, J. Taillades, O. Vandenabeele-Trambouze, H. Cottet, J.P. Biron, R. Plasson, L. Mion, O. Lagrille, H. Martin, F. Selsis, M. Dobrijevic, *Polym. Int*., **2002**, 51, 661-665.

[28] J. P. Ferris, A. R. Hill, R. H. Liu, L. E. Orgel, *Nature*, **1996**, 381, 59-61.

[29] H. R. Kricheldorf, *Angew. Chem. Int. Ed*., **2006**, 45, 5752-5784.

[30] V. Vasas, C. Fernando, M. Santos, S. Kauffman, E. Szathmary, *Biol. Direct*, **2012**, 7 (1).

[31] E. Szathmary, I. Gladkih, *J. Theor. Biol.*, **1989**, 138, 55-58.

[32] E. Szathmary, *Trends Ecol. Evol.*, **1991**, 6, 366-370.

[33] M. P. Robertson, G. F. Joyce, *Cold Spring Harbor Perspect. Biol.*, **2012**, 4, a003608.

[34] G.F. Joyce, *Nature*, **1989**, 338, 217 – 224.

[35] G. von Kiedrowski, *Angew. Chem. Int. Ed.*, **1986**, 25, 932-935.

[36] T. Li, K. C. Nicolaou, *Nature*, **1994**, 369, 218-221.

[37] W. S. Zielinski, L. E. Orgel, *Nature*, **1987**, 327, 346-347.

[38] D. Sievers, G. von Kiedrowski, *Nature*, **1994**, 369, 221-224.

[39] D. Sievers, G. von Kiedrowski, *Chem. Eur. J*., **1998**, 4, 629-641.

[40] X. Li, D. R. Liu, Angew. Chem. Int. Ed. 2004, 43, 4848-4870.

[41] T.A. Lincoln, G.F. Joyce, *Science*, **2009**, 323, 1229-1232.

[42] T. Tjivikua, P. Ballester, J. Rebek, *J. Am. Chem. Soc.,* **1990**, 112, 1249-1250.

[43] J. S. Nowick, Q. Feng, T. Tjivikua, P. Ballester, J. Rebek, *J. Am. Chem. Soc.*, **1991**, 113, 8831-8839.

[44] Q. Feng, T. K. Park, J. Rebek, *Science*, **1992**, 256, 1179-1180.

[45] A. Vidonne, D. Philp, *Tetrahedron*, **2008**, 64, 8464-8475.

[46] J. W. Sadownik, D. Philp, *Angew. Chem. Int. Ed.*, **2008**, 47, 9965-9970.

[47] E. Kassianidis, D. Philp, *Angew. Chem. Int. Ed.*, **2006**, 45, 6344-6348.

[48] B. Wang, I. O. Sutherland, *Chem. Commun.*, **1997**, 1495-1496.

[49] M. Kindermann, I. Stahl, M. Reimold, W. M. Pankau, G. von Kiedrowski, *Angew. Chem. Int. Ed.,* **2005**, 44, 6750-6755.

[50] A. Vidonne, D. Philp, *Eur. J. Org. Chem.,* **2009**, 593-610.

[51] I. Stahl, G. von Kiedrowski, *J. Am. Chem. Soc.,* **2006**, 128, 14014-14015.

[52] V. Borsenberger, M.A. Crowe, J. Lehbauer, J. Raftery, M. Helliwell, K. Bhutia, T. Cox, J.D. Sutherland, *Chem. Biodiversity,* **2004**, 1, 203-246.

[53] J.M. Smith, V. Borsenberger, J. Raftery, J.D. Sutherland, *Chem. Biodiversity,* **2004**, 1, 1418-1451.

[54] S. L. Miller, *Science*, **1953**, 117, 528-529.

[55] A.P. Johnson, H.J. Cleaves, J.P. Dworkin, D.P. Glavin, A. Lazcano, J.L. Bada, *Science,* **2008**, 322, 404-404.

[56] S.L. Miller, L.E. Orgel, *The Origins of Life on Earth, Prentice Hall, Englewood Cliffs, NJ*, **1974**.

[57] S.W. Fox, K. Dose, *Molecular Evolution and the Origin of Life, Dekker, NY*, **1977**.

[58] G. Danger, R. Plasson, R. Pascal, *Chem. Soc. Rev.*, **2012**, 41, 5416-5429.

[59] D. H. Lee, J. R. Granja, J. A. Martinez, K. Severin, M. R. Ghadiri, *Nature*, **1996**, 382, 525-528.

[60] S. Yao, I. Ghosh, R. Zutshi, J. Chmielewski, *Angew. Chem. Int. Ed*., **1998**, 37, 478-481.

[61] Z. Dadon, M. Samiappan, E. Y. Safranchik, G. Ashkenasy, *Chem. Eur. J.*, **2010**, 16, 12096-12099.

[62] S. Yao, I. Ghosh, R. Zutshi, J. Chmielewski, *Nature*, **1998**, 396, 447-450.

[63] A. Saghatelian, Y. Yokobayashi, K. Soltani, M. R. Ghadiri, *Nature,* **2001**, 409, 797-801.

[64] B. Rubinov, N. Wagner, A. Rapaport, G. Ashkenasy, *Angew. Chem. Int. Ed.*, **2009**, 48, 6683-6686.

[65] J.M.A. Carnall, C.A. Waudby, A.M. Belenguer, M.C.A. Stuart, J.J.-P. Peyralans, S. Otto, *Science*, **2010**, 327, 1502-1506.

[66] Jacqui Carnall's thesis, University of Cambridge, **2009**.

Chapter II
Exponential replication enabled through a fibre elongation/breakage mechanism

The following Chapter describes a peptide system capable of undergoing self-replication resulting in exponential growth. This system is relevant in the context of prebiotic chemistry, since, in order for life to appear as we know it, replicating molecules had to compete with each other, under conditions where only the most efficient ones were able to survive. Such systems synthesized in a laboratory may further our understanding of Darwinian evolution at the molecular level, and may provide leads for the design of de-novo life.

Parts of this chapter have been published:
M. Colomb-Delsuc, E. Matia, J. W. Sadownik, S. Otto, *Nature communications*, **2015**, 6, 7427

II.1- Concept of exponential growth

The understanding of our prebiotic world and how complexity emerged from a mixture of simple molecules represents an important challenge in modern science. Several parameters and mechanisms remain to be studied in order to understand the emergence of the first prebiotic systems, and before we will be able to synthesize life de-novo.
Chemical systems sharing some of the characteristics of living cells, but displaying much simpler mechanisms than the ones in our modern biological world should be developed, in order to mimic the mechanisms that could have been ruling the emergence of life in the prebiotic world. Important aspects are (i) compartmentalisation[1,2,3,4,5]: each entity of a species should be contained in a well-defined space; (ii) metabolism: a living system should be able to gather energy and building blocks from its environment, and use these for the chemical reactions needed to sustain itself; and (iii) replication: for a species to stay alive, it needs to be able transmit its information to the next generation by replicating in an efficient manner.
Simple autocatalytic systems[6] featuring self-replication or cross-replication mechanisms[7,8] have been described, in different fields of chemistry, by using small biomolecules such as peptides[9,10], nucleic acids[11,12], or through the design of fully synthetic molecules[13,14,15].

In a synthetic system consisting of a pool of several species in competition with each other for a given food niche, only one is capable to sustain itself, while the population of the others decreases, until total extinction. This is the very principle of Darwinian evolution. This process is possible if the species in competition undergo cycles of replication/destruction with different efficiencies. The replication corresponds to a growth in the species population through the consumption of food, while the destruction corresponds to the disassembly of the species, which may lead to their conversion back into food. In such a system, the most efficient replicator will dominate, while the other competing species are being destroyed, and eventually go extinct.[16,17,18] Therefore, replication rate and destruction rates are two obvious determining parameters to be considered when studying complex systems in which several species are in competition. However, it turns out that also reaction orders play an important role (*vide infra*).

The following equations describe the kinetics of reaction of a simple replicator, and introduce the replication rate law:

$$F \xrightarrow{R} R \tag{1}$$

$$R + D \rightarrow F + W \tag{2}$$

$$\frac{d[R]}{dt} = k_R[F]^f[R]^r - k_D[R]^d[D]^x \tag{3}$$

F represents a food molecule, consumed by the replicator *R* in order to give more of itself. *D* is a destroying agent acting on the replicator, leading to the production of food, ready to be used to form more replicator, and some waste molecules *W*. The rate of replicator formation is given by equation (3), in which k_R represents the rate constant of the replication and k_D the rate constant of the destruction reaction. The order of the replication process in food and replicator are given by *f* and *r*. The order of the destruction process in replicator, and destroying agent are given by *d* and *x*.

Autocatalytic systems where the order in replication reaches a value of 1 are commonly referred as exponentially growing.[15,16,19] Most of the autocatalytic systems currently described suffer from inefficient dissociation of the products of replication, as already discussed in Chapter I of this thesis. Therefore, in such systems, the product of the replication cannot participate efficiently in a new replication cycle, leading to an order in replicator of 0.5, corresponding to parabolic growth.[20,21,22,23]

In a scenario where several species are competing for a same food niche, a limitation in replication order (i.e. $r < 1$) has been shown to prevent species from going extinct, leading to their indefinite coexistence[18]. Such a system is not compatible with Darwinian evolution, in which one of the species should be capable to outcompete the others, leading to their total annihilation.
It is possible to reach complete destruction of the other species in competition only if the order in replicator in the replication process is higher than, or equal to the order in replicator in the destruction process (i.e. $r \geq d$)[16,17,18]. In most of the cases the product of the replication can be eliminated either by an external molecule able to destroy it through a chemical reaction, or by being physically moved out of the system, leading to an order in replicator in the destruction process d equals to 1. The design of a system able to reach exponential growth (i.e. $r = 1$) is therefore a prerequisite for achieving Darwinian evolution at a molecular level.

Some examples of systems able to undergo exponential growth have been described previously. It was first achieved by following non-autonomous pathways, in which intervention is required between the different replication steps.[24,25,26] The first example of a system capable of exponential growth, in a non-autonomous manner, was introduced as Surface-Promoted Replication and Exponential Amplification of DNA analogues (or SPREAD), by Günter Von Kiedrowski et al.[24] Scheme II.1.a shows the system he described. In order to achieve exponential growth, a DNA single strand is first immobilized on a solid support. Building blocks are then added to the system, and a new strand, complementary to the first one, is formed by a step of recognition (or annealing) followed by a ligation process. The freshly formed strand is then separated by changing conditions, and the newly liberated DNA single strand is ready to be fixed on the solid support for a new cycle of replication. The support here avoids product inhibition by impeding duplex reassociation and facilitating product isolation and handling. This method allows to double the amount of replicating material in solution after each cycle of replication, achieving therefore replication in an exponential manner. However, the need of a treatment after each step represents a limitation. It was nevertheless the first description of an exponential system, and opened the way for the development of autonomous exponentially replicating systems, which few systems managed to achieve to date. Scheme II.1.c shows one of the rare examples, described by Ashkenasy and al.[27] Their system uses a peptide able to form β-sheets. Two peptide building blocks form β-sheet interactions with a long peptide template, which brings them close enough to speed up native ligation. The newly formed peptide is then ready to link to two new building blocks through a new cycle of replication. Another example was introduced by Joyce,[12] depicted in Scheme II.1.b, which is limited by the need of large biomolecules, developed with the help of other biomolecules, to reach exponential growth, when an ideal system would use only small building blocks which synthesis is easy to handle, in order to be closer to prebiotic conditions. While these last examples describe autonomous exponential growth, they lack the description of the precise mechanism leading to exponential replication.

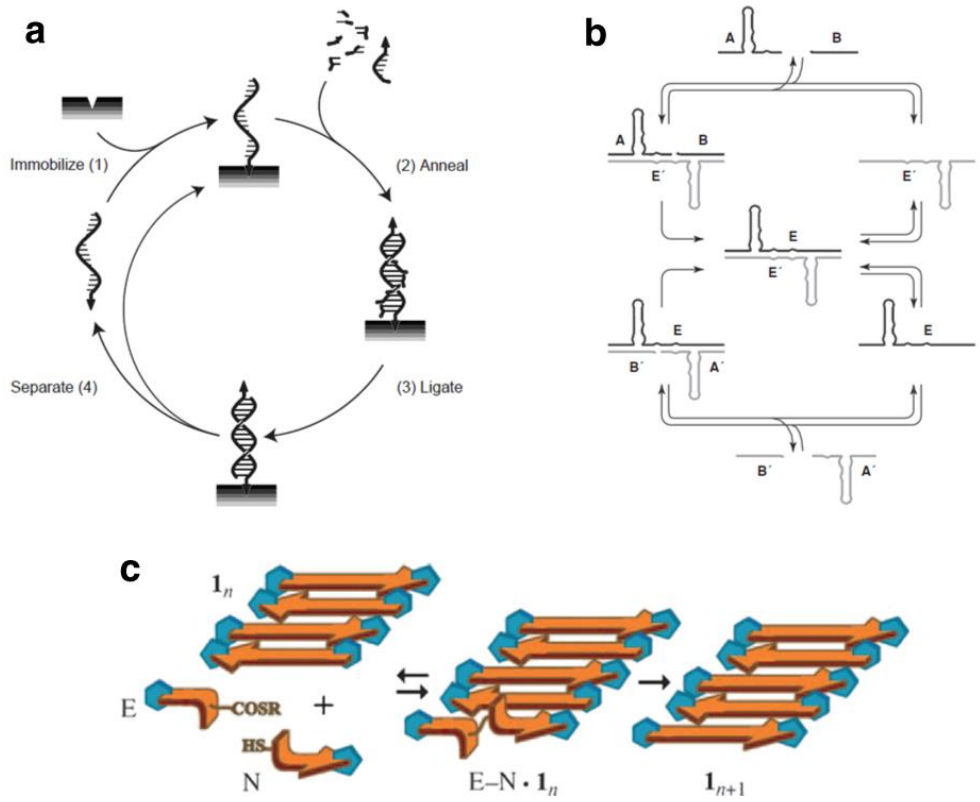

Scheme II.1. *Examples in the literature where exponential growth is reached. a. SPREAD system[24] b. System described by Joyce[12], where E represents the template, and A and B are the precursors. A', B', and E' are the complementary nucleotide sequences to their corresponding letter. c. Peptide system described by Ashkenasy[27]. Reproduced from references 12, 24 and 27.*

This chapter demonstrates exponential replication in a peptide system developed in our group, and gives unique insights into the mechanism of replication.

II.2. Introduction of the peptide system

The following study uses Dynamic Combinatorial Libraries[28,29] made from peptide building block **1**, represented in Scheme II.2, which has been developed some years ago in our group, and has been under study since then for different purposes[30,31]. In this chapter we have analysed the extent to which this system is capable of exponential growth.

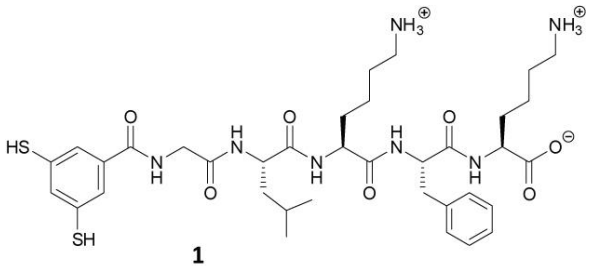

1

Scheme II.2. *Peptide building block used in this study.*

Building block **1** is composed of an aromatic dithiol capable of undergoing oxidation, leading to a dynamic combinatorial library composed of different-sized macrocycles, the composition of which may change over time due to the reversible covalent disulfide bonds linking the macrocycles (see Scheme II.3).

The system was monitored by HPLC/UPLC analyses, with which the changes in composition of the libraries can be followed, by extracting the data from the chromatograms and plotting the amount of each species against time.

A control compound equipped only with a carboxylate group (compound **2**), oxidises to different species, and after some days reaches an equilibrium composition which is dominated by cyclic trimers and tetramers.[30]

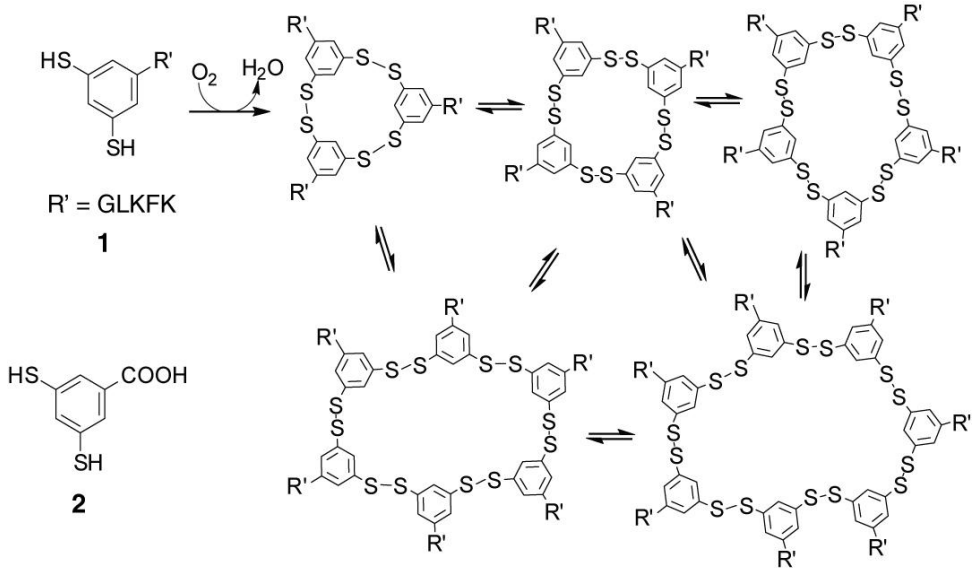

Scheme II.3. *Oxidation of the building block **1** to larger species, and dynamic exchange of the formed macrocycles.*

When equipped with a peptide chain, designed in order to form β-sheet structures by alternating hydrophobic and hydrophilic residues, the larger macrocycles formed by oxidation of **1** are able to stack on top of each other through peptide interactions, leading to the formation of amyloid-like long fibres (Scheme II.4), observable by TEM.

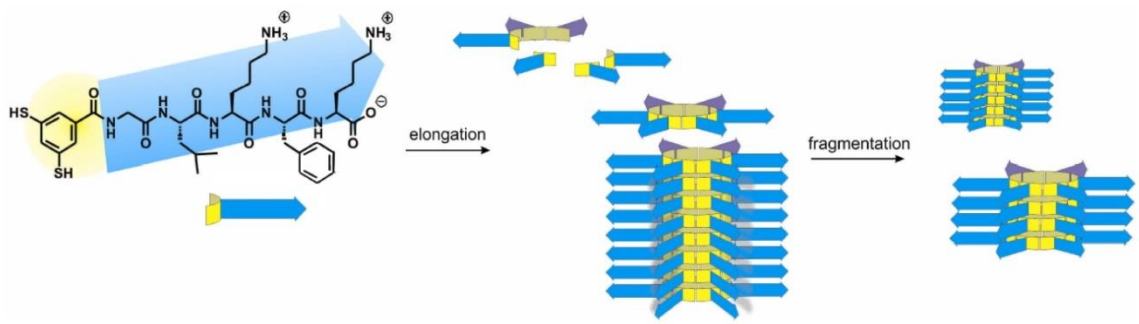

Scheme II.4. *Elongation and fragmentation of the fibres made from hexameric macrocycles of **1**.*

These fibres represent a kinetic trap, reducing the dynamicity of the macrocycles included in them. They trigger a self-replication process in which the species that are still in solution are oxidised to hexamers and are included on top of the fibres, leading to a growth in fibre length.

Fibres made from smaller macrocycles than hexamers are not observed for this system, probably due to the relatively weak interactions between the peptide chains, which are not sufficient to allow the smaller macrocycles to stack on top of each other. On the other hand, hexamer macrocycles are able to stack onto each other since the β-sheet interactions coming from the six peptide chains together are strong enough.

Upon mechanical stress, the fibres formed from the self-assembly of the hexamers macrocycles are broken into smaller ones. However, the fibre elongation, corresponding to an incorporation of the newly formed hexamer species to the fibres, happens at the fibre ends. Therefore, fibre breakage, by increasing the number of fibres in the library, also increases the number of elongation sites, overcoming the earlier discussed problem of dissociation of the products of replication.

As discussed before, the order of the replication reaction *r*, from equation (3) should be equal to 1 for the growth in replicator concentration to be considered exponential. In absence of a destruction mechanism in our system, equation (3) simplifies to equation (4):

$$\frac{d[R]}{dt} = k_R[F]^f[R]^r \tag{4}$$

In order to be able to experimentally determine the order in replicator *r*, a logarithmic regression on equation (4) gives the following equation:

$$\log\frac{d[R]}{dt} = \log k_R + f\log[F] + r\log[R] \tag{5}$$

When considering only the initial stage of the replication, the food is not significantly consumed and therefore its concentration can be approximated to be constant. Consequently, log $k_R + f\ log[F]$ is constant. This implies that the replication order *r* of the reaction can be determined from the slope of a plot of log(d[R]/dt) versus log[R]. The relevant data was acquired through a set of seeding experiments.

II.3. Seeding experiments

In order to assess the initial rate of replication experimentally, a series of seeding experiments were performed, by addition of a solution containing the replicating species, fibres of hexamer macrocycles in the present case, to a young library not fully oxidised, composed of the intermediate species, including monomer, trimer and tetramer.
The protocol by which those seeding experiments were performed is the following: A solution of 3.8 mM of monomer of **1** dissolved in borate buffer 50 mM was oxidized by adding 70 mol% of a solution of sodium perborate (with respect to the monomer) in order to reach within 30 minutes a library composed of monomer, trimer, and tetramer species. A UPLC analysis of a library after sodium perborate oxidation, ready to be seeded is shown in Figure II.1.b.

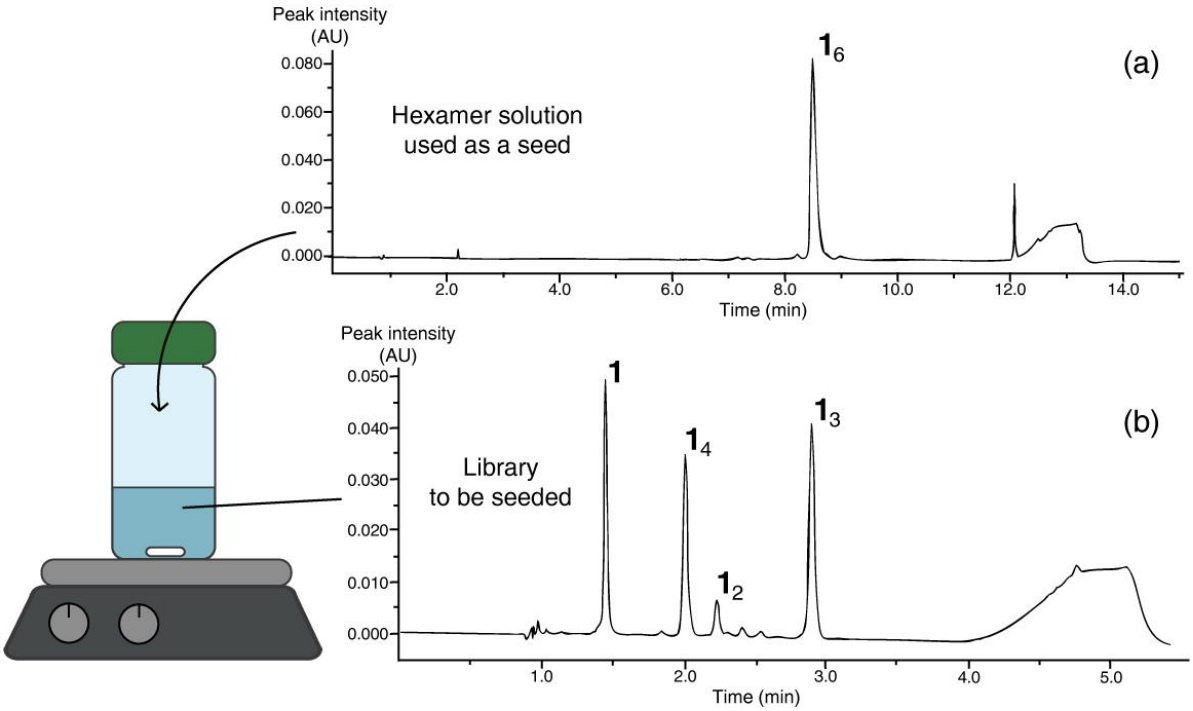

Figure II.1. *Seeding experiment in which the seed (a) is added to a library rich in the small macrocycles (b).The broad peak at the end of the chromatograms reflects an increase in absorbance due to an increase in acetonitrile content in the mobile phase.*

At this stage, the monomer represents for this example 27% of total peak area of the library, the linear dimer 6%, the cyclic trimer 36% and the cyclic tetramer 26%. Although the hexamer grows seemingly from the tetramer and the trimer, it is important to keep some monomer in the solution in order to keep enough thiolate species, providing dynamicity to the system. This library was then split into 4 samples, each one equipped with a small stirring bar. To these libraries, a library rich in hexamer, obtained from the oxidation and exchange of a library prepared from a solution of 3.8 mM of monomer of **1** dissolved in borate buffer (50 mM, pH 8.1), was added in different amounts corresponding to 5 mol%, 10 mol %, 15 mol%, and 20 mol% of the material in the libraries to be seeded. A UPLC chromatogram of the hexamer used as a seed is shown in Figure II.1.b. There is a peak observable at the beginning of the washing of the column (corresponding to an increase in acetonitrile in the eluents, and observable in the chromatogram as a hump from 12.0 to 13.5 min). This peak, also observed in blank samples, may correspond to some compound trapped previously in the column.

Immediately after the seed was added to all the libraries, they were stirred at 1200 rpm and monitored by a sampling them every 8 minutes. The sampling was done by withdrawing 2 µL of a library, and diluting this sample in 98 µL of a solution of ddH_2O containing 0.6% of TFA. This procedure quenched the sample, by diluting it and placing it in an acidic environment, preventing disulfide exchange and therefore further changes in the library composition.

The libraries were monitored for 100 min following this methodology, and then all the samples were analysed by UPLC. From the chromatograms, the concentration of hexamer with respect to the other species was determined, by measurement of the peak areas. Figures II.2 and II.3 show an example of the results obtained from a seeding experiment where the seed was added in 20 mol% with respect to the monomer in the seeded library.

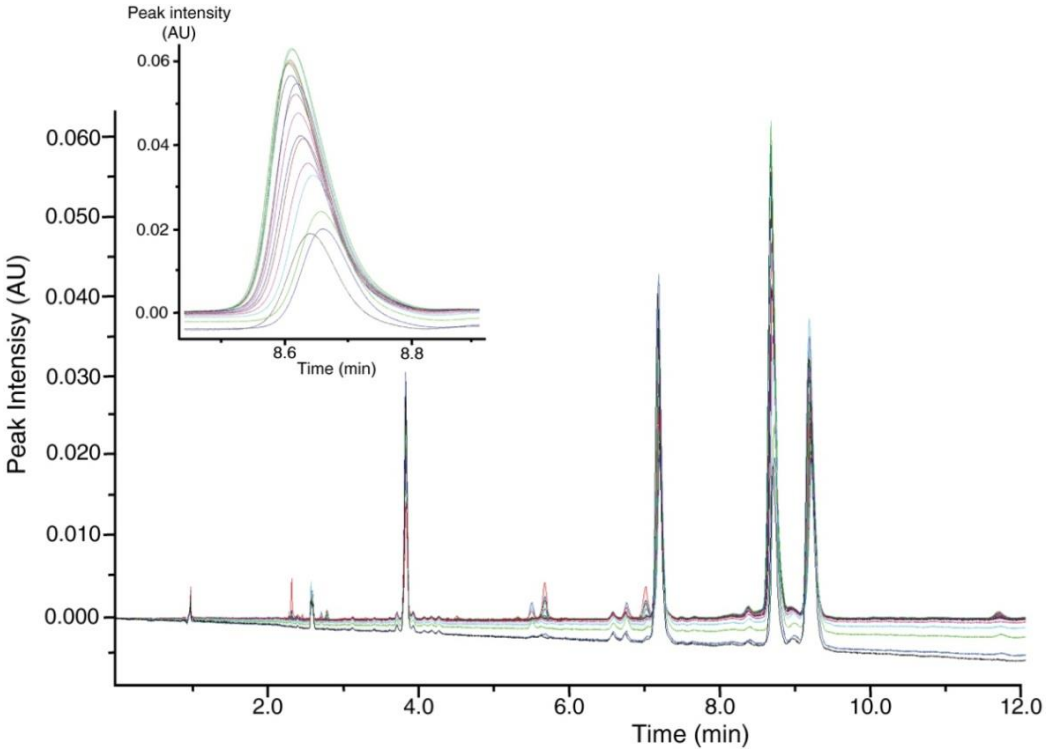

Figure II.2. *Example of the UPLC chromatograms obtained from a seeding experiment (20 mol% of seed was added in this example) from 0 to 120 min. Each line represents a UPLC measurement. The inset shows the growth of the hexamer species.*

Figure II.2 shows an increase of the concentration of hexamer with time. In order to confirm this trend with more accuracy, the peak area of each peak was measured, and from the total peak area, the relative concentration of each species could be determined. When plotting the library distribution against time, the kinetics of growth or disappearance of the different species in solution can be observed. Figure II.3 represents the kinetic profile corresponding to the data extracted from the integration of the chromatograms shown in Figure II.2.

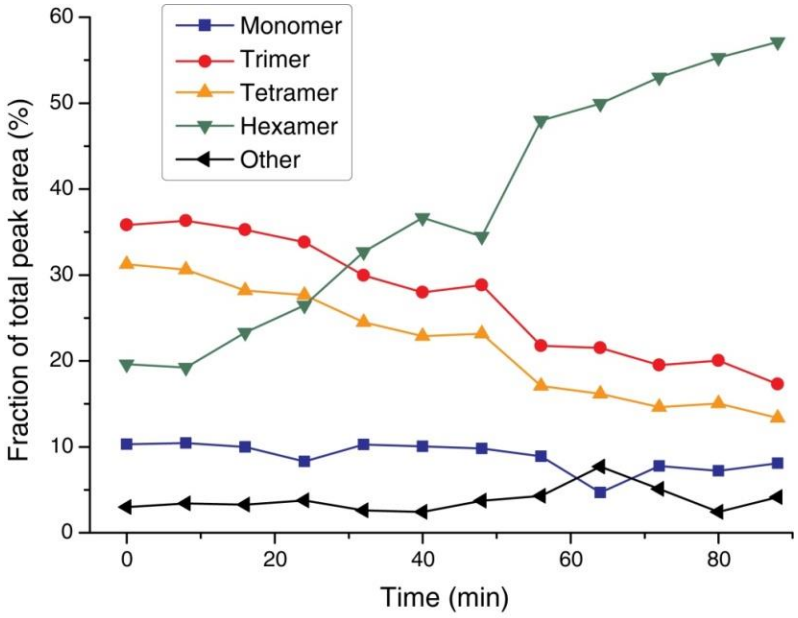

Figure II.3. *Kinetics of growth of the hexamer, and change in concentrations of the other species in solution during a seeding experiment. The amount of seed added was 20 mol% with respect to the initial monomer concentration.*

It can be observed that the hexamer concentration is growing at the expense of tetramer and trimer, and the monomer concentration is slightly decreasing, but stays relatively stable. The other species (mainly composed of the linear dimer and some small amounts of pentamer) stay around 3% of the total peak area.

In order to determine as accurately as possible the rate of growth of the hexamer, several sets of seeding experiments at different seed concentration were performed, following the methodology described above, and an arithmetic average of the obtained values was calculated. The kinetics of growth of hexamers for different seeded libraries, at different seed concentrations is depicted in Figure II.4.

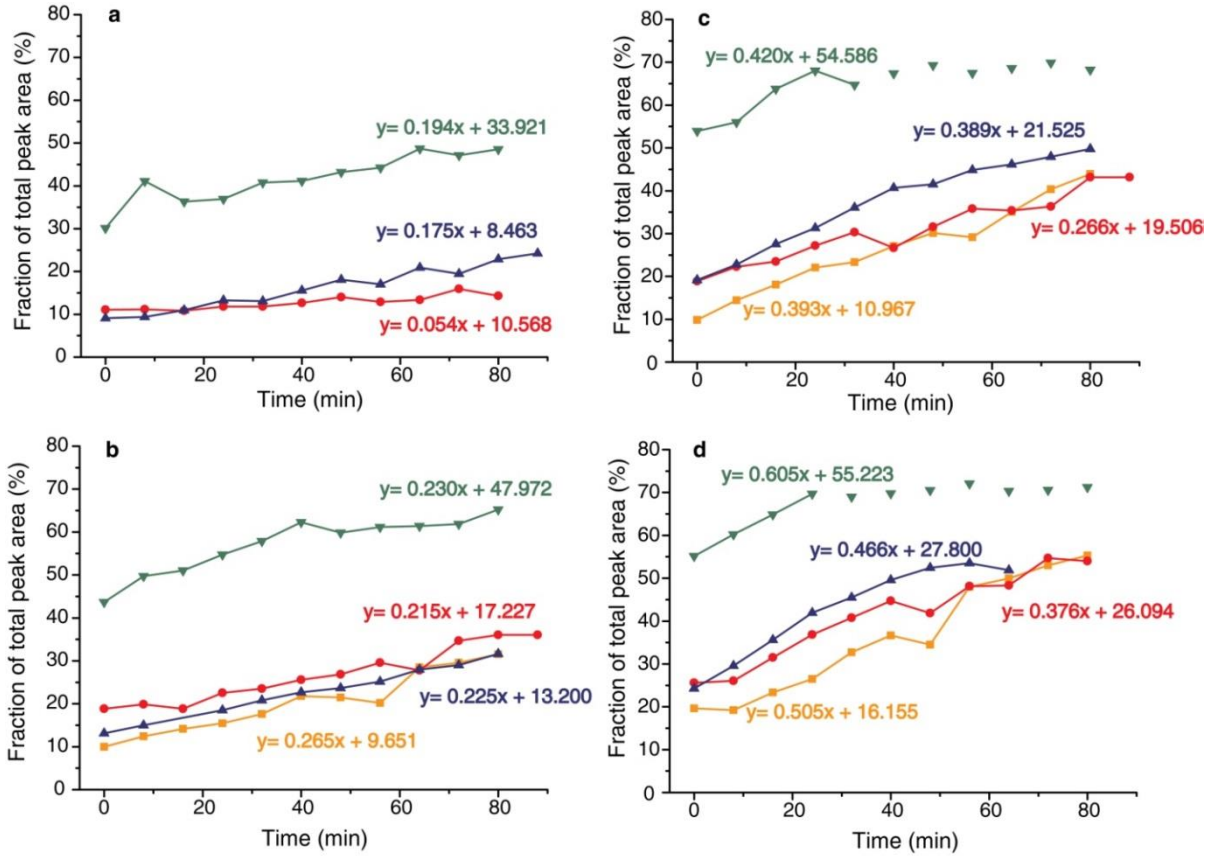

Figure II.4. *Kinetics of replicator growth in seeded libraries at 5% (a), 10% (b), 15% (c), 20% (d) of initial seed. Each colour corresponds to a set of seeding experiments done on the same batch.*

All the experiments depicted here follow a clear trend. The more seed was added, the faster the hexamer concentration increases, which can be considered as evidence for autocatalysis. One set of measurements (green triangles) gave an initial replication concentration higher than for the other sets of experiments, leading to a faster saturation when seeded at 15% and 20%. For this reason, the initial replication rate was determined using the data points before reaching the plateau.

In order to determine the actual growth rate of the replicator, the values of the slopes from Figure II.4 were extracted, their corresponding logarithm was calculated and plotted against log(d[R]/dt). The results are shown in Figure II.5. According to equation (5), the slope of this plot corresponds to the order of the reaction *r*, which is 0.993 ± 0.17 in the present case.

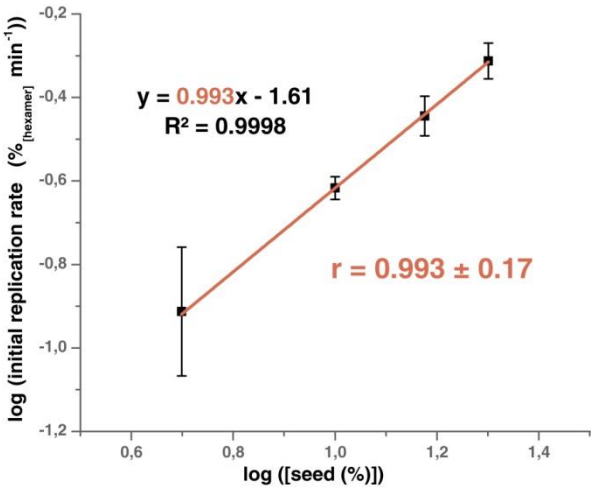

Figure II.5. *Experimental determination of the order in replicator. Initial replication rates against initial replicator concentration. The error bars on the data points correspond to one standard deviation for each seed concentration and the error on the slope is the standard deviation based on the complete set of measurements.*

This value is consistent with exponential growth occurring in our system. Note that exponential growth occurs autonomously, since all the steps happen in one vial without any human interference other than dissolving monomer in a buffer at the initial stage and mechanical agitation. This is one of the few systems described to date capable of autonomous exponential growth.

However, the large error on this data led us to do further experiments in order to confirm experimental growth and to obtain some insights into the mechanism leading to exponential growth. Moreover, a theoretical model of the system, and computational simulations, were also used in order to further verify our hypotheses.

II.4. Insights into the mechanism of replication

II.4.a. Influence of the stirring rate on fibre breakage

In order to assess the validity of the proposed fibre breakage mechanism, we investigated the effect of shear stress on the fibre length distributions. If shear stress has an influence on fibre breakage, then exposing the system to higher stirring rates should lead to a more pronounced breakage, and therefore shorter fibres should be observed in such libraries.
In order to prove this hypothesis, a series of experiments were performed in which a library made by dissolution of 3.8 mM of **1** in borate buffer (50 mM, pH 8.1) was split into several samples. Each of them was equipped with a stirring bar and put on a stirring plate. These libraries were then stirred at stirring rates of 200 rpm, 400 rpm, 800 rpm, 1000 rpm, 1200 rpm, and 1500 rpm. Their library composition was monitored by UPLC, by a regular sampling of the libraries.

After they reached constant composition in which the hexamer was the main species present for all the samples, a series of TEM measurements were performed on each sample, and an average fibre length distribution was measured. The obtained micrographs, shown in Figure II.6, demonstrate that

fibres can be observed for all of the libraries, confirming that the self-replication process occurs at all the stirring rates studied.

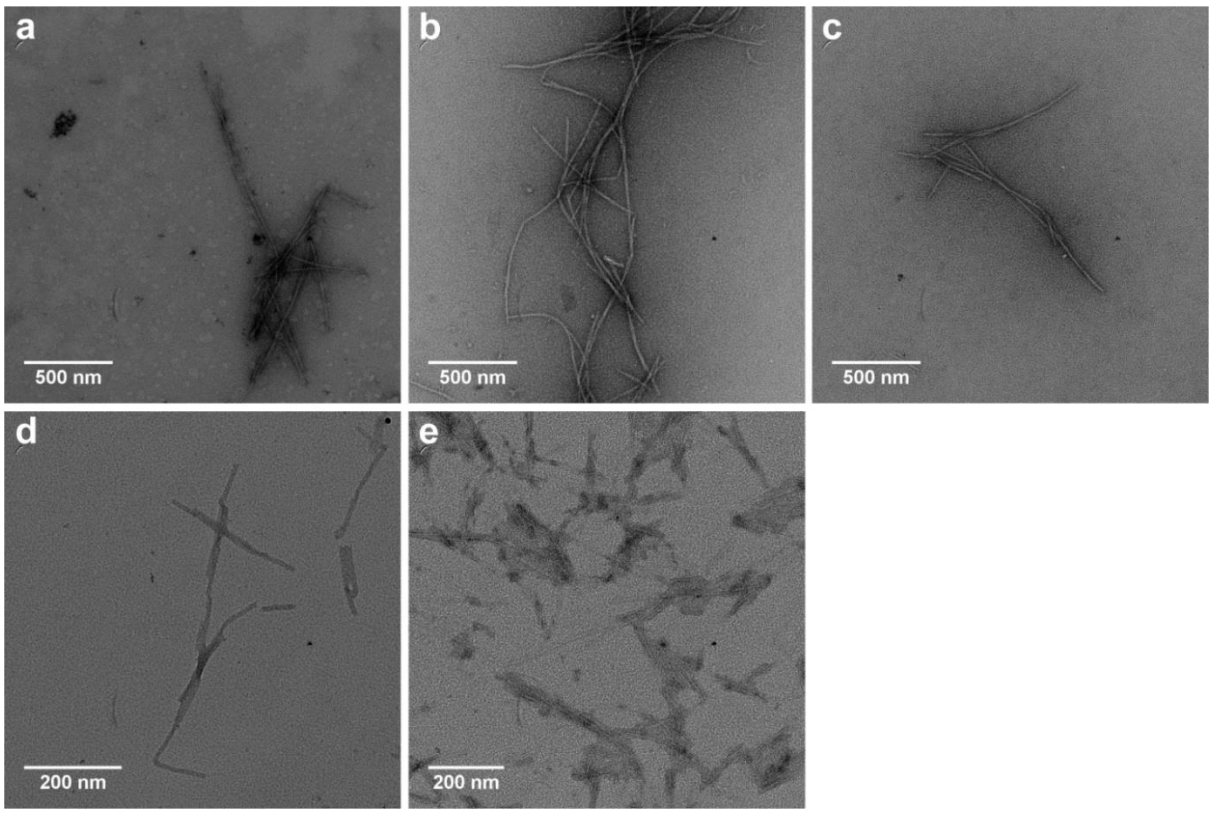

Figure II.6. *TEM analysis of fibre length distribution at different stirring rates. After complete oxidation, and once the hexamer prevailed in all libraries, TEM measurements were made. The micrographs correspond to stirring rates of 200 rpm (a), 400 rpm (b), 800 rpm (c), 1000 rpm (d), and 1500 rpm (e).*

Moreover, fibre measurements, made with the software ImageJ, and then processed in MS Excel, gave a different average fibre length for each library studied. Figure II.7 depicts the average fibre length obtained as a function of the stirring rate. A clear trend shows that at first, the average fibre length decreases dramatically with increasing stirring rates, but this decrease is more moderate at higher shearing rates. It appears that, when reaching shorter lengths, the fibres are more resistant to shear stress, and more energy is therefore required to break them.

(a)

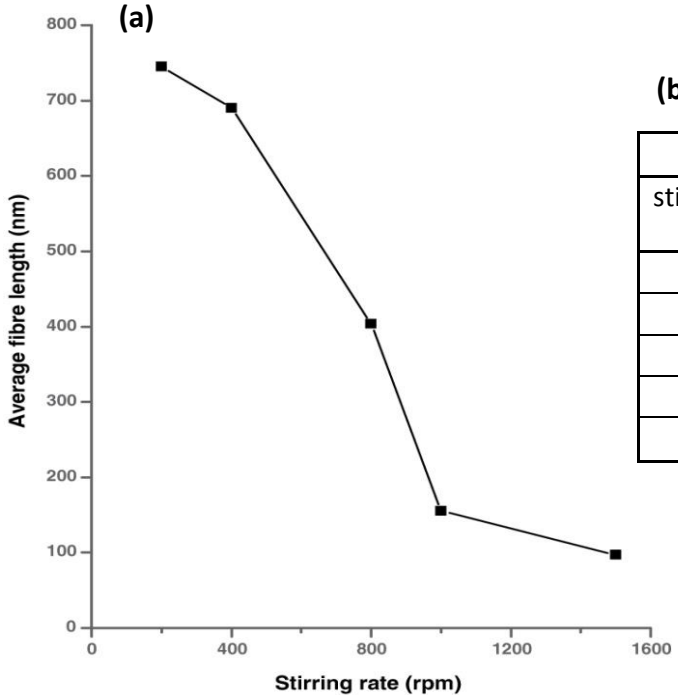

(b)

XGLKFK		
stirring rate (rpm)	average length (nm)	measurements
200	745	37
400	690	35
800	404	38
1000	155	77
1500	97	30

Figure II.7. *Influence of the stirring rate on the average fibre length. a. Average fibre length against stirring rate. b. Values of the observed average fibre length and number of length measurements for each sample at different stirring rates.*

From these measurements, the fibre length distributions of the samples were also determined. The obtained results are shown in the Chapter III of this thesis, where they are further discussed, and compared with the results obtained with other peptide sequences.

These results are in accordance with our postulate that the shear stress applied to the system affects the average fibre length, and supports the proposed mechanism of an exponential growth induced by fibre breakage.

II.4.b. Effects of the shear rate on the rate of growth of the replicator

At the same time and on the same libraries as the ones used for the fibre length distribution measurements discussed in the previous paragraph, the change in composition of the libraries stirred at different rates was monitored, with a particular focus on the concentration of hexamer.
The sampling was done according to the procedure described in paragraph II.3, and the relative concentration of the species in solution was determined by plotting the peak areas obtained from the chromatograms.
Figure II.8 shows the amount of hexamer in time, depending on the stirring rate applied to the system. It can be observed that the hexamer growth happens earlier when the libraries are subjected to increasing shear stress. This means that for a library in which the stirring rate, and therefore the shear stress applied, is low, it will take more time for the hexamers to form and to start stacking on top of each other in order and form fibres.

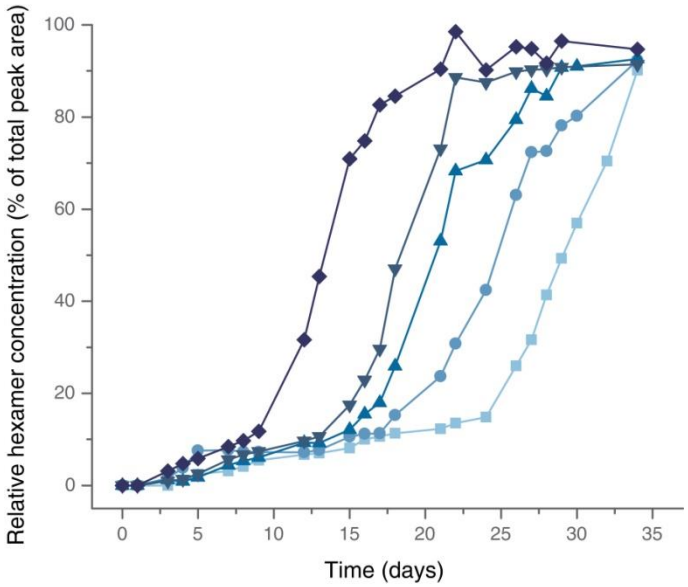

Figure II.8. *Kinetics of replicator growth at various stirring rates (lighter to darker blue: 200, 400, 800, 1000 and 1500 rpm).*

However, it is interesting to notice that the slopes of the different hexamer growth cruves, despite starting at different times, seem to be relatively comparable, meaning that as soon as the hexamer concentration becomes significant, its self-replication speed seems to be only little dependent on the shear stress.
This observation suggests that during the advance phase of replication process, the average fibre length does not play a significant role since, despite strong differences in fibre length averages (Figure II.7.a), the replication efficiency of those libraries seems to be similar, independent of the stirring rate.
Apparently some other process that is independent of the number of fibre ends becomes rate limiting which may be the production of hexamers in solution.

In order to assess the relationship between average fibre length, and kinetics of self-replication, the time that it takes for the hexamer to reach 50% of the total peak area, i.e. of the total relative concentration of the species in solution, referred as t_{50}, was determined, and plotted against the data accumulated from the average fibre length measurements. The results from this analysis are depicted in Figure II.9.

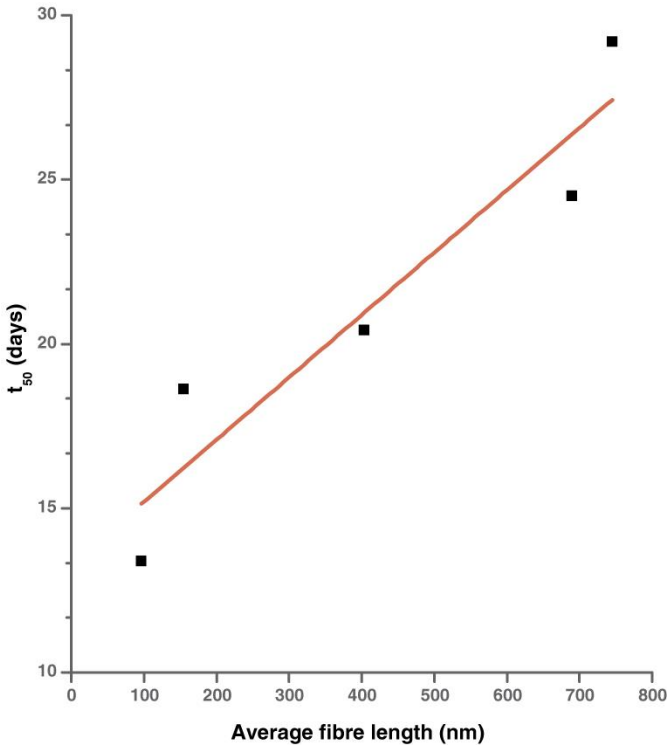

Figure II.9. *t_{50} , i.e., the time needed for the replicator to represent 50% of the library material, as a function of the average fibre length; the line represents a linear fit of the data.*

It can be seen that the time it takes for the replicator to represent 50% of the library material appears to be roughly proportional to the average fibre length, confirming the observations made on Figure II.8.

II.4.c. Monitoring the average fibre length during the replication process

When relating equation (4) to our system, it can be observed that in order to have a replication order of 1, the average fibre length has to be constant throughout the replication process, since the concentration of fibre ends, corresponding to the concentration of replication sites, depends exclusively on the replicator concentration only in the case where the average fibre length stays constant.
To verify whether the fibre length average is indeed constant during replication a seeding experiment was done during which the fibre length was monitored during the entire replication process.

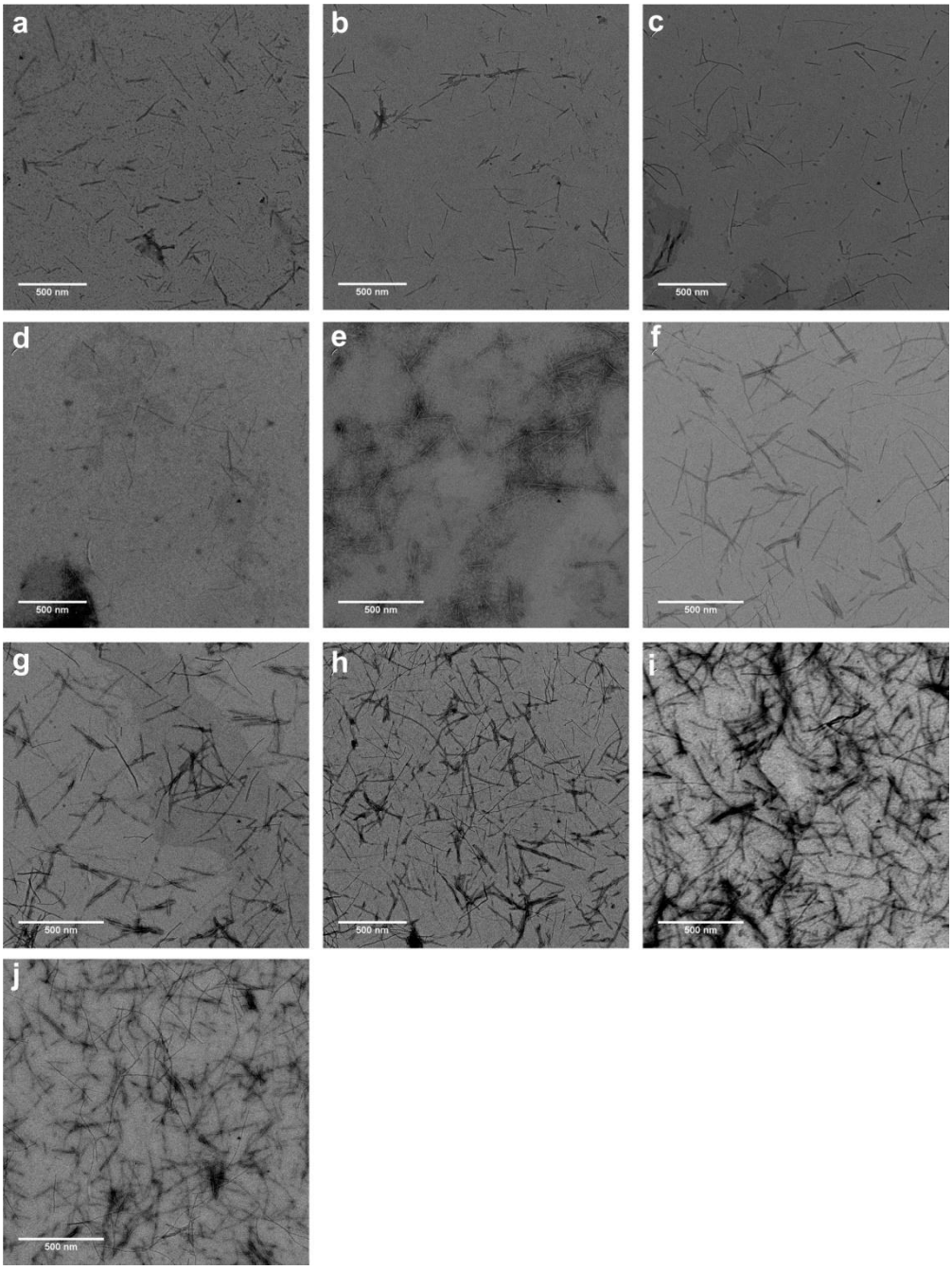

Figure II.10. *TEM analysis of fibre length average over time during replication. A library was seeded with 20 mol % of a sample rich in hexamer of* ***1****, and observed at different times after the addition of the seed. The micrographs correspond to times of 0 min (a), 8 min (b), 16 min (c), 24 min (d), 32 min (e), 40 min (f), 48 min (g), 56 min (h), 72 min (i), 88 min (j). The sample was stirred at 1200 rpm during the measurements.*

A seeding experiment was performed as described in section II.3 of this chapter, but now every 8 minutes an aliquot was withdrawn from the library, diluted 40 times in double distilled water and immediately after deposited on a glow-discharged carbon coated TEM 400 mesh copper grid. The solution was blotted on filter paper after 30 seconds, and stained 20 seconds with a solution of 2% uranyl acetate and then blotted again on filter paper. The staining process was repeated a second

time, in order to enhance the contrast. The grids were then observed by TEM, and the obtained micrographs are depicted in Figure II.10.

As expected, fibres are observed in every sample. While all the samples were diluted the same way, the observed fibre concentration increases with time, confirming that in the course of the experiment the increase in hexamer concentration observed by UPLC measurements is accompanied by an increase in the number of fibres, suggesting that the newly formed hexamer is incorporated into the fibres.

From the obtained micrographs, fibre length measurements were performed, in order to obtain and compare their corresponding fibre length averages. The results from these measurements are shown in Figure II.11.

(a)

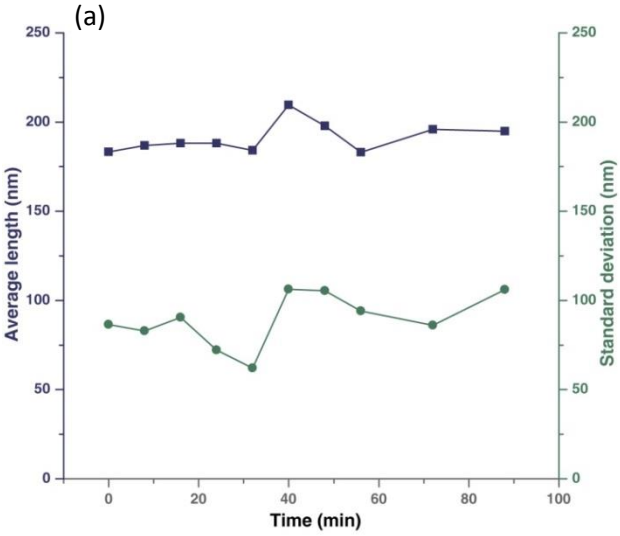

(b)

Time (min)	average length (nm)	sample size (number of measurements)
0	183,4	81
8	186,8	88
16	188,2	106
24	188,2	84
32	184,1	117
40	209,6	118
48	197,7	95
56	183,0	126
72	196,0	33
88	194,9	68

Figure II.11. *Average fibre length over time during replication. a. Average fibre length (blue squares) and associated standard deviation of the fibre length distribution (green circles) of this seeded library as a function of time (determined by TEM). b. The number of length measurements for each sample at different times after the library was seeded with 20 mol% of a sample rich in hexamer of* ***1****.*

It can be observed that the average fibre length is relatively stable throughout the seeding experiments.

In order to give further support for the proposed mechanism, a series of computer simulations were performed based on a model designed in our group.

II.5. Computational support

Due to inherent limitations in the experimental system, and in order to further confirm our proposed theory, a computational model of the system was developed and studied by Elio Mattia.[32]

The model includes different parameters that are according to our theory necessary for self-replication, and puts them together in order to see how the system can behave. The parameters considered in this model are the exchange reactions for the different non-assembled species present in solution, their organisation leading to fibre nucleation and elongation, and the breakage of long fibres into short ones.

Scheme II.5 represents the different parameters involved in the model, and their relationships.

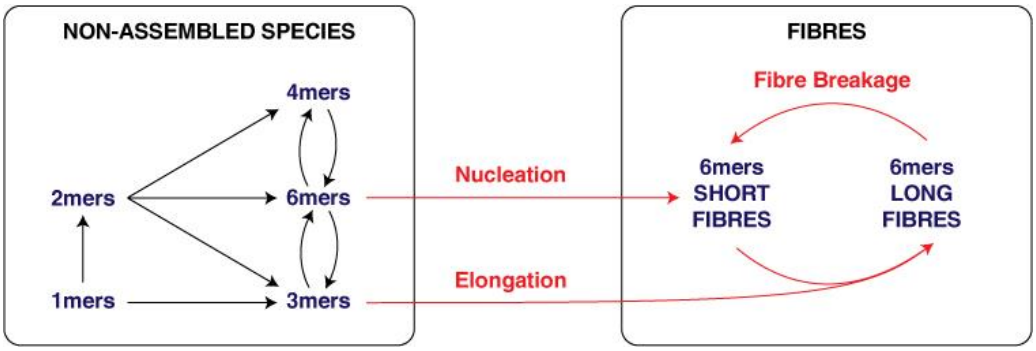

Scheme II.5. *Computational model used for the study of the replicating system.*

As previously discussed, in order to determine the order in replication *r* by using equation (5), the concentration of food molecules *F* has to be constant. Therefore, the concentration of non-assembled species was kept constant throughout the simulations.
The logarithm of replication rate versus the logarithm of replicator concentration was determined, and the central region of a plot simulating the hexamer growth is represented in Figure II.12.

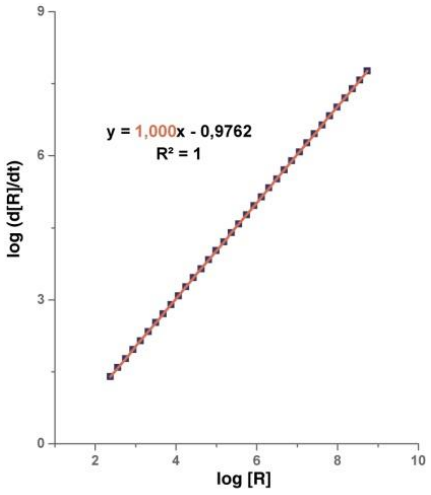

Figure II.12*. Central region of the growth of hexamer.*
It can be observed that in that case, the replication order r=1.000, confirming that an elongation/breakage mechanism leads to exponential growth.

Further studies done with the computational model[32] led to interesting insights. Without a fibre breakage mechanism, the replication order goes down to 0,5, further underlining the importance of fibre breakage for attaining exponential growth. Other investigations with this model also showed that, as observed experimentally, the fibre length distribution stays constant throughout the replication process.
These computer simulations confirm therefore the results obtained experimentally.

II.6. Conclusions

In conclusion, this study shows that the peptide system developed in our group is capable of exponential growth. This was demonstrated both experimentally and computationally. Moreover, further experiments gave some interesting insights into the mechanism, providing proof that the shear stress applied to the system induces the breakage of the obtained fibres, which is mechanistically the key point for exponential growth. The corresponding mechanism is shown in Scheme II.6. Upon oxidation, the peptide building block gives rise to a pool of interchanging macrocycles from which a replicator emerges to form a fibre nucleus (primary nucleation). This fibre nucleus elongates through self-assembly thanks to β-sheet interactions by using the food present in solution, and eventually results in a long fibre that, upon mechanical agitation, may fragment into smaller ones, the ends of which can act as secondary nucleation sites for further growth.

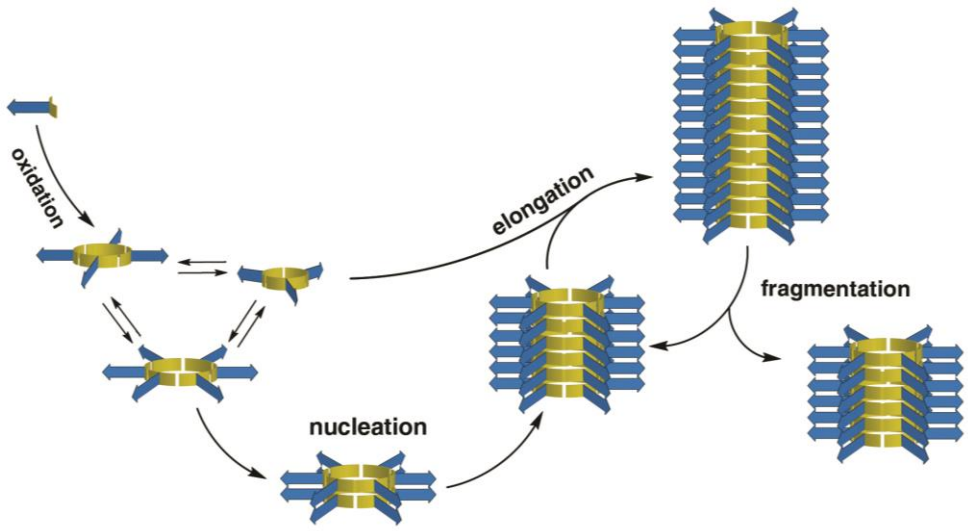

Scheme II.6. *Oxidation of the peptide building block, and exponential replication of the obtained hexamer species.*

It is interesting to notice that the growth mechanism presented here has some strong similarities with the growth of amyloid systems. Indeed, it is well established that mechanical stress is strongly influencing the secondary nucleation of amyloid fibrils[33]. These resemblances in growth mechanism, together with the sharing of some properties, like similar responses to specific dyes[31], demonstrate that a clear parallel can be made between the purely synthetic chemical system developed in our group, and well defined complex biological systems such as amyloid fibrils.

In a more general context, this study gives further insights into exponentially self-replicating systems, and is a step towards achieving Darwinian evolution at the molecular level. Although this study focusses on a rather specific example, it has revealed for the first time a mechanism for attaining exponential replication that is potentially generalizable. In a context of a competitive scenario where several species would be growing from the same source of food, such a system would represent a good candidate for achieving Darwinian evolution with fully synthetic molecules.

II.7. Experimental Section

II.7.a. Materials and methods

Peptide building block **1** was synthesized by Cambridge Peptides Ltd (Birmingham, UK) from 3,5-bis(tritylthio)benzoic acid, which was prepared via a previously reported procedure.[30] Doubly distilled water, boron oxide and potassium hydroxide utilized for the preparation of buffers were obtained from in-house double distillation facilities, Aldrich and Merck Chemicals, respectively. Sodium perborate used for the oxidation of the libraries was purchased from Sigma Aldrich. Acetonitrile (ULC/MS grade) and Water (ULC/MS grade) were obtained from Biosolve BV. Trifluoroacetic acid was purchased from Aldrich. Libraries were prepared in clear HPLC glass vials (12 × 32 mm) closed with Teflon-lined snap caps purchased from Jaytee. Magnetic stir bars used to stir the libraries were Teflon coated (2 × 2 × 5 mm) and obtained from VWR. Samples were stirred on IKA RCT basic magnetic stirrers.

II.7.b. UPLC analysis

UPLC analyses were performed on a Waters Acquity UPLC I-class system equipped with a PDA detector. All analyses were performed using a reversed-phase UPLC column (Aeris Widepore 3.6 μm XB-C18 150 × 2.10 mm, purchased from Phenomenex). UV absorbance was monitored at 254 nm. Column temperature was kept at 35 °C.
For the UPLC chromatogram on Figure II.1.a, the seeding experiments (section II.3.) and the kinetics of growth depending on the stirring rate (section II.4.b.), the following method was used:

Injection volume: 5 μL of a 3.8 mM library subjected to a 1:50 dilution in a solution of 0.6 v% of trifluoroacetic acid in doubly distilled water.
Eluent flow: 0.3 mL/min.
Eluent A: UPLC grade water (0.1 v% trifluoroacetic acid)
Eluent B: UPLC grade acetonitrile (0.1 v% trifluoroacetic acid)

Method:

time (min)	%A	%B
0,0	90,0	10,0
1,0	90,0	10,0
1,3	75,0	25,0
3,0	72,0	28,0
11,0	69,0	31,0
11,5	5,0	95,0
12,0	5,0	95,0
12,5	90,0	10,0
15,0	90,0	10,0

For the UPLC chromatogram depicted on Figure II.1.b, the method used was the following:

Injection volume: 5 µL of a 3.8 mM library subjected to a 1:50 dilution in doubly distilled water.
Eluent flow: 0.3 mL/min.
Eluent A: UPLC grade water (0.1 v% trifluoroacetic acid)
Eluent B: UPLC grade acetonitrile (0.1 v% trifluoroacetic acid)
Method:

time (min)	%A	%B
0,0	90,0	10,0
1,0	90,0	10,0
1,3	72,0	28,0
3,0	64,0	36,0
3,5	5,0	95,0
4,0	5,0	95,0
4,5	90,0	10,0
6,0	90,0	10,0

II.7.c. Negative staining TEM measurements

An aliquot of a sample taken from a peptide library was diluted 40 times in doubly distilled water. Shortly thereafter, a small drop of the diluted sample was deposited on a 400 mesh copper grid covered with a thin carbon film. After 30 seconds, the droplet was blotted on filter paper. The sample was then stained with a solution of uranyl acetate deposited on the grid and blotted on filter paper after 30 seconds. The staining process was repeated in order to have an enhanced contrast. The grids were observed in a Philips CM12 electron microscope operating at 120 kV. Images were recorded on a slow scan CCD camera.

II.8. References

[1] A. Brizard, M. Stuart, K. van Bommel, A. Friggeri, M. de Jong, J. van Esch, Angew. Chem., **2008**, 120, 2093-2096.

[2] P.-A. Monnard, D.W. Deamer, *Anat. Rec.*, **2002**, 268, 196-207.

[3] Y. Schaerli , F. Hollfelder, *Mol. BioSyst.*, **2009**, 5, 1392-1404.

[4] (a) P. L. Luisi, P. Stano, *Nature Chemistry*, **2011**, 3,755-756 ; (b) T. Pereira de Souza, P. Stano, P. L. Luisi, *Chem. Bio. Chem.*, **2009**, 10, 6, 1056-1063; (c) P. Walde, K. Cosentino, H. Engel, P. Stano, *Chem. Bio. Chem.*, **2010**, 11, 7, 848-865.

[5] (a) T. F. Zhu, J. W. Szostak, *J. of Syst. Chem.,* **2011**, 2:4; (b) I. Budin, R. J. Bruckner, J.W. Szostak, *J. Am. Chem. Soc.*, **2009**, 131, 9628-9629.

[6] A. J. Bissette, S. P. Fletcher, *Angew. Chem. Int. Ed.*, **2013**, 52, 12800 – 12826.

[7] V. Patzke, G. von Kiedrowski, *Arkivoc*, **2007**, v, 293-310.

[8] A. Vidonne, D. Philp, *Eur. J. Org. Chem.*, **2009**, 593-610.

[9] D.H. Lee, J.R. Granja, J.A. Martinez, K. Severin, M.R.A. Ghadiri, *Nature*, **1996**, 382, 525-528.

[10] M. Samiappan, Z. Dadon, G. Ashkenasy, G. *Chem. Commun.*, **2011**, 47, 710-712.

[11] G. von Kiedrowski, *Angew. Chem. Int. Ed. Engl.*, **1986**, 25, 932-935.

[12] T.A. Lincoln, G.F. Joyce, *Science*, **2009**, 323, 1229-1232.

[13] T. Tjivikua, P. Ballester, J. Rebek, *J. Am. Chem. Soc.*, **1990**, 112, 1249-1250.

[14] E. Kassianidis, R.J. Pearson, E.A. Wood, D. Philp, *Faraday Discuss.*, **2010**, 145, 235-254.

[15] A. Dieckmann, S. Beniken, C. Lorenz, N.L. Doltsinis, G. von Kiedrowski, *J. Syst. Chem.*, **2010**, 1, 10.

[16] S. Lifson, H. Lifson, *J. Theor. Biol.*, **2001**, 212, 107-109.

[17] E. Szathmary, I. Gladkih, *J. Theor. Biol.*, **1989**, 138, 55-58.

[18] E. Szathmary, *Trends Ecol. Evol.*, **1991**, 6, 366-370.

[19] G. von Kiedrowski, *Bioorg. Chem. Front.*, **1993**, 3, 113-146.

[20] B. Wang, I.O. Sutherland, *Chem. Commun.*, **1997**, 1495-1496.

[21] R. Issac, J. Chmielewski, *J. Am. Chem. Soc.*, **2002**, 124, 6808-6809.

[22] X.Q. Li, J. Chmielewski, *J. Am. Chem. Soc.*, **2003**, 125, 11820-11821.

[23] M. Kindermann, I. Stahl, M. Reimold, W.M. Pankau, G. von Kiedrowski, *Angew. Chem. Int. Ed.*, **2005**, 44, 6750-6755.

[24] A. Luther, R. Brandsch, G. von Kiedrowski, *Nature*, **1998**, 396, 245-248.

[25] K. Montagne, R. Plasson, Y. Sakai, T. Fujii, Y. Rondelez, *Mol. Syst. Bio.*, **2011**, 7, 466.

[26] R. Schulman, B. Yurke, E. Winfree, *Proc. Nat. Ac. Sci.*, **2012**, 109, 176405-6410.

[27] B. Rubinov, N. Wagner, A. Rapaport, G. Ashkenasy, *Angew. Chem. Int. Ed.*, **2009**, 48, 6683-6686.

[28] P.T. Corbett, J. Leclaire, L. Vial, K.R. West, J.-L. Wietor, J.K.M Sanders, S. Otto, *Chem. Rev.*, **2006**, 106, 3652-3711.

[29] *J. Li, P. Nowak, S. Otto*, *J. Am. Chem. Soc.*, **2013**, 135, 25, 9222-9239

[30] J.M.A. Carnall, C.A. Waudby, A.M. Belenguer, M.C.A. Stuart, J.J.-P. Peyralans, S. Otto, *Science*, **2010**, 327, 1502-1506.

[31] M. Malakoutikhah, J. J-P. Peyralans, M. Colomb-Delsuc, H. Fanlo-Virgos, M.C.A. Stuart, S. Otto, *J. Am. Chem. Soc.*, **2013**, 135*,* 18406–18417.

[32] M. Colomb-Delsuc, E. Mattia, J. Sadownik, S. Otto, *manuscript in preparation*.

[33] (a) P. Arosio, M. Beeg, L. Nicoud, M. Morbidellin, *Chem. Eng. Sci.*, **2012**, 78, 21-32; (b) J. E. Gillam, C. E. MacPhee, *J. Phys.: Condens. Matter*, **2013**, 25, 373101; (c) E. K. Hill, B. Krebs, D. G. Goodall, G. J. Howlett, D. E. Dunstan, *Biomacromol.*, **2006**, 7, 10-13; (d) A.T. Petkova, R. D. Leapman, Z. Guo,W.-M. Yau, M. P. Mattson, R. Tycko, *Science*, **2005**, 307, 262-265; (e) C. L. Teoh, I. B. Bekard, P. Asimakis, M. D. W. Griffin, T. M. Ryan, D. E. Dunstan, G.J. Howlett, *Biochemistry*, **2011**, 50, 4046-4057.

Chapter III
Peptide fibres response to shear stress

Fibres formed in the process of self-replication of different peptide containing macrocycles are affected by mechanical forces, and can break apart upon stirring. Fibre breakage has an influence on the speed of replication of the macrocycles. The changes in fibres length depending on the stirring rate were investigated, leading to further insights onto the response of the system to shear stress.

III.1. Introduction

The study of the emergence of life and the development of synthetic systems tending to go towards life are among the most stimulating challenges of modern science.
In order to reach rudimentary forms of life, not only the chemical and supramolecular interactions between the molecules involved in the system should be taken into account, but also the external factors surrounding the systems, which may have a relevant influence on it.

A famous example of the effect of external parameters, introduced by K. Soai in 1995[1], concerns the emergence of chirality through symmetry breaking[2], which has proven to be induced efficiently by several external parameters, including physical interactions[3]. These findings led chemists to rethink the role played by the environment at a molecular level, and investigations of other external parameters were performed. For instance, the medium in which the systems develop plays a significant role, as illustrated in the domain of prebiotic peptide science by the numerous studies done on the emergence of natural amino acid precursors from simple molecules[4], and their development[5]. It was demonstrated that clays[6], aerosols[7], or interactions at the interface between minerals and aqueous systems[8] can enhance the formation and activation of amino acids or other simple prebiotic molecules.
Moreover, the importance of controlling the fluid mechanics in which the reactions take place has been proven,[9] by showing that the sense in which the sample is stirred can give different outcomes in the symmetry breaking of a racemic system to a chiral one, and was recently highlighted in the case of supramolecular assemblies[10].

Mechanistic studies describing the fragmentation of fibril structures under shearing conditions have been widely reported, predominantly in material sciences[11] and nanotechnologies[12]. More recently, some well-defined biological assemblies such as amyloid-like fibrils are also showing a response when shear stress is applied to the system.[13] Their mechanical properties have been defined[14] and it has been demonstrated that the fibre length plays a biological role on the viability of cell exposed to amyloid-like fibrils[15]. As described in Chapter II of this thesis, the peptide system developed in our group displays some similarities with amyloids. Interestingly, shear stress has already proven to be strongly influencing the system by giving different outcomes depending on the shearing conditions[16], or by influencing the kinetics of growth of a replicating peptide through changes in the stirring rate, as seen in Chapter II. For these reasons, there is a strong incentive to further investigate the role of the shear stress on peptide fibre breakage.

Furthermore, it has been recently reported in a different context that the hydrophobicity of the building block, tuned by changes in the peptide sequence, influences the obtained replicator macrocycle size[17] (for more information on this topic, see chapter V). In order to broaden the scope of this study, and have a better the understanding of the role of shear stress, the effect of stirring rate upon fibre breakage and the obtained fibre lengths was therefore investigated for a set of building blocks differing in hydrophobicity. Indeed, the fibre length has already proven to be a parameter playing an important role in the self-replication process, and it would be interesting to be able to determine the optimal conditions for a replication process, and also to see if some peptide sequences can potentially lead to more efficient replication than others, since a different macrocycle size may mean different resistance to shear stress.

We therefore set out to investigate further the effect of shear stress on fibres formed by replicators emerging from different peptide libraries in which the peptide sequence differs.

III.2. Kinetics of formation of the different peptide macrocycles

The influence of the shear stress on different peptide libraries will be discussed in this chapter. A set of libraries made from peptide building blocks varying in hydrophobicity were studied at different stirring rates. The kinetics of growth of the replicator, and the fibre length distribution depending on the stirring rate were monitored.

The self-replicating behaviour of the peptide building blocks **1**, **2** and **3** used for this study has been previously reported.[13] Through oxidation of the thiols to disulfides, the building blocks assemble into larger species through a dynamic exchange, eventually leading to large macrocycles displaying enough interactions with each other to enable the formation of stacks, resulting in fibres, as discussed in **section II.2** of this thesis.

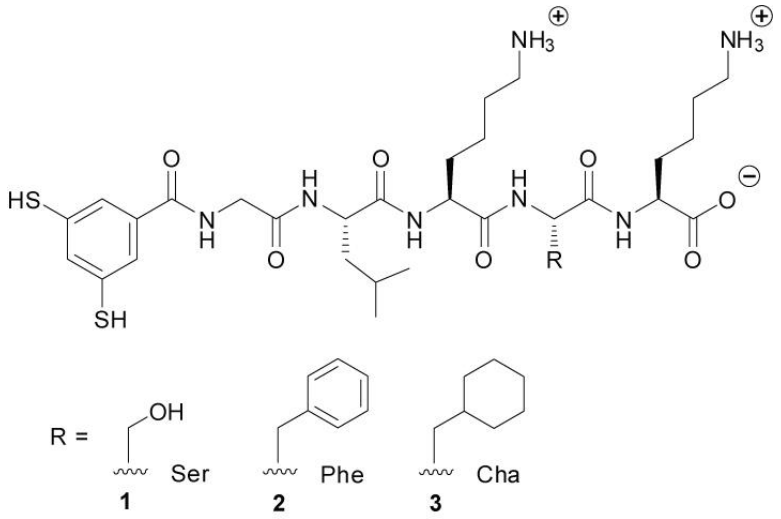

Scheme III.1. Structure of the different peptide building blocks used in this Chapter.

The peptides chosen for this study, which differ from each other in hydrophobicity (**Table III.1**, determined by Morteza Malakoutikhah), lead to different outcomes in terms of replicator size, due to differences in interactions between the macrocycles resulting of the oxidation of those building blocks. Peptide **1**, the most hydrophilic, leads through self-replication to fibres made of octameric rings $\mathbf{1}_8$, whereas **2**, a more hydrophobic peptide[18] and **1**, a non-natural amino acid displaying the most pronounced hydrophobicity,[17] lead both to fibres made of hexameric rings, respectively $\mathbf{2}_6$ and $\mathbf{3}_6$.

These three building blocks represent therefore an interesting pool to study the role of the shear stress since the role of the hydrophobicity and of the replicator size on fibre breakage may be investigated.

Peptide	Sequence	Retention Time (min)
1	X-Gly-Leu-Lys-***Ser***-Lys-COOH	9.4
2	X-Gly-Leu-Lys-***Phe***-Lys-COOH	11.1
3	X-Gly-Leu-Lys-***Cha***-Lys-COOH	12.3

Table III.1. *Peptide sequences and their retention time in reversed-phase HPLC, with a gradient from 5 to 95% CH_3CN in water in 30 min using a Phenomenex phenylhexyl C18 column 4.6 × 75 mm, 3 µm. X: 3,5-dimercaptobenzoic acid.*

Dynamic combinatorial libraries at a concentration of 3.8 mM in borate buffer (50 mM, pH 8.2) were prepared for those three building blocks, and were stirred from the beginning at different stirring rates, ranging from 200 rpm to 1500 rpm. The kinetics of evolution of the replicator in those libraries was monitored by HPLC or UPLC, as represented in **Figure III.1**.

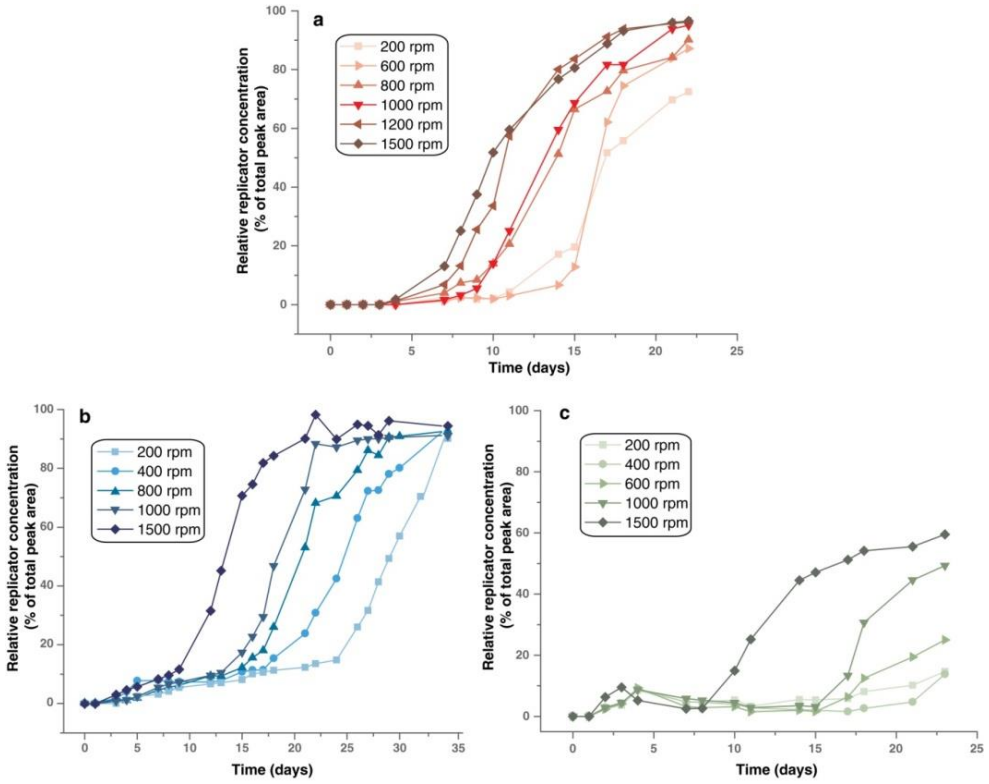

Figure III.1. Kinetics of appearance of the replicators $\mathbf{1}_8$ (a), $\mathbf{2}_6$ (b), and $\mathbf{3}_6$ (c), depending on the stirring rate.

Interestingly, the time at which replication is fastest, corresponding to an inflexion in the replicator's concentration curve, is dependent on the stirring rate. The libraries in which the stirring rate is higher show faster kinetics than the ones stirred at lower rates. This phenomenon, already evoked in **section II.2** of this thesis, is now confirmed with other sequences, and further underlines the importance of stirring rate, and therefore shear stress applied to the system, on the kinetics of growth of the replicator.

One of the hypotheses that may explain this behaviour comes from the fact that during the replication process, the fibres growth occurs at the fibre ends. For a given concentration of peptide building block, the fibre ends concentration will depend upon the length of the fibres present in solution. Shorter fibre lengths, and therefore higher fibre end concentrations, will give rise to faster replication. In the case of the system presented here, this would mean that higher stirring rates give a more efficient fibre breakage, therefore enhancing the speed of replication.
It is interesting to notice that for the different peptide sequences studied, the times and ranges of appearance of replicator are different. For example, the replicator $\mathbf{1}_8$ stirred at 1500 rpm starts to rapidly grow after 7 days, while the slowly stirred sample at 200 rpm shows a growth in replicator $\mathbf{1}_8$ after 15 days; a difference of 8 days. However, in the case of the peptide building block **2**, the replicating species $\mathbf{2}_6$ in the sample stirred at 1500 rpm grows significantly only after 10 days, when in the sample stirred at 200 rpm this phenomenon is observed around 26 days, making a difference of 16 days between the two samples, corresponding to twice the difference that was observed with peptide **1**.

III.3. TEM measurements and average fibre length

In order to confirm the role of fibre length distribution in the kinetics of growth of the replicator, a series of fibre length measurements were done on the oxidised libraries previously described. This was achieved by observing a sample of each library by TEM, measuring the fibre lengths on the obtained micrographs, and plotting histograms depicting the fibre length distributions.

III.3.a. XGLKSK

The histograms depicting the fibre length distribution of peptide **1** are presented in **Figure III.2**.

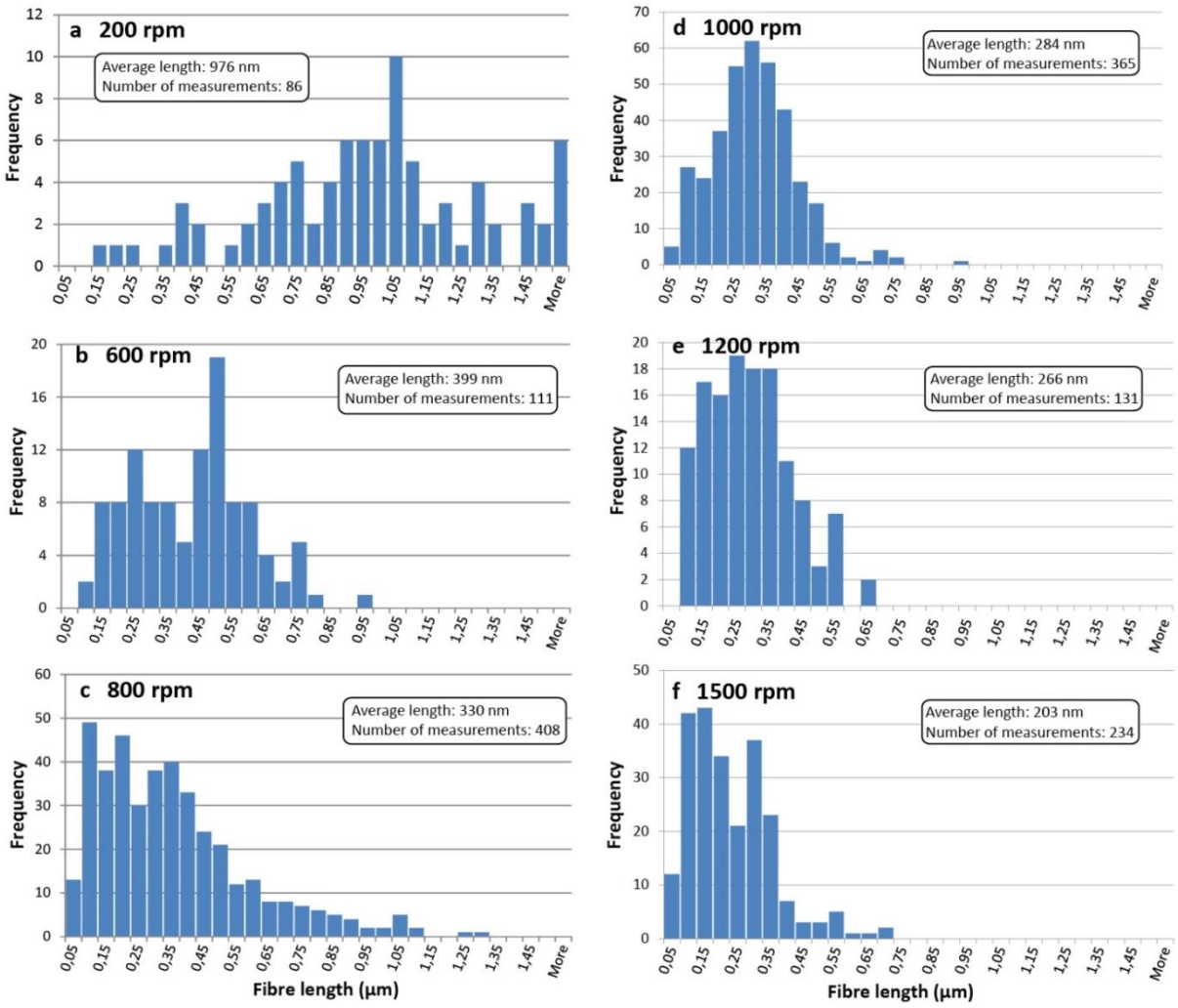

Figure III.2. Fibre length distributions in fully oxidized libraries made of $\mathbf{1}_8$ stirred at rates of **a**: 200 rpm, **b**: 600 rpm, **c**: 800 rpm, **d**: 1000 rpm, **e**: 1200 rpm and **f**: 1500 rpm

A first glance at these histograms reveals that the average length increases when the stirring rate decreases. This observation confirms that the shear stress applied to the system has a direct influence on the fibre breakage.

A direct observation of the TEM micrographs (**Figure III.3**) confirms those results by showing that fibres tend to be longer at lower stirring rates.

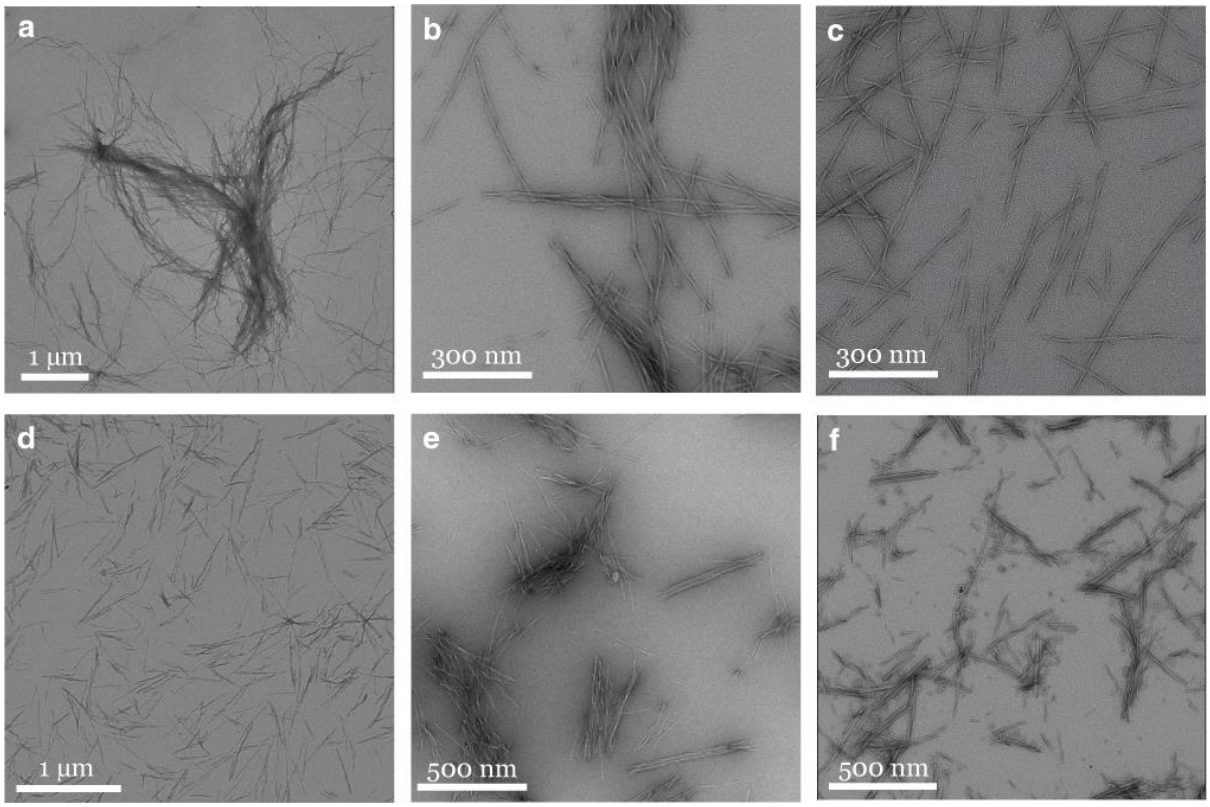

Figure III.3. TEM images of libraries made of $\mathbf{1}_8$ stirred at rates of **a**: 200 rpm, **b**: 600 rpm, **c**: 800 rpm, **d**: 1000 rpm, **e**: 1200 rpm and **f**: 1500 rpm

Although the fibre length distribution is more readily apparent from the histograms, observing the micrographs gives some insights on the shape of the fibres. It is for example interesting to notice that the long fibres coming from the library stirred at 200 rpm tend to aggregate. It is unclear to what extend this aggregation may be due to drying effects. For the micrographs shown at higher magnifications (**Figure III.3.b** and **III.3.c**), twisted bundles of fibres can be observed.

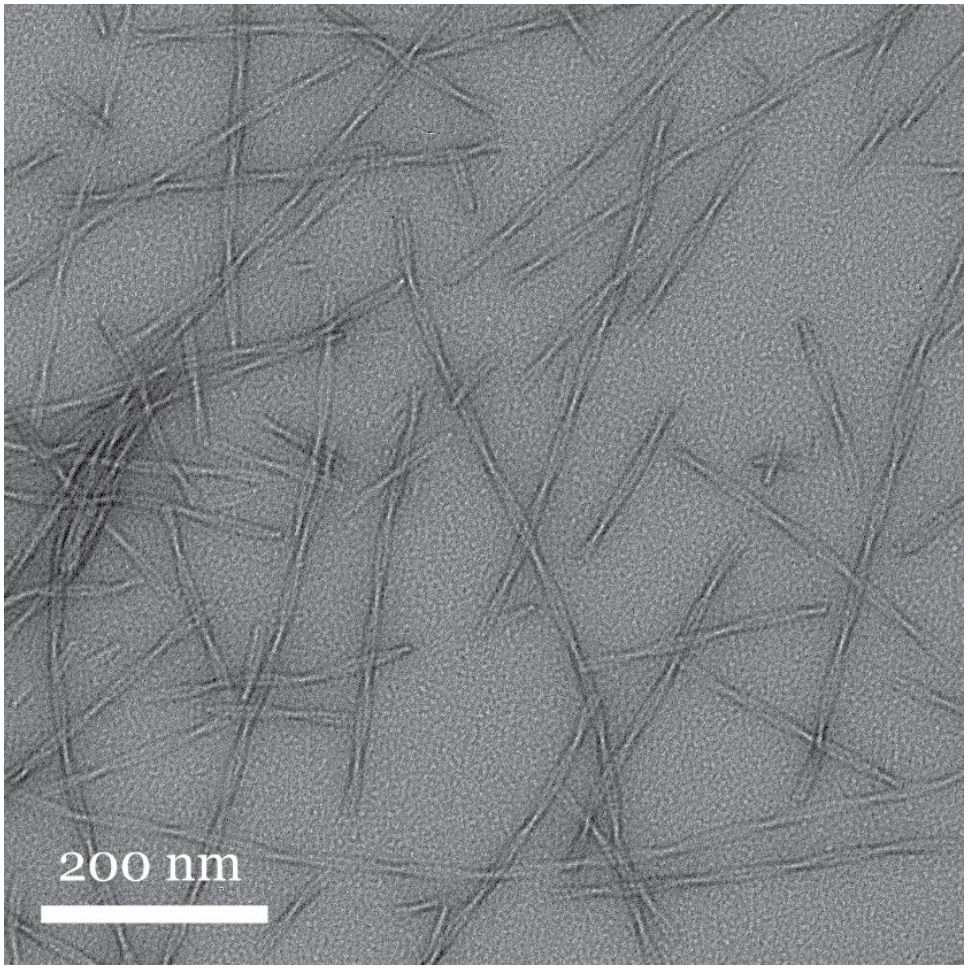

Figure III.4. TEM micrograph of a library composed of $\mathbf{1}_8$ stirred at 800 rpm.

A more accurate investigation done by measuring the fibres width, shows an average bundle thickness of 11.4 ± 1.9 nm, which corresponds to two fibres per bundle. Measurements of the fibre lengths and the number of twists for each of them were done on the sample stirred at 800 rpm (**Figure III.4.**). The results show a uniform twisting, with a pitch of 83.9 ± 3.2 nm. This uniformity suggests that the twisting of the bundles fibres is not random but is rather governed by some interactions occurring between the lateral peptide chains of macrocycles from two adjacent fibres.
Further details on the determination of the fibre thickness and twist pitch can be found in the experimental section of this chapter.

III.3.b. XGLK(Cha)K

The same set of studies was performed on peptide **3**, which, after full oxidation of the library, gives rise to hexamers $\mathbf{3}_6$. The results, presented in **Figure III.5.**, share some similarities with the observations made for peptide **1**, in that there is a clear tendency of the average fibre length to be inversely dependent to the stirring rate.

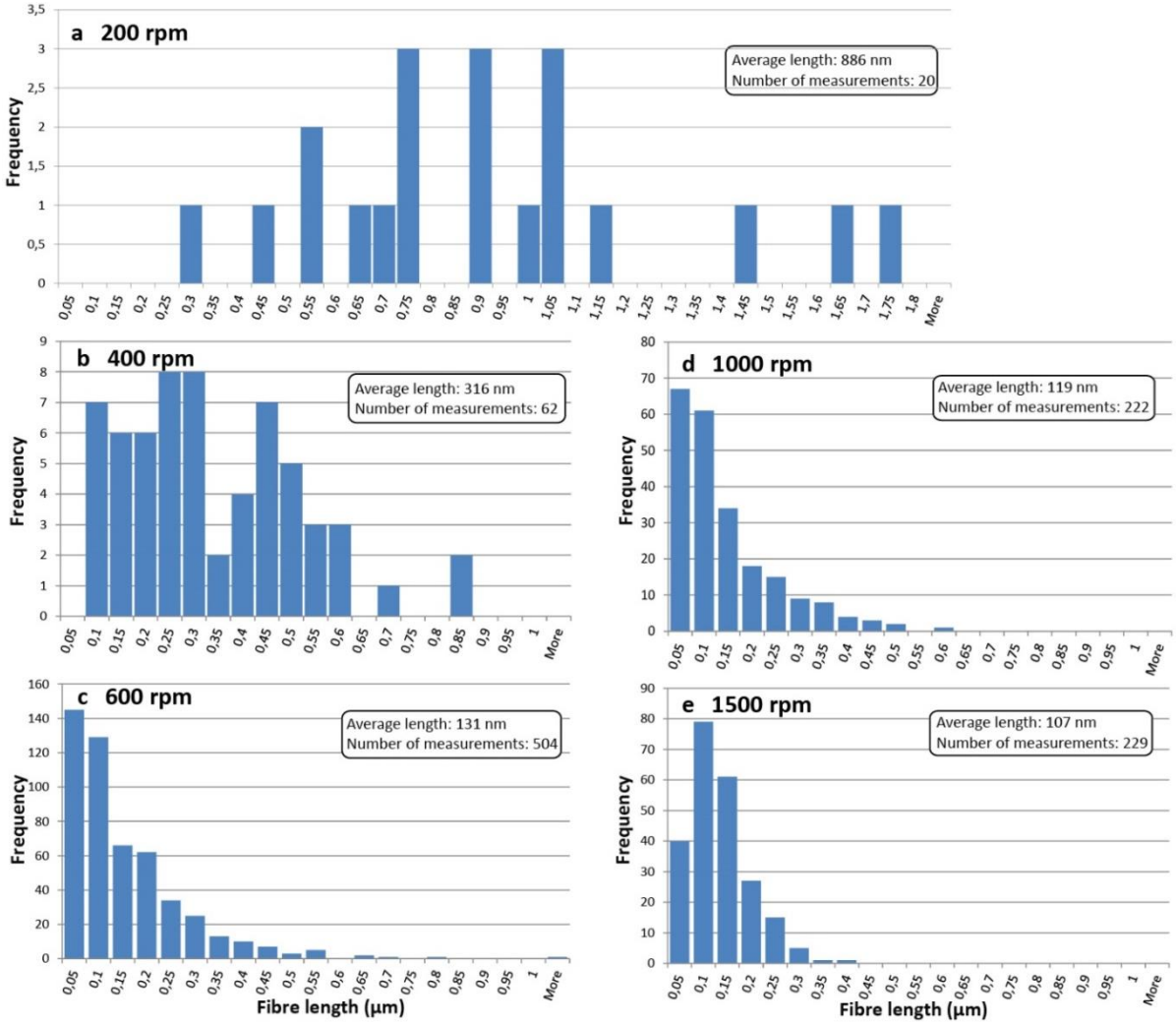

Figure III.5. Fibre length distributions in fully oxidized libraries made of $\mathbf{3}_6$ stirred at rates of **a**: 200 rpm, **b**: 400 rpm, **c**: 600 rpm, **d**: 1000 rpm and **e**: 1500 rpm.

The fibre length distribution is at first broad, and despite a small number of measurements at 200 rpm, due to aggregation making measurements of isolated fibres difficult, long fibres up to 1.8 µm are observed.

For libraries exposed to higher stirring rates, from 600 rpm in the present case, the distribution tends to become narrower and goes towards shorter fibre lengths, with a range staying relatively narrow in the case of a sample stirred at 1500 rpm.

Interestingly, in the case of the sample stirred at 400 rpm, it can be observed that, for shorter lengths, the distribution is relatively flat, but suddenly drops at a value of 0.35 µm, and increases again, before decreasing when reaching higher values. These observations suggest a bimodal distribution. Similar behaviour can be observed in Figure III.2.b, for peptide **1** stirred at 600 rpm.

The TEM micrographs from the libraries made at different stirring rates using peptide **3**, depicted in **Figure III.6.**, give some interesting insights into the morphology and interactions between the fibres. Indeed, aggregation can be observed for the libraries stirred at 200 rpm, and 400 rpm, which is not observed for the other stirring rates. This may be due to the fact that when having longer lengths, interactions between the fibres are strong enough to keep them together, providing a stronger resistance to breakage, which may be one of the reasons for their longer average length.

Interestingly, the fibres observed here are single ones which are not twisted, compared to what could be observed in the libraries made from peptide **1**. Although it is hard to account for those differences in morphologies, the number of peptide building blocks incorporated in macrocycles forming the replicating species, which is six in the present case, and was eight in the case of the peptide building block **1**, may influence the interactions between the peptide chains of two fibres in the vicinity of each other, leading to twisted bundles in one case, and single straight fibres in another.

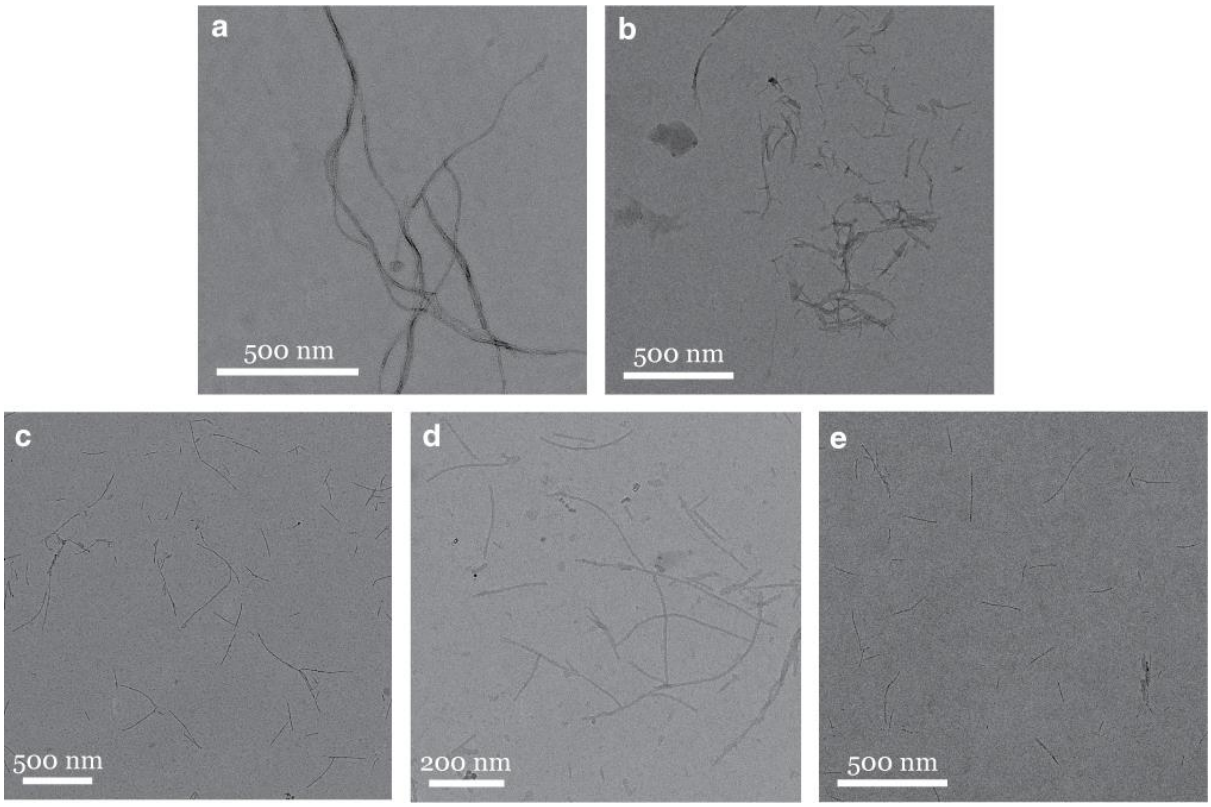

Figure III.6. TEM images of libraries made of $\mathbf{3}_6$ at stirred at rates of **a**: 200 rpm, **b**: 400 rpm, **c**: 600 rpm, **d**: 1000 rpm and **e**: 1500 rpm

III.3.c. XGLKFK

In order to further investigate the role of the peptide sequence on the fibre breakage, the influence of the stirring rate on fibre breakage was performed with peptide building block **2**, which gives rise to the self-replicating macrocyclic hexamers $\mathbf{2}_6$. These replicators have the same size as peptide **3**, , but have a different peptide chain hydrophobicity.

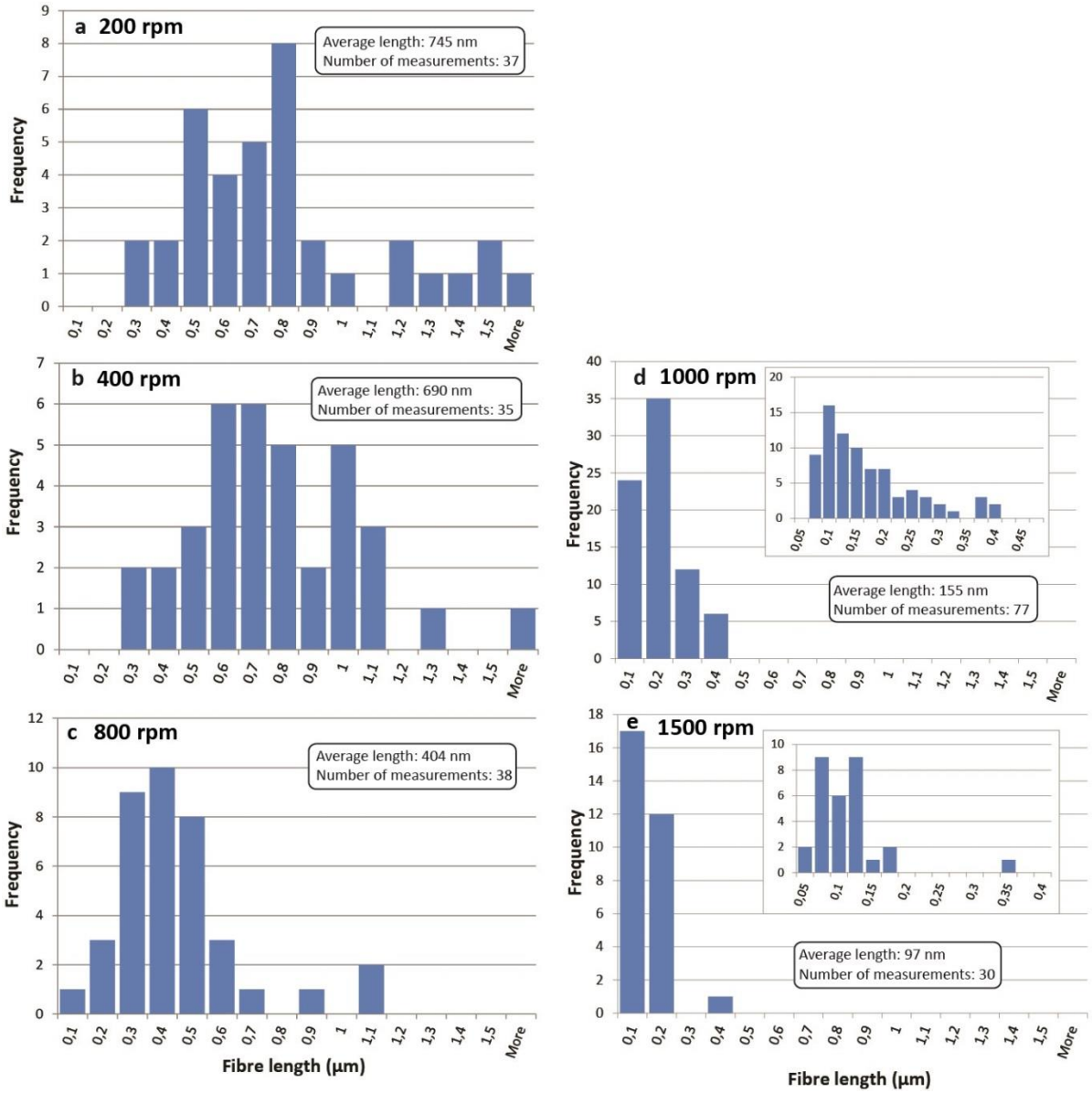

Figure III.7. Fibre length distributions in fully oxidized libraries made of $\mathbf{2}_6$ stirred at rates of **a**: 200 rpm, **b**: 400 rpm, **c**: 800 rpm, **d**: 1000 rpm and **e**: 1500 rpm.

The results of these experiments, presented **Figure III.7.**, share some similarities with the observations made from peptide **1** and **3**, in that there is a clear tendency of the average fibre length to be inversely dependent on the stirring rate.

Moreover, it can be observed that the library stirred at 200 rpm (**Figure III.7.a**) has a really broad fibre length distribution, ranging from short fibres of 260 nm long to long ones, being up to 1.7 µm long.

The sample, which was stirred at 400 rpm (**Figure III.7.b**), shows signs of a bimodal distribution, with a minimum around 900 nm, although given the small sample size this observation is probably not statistically significant. In contrast, the fibre length distribution of the library stirred at 800 rpm (**Figure III.7.c**), which distribution follows the shape of a Gaussian curve, with a maximum peak in fibre lengths at 400 nm. Although the average fibre length of the sample stirred at 1000 rpm (**Figure III.7.d**) is smaller than for the lower stirring rates, its distribution has a long tail, much longer than the one observed at 1500 rpm (**Figure III.7.e**). This library has a narrow length distribution.

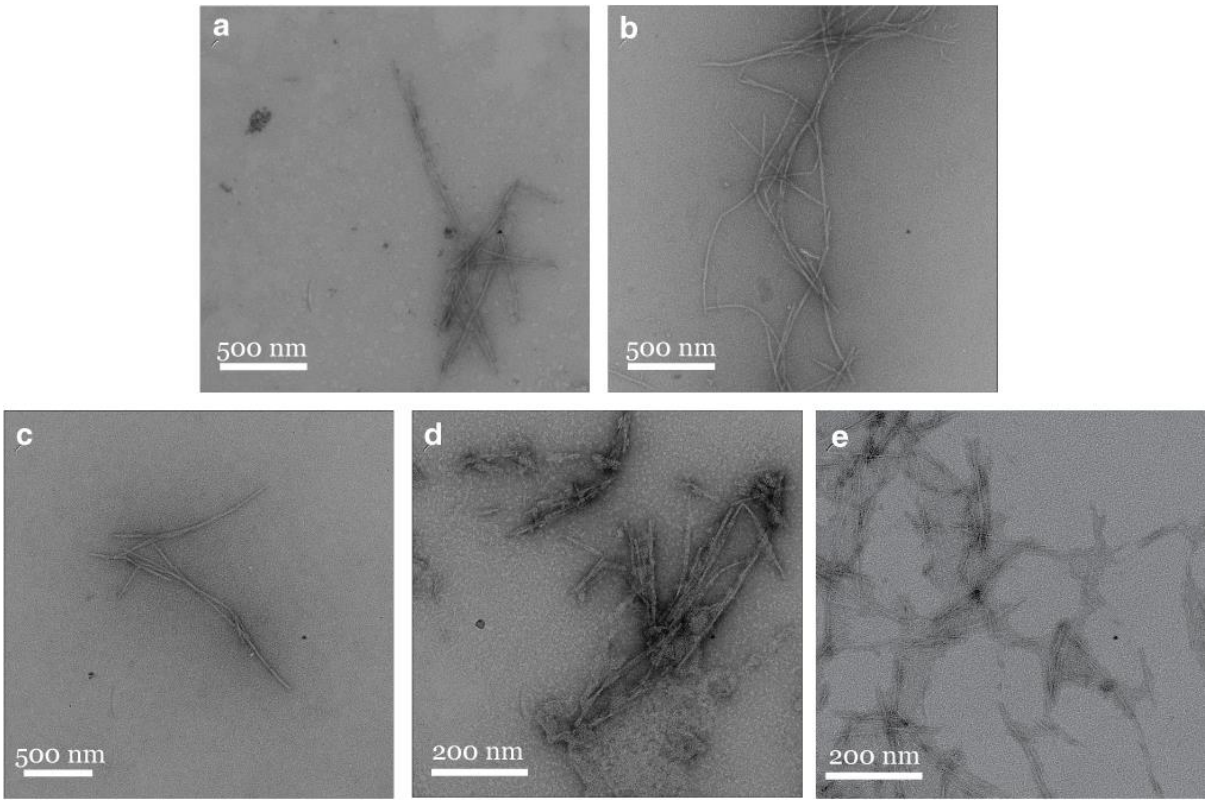

Figure III.8. TEM images of libraries made of $\mathbf{2}_6$ at stirred at rates of **a**: 200 rpm, **b**: 400 rpm, **c**: 800 rpm, **d**: 1000 rpm and **e**: 1500 rpm

The TEM micrographs from the libraries, presented in Figure III.8., give some interesting insights into the nature of the fibres present in the stirred libraries. It can qualitatively be observed that the fibres are long at high stirring rates, and get shorter with increased stirring rate, which is in accordance with the observations made from the histograms of the fibre length distributions discussed in the previous paragraph. Moreover, the fibres tend to aggregate, limiting the number of length measurements that could be performed. Although they tend to aggregate, no bundling of fibres can be formally observed, and the fibres are quite straight, and do not appear to twist, as was observed earlier with peptide **1**.

III.4. Fibre length averages and polydispersity index.

In order to determine at which stirring rate, and for which sequences the replication process was optimal, an average fibre length was determined for each library of the samples described above.
This parameter plays an important role in the replication process, since the average fibre length determines the concentration of fibres ends, and, as discussed in the previous chapter of this thesis, the fibre end concentration is a parameter that may influence the rate of growth of the fibres, since fibres are growing from the fibre ends.
It is important to notice that the avergage fibre length is here the relevant parameter, and not the fibre length distribution, which does not play a role in the replication process since the number of fibre ends, at a given average fibre lengh and a given amount of replicator, is independent of the fibre length distribution. This statement follows directly from the definition of the average fibre

length which equals the sum of the lengths of all fibres divided by the number of fibres. The first term is constant and determined by the replicator concentration (assuming all replicator to be incorporated into the fibres) while the second term equals half the number of fibre ends.
The average lengths were plotted in function of the stirring rate for the different peptide building blocks studied. The results are displayed in Figure III.9.

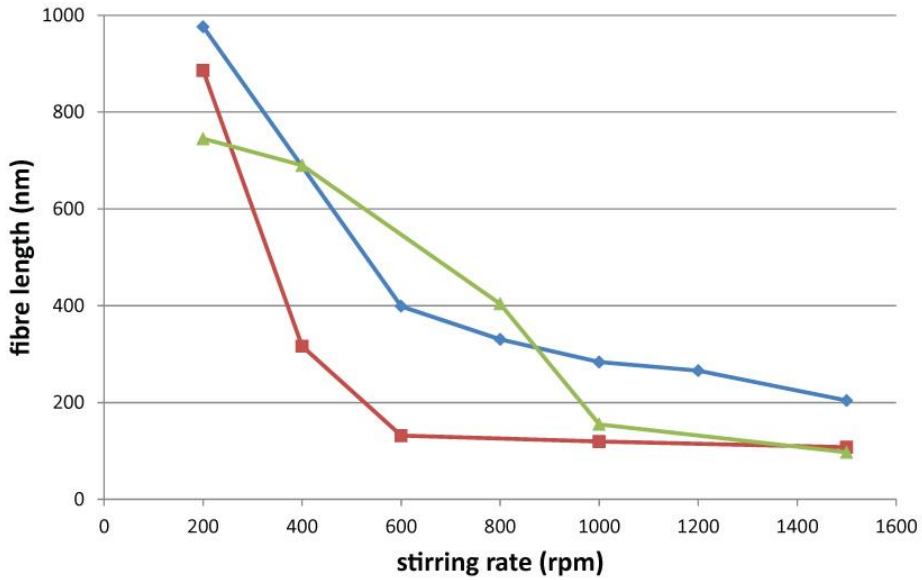

Figure III.9. Fibre length average in function of the stirring rate for **1** (blue diamonds), **2** (green triangles), and **3** (red squares).

As seen from fibre length distributions discussed earlier, shorter average fibre lengths are observed at higher stirring rate, for each of the sequences studied.
The fibre length averages are decreasing quickly at first, but stabilize at higher stirring rates, reaching a plateau. This observation is particularly clear in the case of peptide **3**.

Moreover, peptides **2** and **3** are both reaching a minimal average fibre length close to 100 nm at 1500 rpm (97 nm in the case of **2**, and 107 nm in the case of **3**), while the peptide sequence **1** has an average fibre length of 203 nm at the same stirring rate. This observation suggests that the fibres made from peptide **2** are more resistant to high stirring rates. The replicating species coming from peptide **1** is the octamer $\mathbf{1}_8$, whereas the replicating species of peptides **2** and **3** are the hexamers $\mathbf{2}_6$ and $\mathbf{3}_6$. Although the individual interactions of the peptide chain of building block **1** are weaker than the ones of **2** and **3**, leading this building block to form fibres made from octameric rings $\mathbf{1}_8$ when the two other species make fibres made of hexameric rings $\mathbf{2}_6$ and $\mathbf{3}_6$, it may be that the sum of the interactions from the side chains of $\mathbf{1}_8$ gives an overall more stable octamer than hexamers of $\mathbf{2}_6$ and $\mathbf{3}_6$. This would explain the longer average fibre length observed at high stirring rates.
Another theory to explain this observation is that fibres formed from $\mathbf{1}_8$ are forming bundles of two fibres. This association may give rise to a stronger resistance to shear stress.

All these observations suggest that, since at higher rates the fibres are shorter, and therefore the concentration of fibre ends is higher, the replication should be more efficient under those

conditions, when a library is stirred above 1000 rpm. Moreover building block **1** should potentially give less efficient replication due to its lower concentration of fibre ends compared to the ones of the other peptides studied at high stirring rate.

The polydispersity indexes (PDI) of the different libraries were calculated (see part III.6.g) and compared. The results, depicted in Figure III.10, show that the PDI profiles vary depending on the peptide sequences. While the PDI of peptide **1** and **3** are moderately affected, varying between 1.18 and 1.44 for peptide **1** and between 1.15 and 1.59 for peptide **3**, peptide **2** undergoes a significant decrease of PDI at stronger stirring rates. These observations suggest that fibres made from peptide **2** have a distribution narrowing down with the stirring rate, as it could be observed on the histograms resulting from this library (Figure III.7). These results suggest that fibres made from **2** follow a different breaking process than the two other sequences studied. This difference may be related to differences in the fibres morphology of this building block.

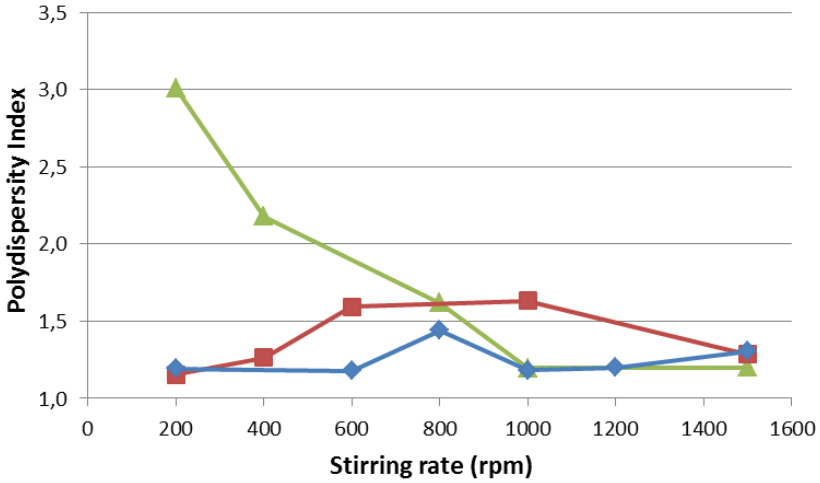

Figure III.10. Polydispersity index depending on the stirring rate for fibres made from $\mathbf{1}_8$ (blue diamonds), $\mathbf{2}_6$ (green triangles), and $\mathbf{3}_6$ (red squares).

III.5. Conclusions

The influence of the shear stress applied to the system by stirring at different stirring rates was investigated for three peptide building blocks differing in their sequence.
It was observed that libraries stirred at high stirring rates have an average fibre length shorter than the ones stirred at lower rates.
Some of the libraries are showing hints of a bimodal distribution, which may mean that the fibre breakage follows in certain cases a precise mechanism and pathway.
The observation of TEM micrographs shows that breakage does not appear to affect fibre morphology, but that fibres do not readily break further, since upon strong shearing, the fibres reach a minimum length. However, fibre length seems to influence aggregation, as longer fibres tend to aggregate more.

Some of them have a higher minimum length than others. The former may therefore be less efficient replicators. Peptide **3** forms twisted bundles, when fibres from other peptide sequences do not.

Unfortunately the stress applied to the system by stirring is not homogenous, and a method allowing to further the control of the fibre breakage will be introduced in the following chapter.

Further investigations with experiments to determinate the replication rate of these peptides depending on the fibre length averages of different peptide libraries may lead to some interesting insights. A competition scenario between libraries composed of several peptide sequences could give to some further understanding on their behaviour in a context comparable to prebiotic conditions. The peptide building blocks used for this study represent good candidates for such investigations, and could put in evidence the role of shear stress in evolution.

III.6. Experimental Section

III.6.a. Materials and methods

Peptide building blocks **1**, **2**, and **3** were synthesized by Cambridge Peptides Ltd (Birmingham, UK) from 3,5-bis(tritylthio)benzoic acid, which was prepared via a previously reported procedure.[12] Doubly distilled water, boron oxide and potassium hydroxide utilized for the preparation of buffers were obtained from in-house double distillation facilities, Aldrich and Merck Chemicals, respectively. Sodium perborate used for the oxidation of the libraries was purchased from Sigma Aldrich. UPLC solvents acetonitrile (ULC/MS grade), water (ULC/MS grade) and HPLC acetonitrile (LC grade) were obtained from Biosolve BV. HPLC doubly distilled water was obtained from in-house double distillation facilities. Trifluoroacetic acid was purchased from Aldrich. Libraries were prepared in clear HPLC glass vials (12 × 32 mm) closed with Teflon-lined snap caps purchased from Jaytee. Magnetic stir bars used to stir the libraries were Teflon coated (2 × 2 × 5 mm) and obtained from VWR. Samples were stirred on IKA RCT basic magnetic stirrers.

III.6.b. UPLC analysis

UPLC analyses were performed on a Waters Acquity UPLC I-class system equipped with a PDA detector. All analyses were performed using a reversed-phase UPLC column (Aeris Widepore 3.6 μm XB-C18 150 × 2.10 mm, purchased from Phenomenex). UV absorbance was monitored at 254 nm. Column temperature was kept at 35 °C.
For the kinetics of growth depending on the stirring rate of peptide **2**, the following method was used:

Injection volume: 5 μL of a 3.8 mM library subjected to a 1:50 dilution in a solution of 0.6 v% of trifluoroacetic acid in doubly distilled water.
Eluent flow: 0.3 mL/min.
Eluent A: UPLC grade water (0.1 v% trifluoroacetic acid)
Eluent B: UPLC grade acetonitrile (0.1 v% trifluoroacetic acid)

Method:

time (min)	%A	%B
0,0	90,0	10,0
1,0	90,0	10,0
1,3	75,0	25,0
3,0	72,0	28,0
11,0	69,0	31,0
11,5	5,0	95,0
12,0	5,0	95,0
12,5	90,0	10,0
15,0	90,0	10,0

III.6.c. HPLC analysis

HPLC analyses were performed on a HP 1050 system equipped with a PDA detector. All analyses were performed using a reversed-phase HPLC column (Phenylhexyl C18 column 4.6 × 75 mm, 3 µm, purchased from Phenomenex). UV absorbance was monitored at 254 nm. Column temperature was kept at 35 °C.
For the kinetics of growth depending on the stirring rate of peptide **1** and **3**, the following method was used:

Injection volume: 5 µL of a 3.8 mM library subjected to a 1:50 dilution in a solution of 0.6 v% of trifluoroacetic acid in doubly distilled water.
Eluent flow: 0.8 mL/min.
Eluent A: Doubly distilled water (0.1 v% trifluoroacetic acid)
Eluent B: Acetonitrile (0.1 v% trifluoroacetic acid)
Method for peptide **1**:

time (min)	%A	%B
0	81,0	9,0
40	74,0	26,0

Method for peptide **3**:

time (min)	%A	%B
0	75,0	25,0
60	60,0	40,0

III.6.d. Negative staining TEM measurements

An aliquot of a sample taken from a peptide library was diluted 40 times in doubly distilled water. Shortly thereafter, a small drop of the diluted sample was deposited on a 400 mesh copper grid covered with a thin carbon film. After 30 seconds, the droplet was blotted on filter paper. The sample was then stained with a solution of uranyl acetate deposited on the grid and blotted on filter paper after 30 seconds. The staining process was repeated in order to have an enhanced contrast. The grids were observed in a Philips CM12 electron microscope operating at 120 kV. Images were

recorded on a slow scan CCD camera. During the measurements, a relatively strong defocus, around - 2500 nm, was applied in order to enhance the contrast on the micrographs and facilitate the length measurements.

III.6.e. Fibre length measurements

TEM micrographs were analysed using imageJ. A scale was set on each micrograph according to its magnification, and an average length of each sample was determined by measuring fibres from the micrograph, using the measuring tool of ImageJ. The data was then transferred in MS Excel, and analysed.

III.6.f. Determination of the fibre thickness for peptide **1**

The average fibre thickness of peptide **1** was obtained from a series of 200 measurements done on a micrograph from a library composed of $\mathbf{1}_8$ stirred at 800 rpm, using ImageJ, and treating the data statistically with MS Excel. A histogram representing the distribution of the measurements is depicted in **Figure III.11**.

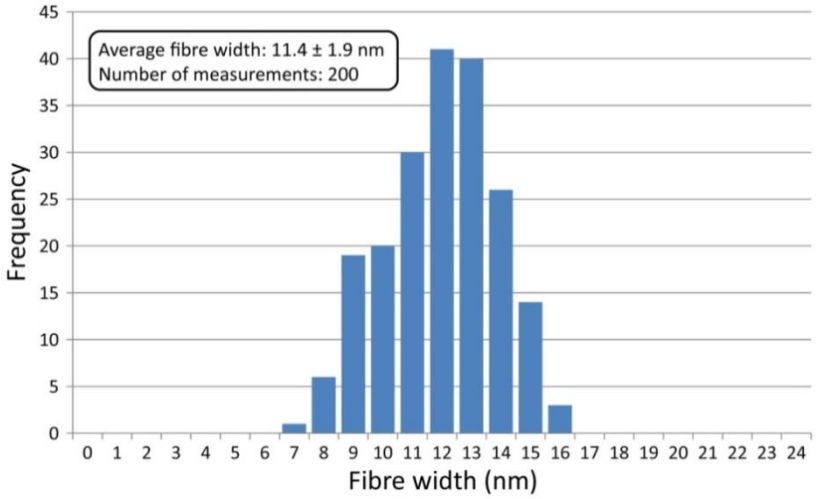

Figure III.11. Average fibre width measured from a micrograph (presented in **Figure III.4**) of a library made of $\mathbf{1}_8$ stirred at 800 rpm.

The average twist step of peptide **1** was obtained from measuring fibre lengths of a library composed of $\mathbf{1}_8$ stirred at 800 rpm, using ImageJ, and treating the data statistically with MS Excel. The results of these measurements are depicted in **Table III.2**.

Input	Measured fibre length (nm)	number of twists	length of one twist (nm)
1	421	5	84,2
2	614	7	87,7
3	973	11	88,5
4	316	4	79,0
5	248	3	82,7
6	420	5	84,0
7	473	6	78,8
8	84	1	84,0
9	176	2	88,0
10	561	7	80,1
11	408	5	81,6
12	82	1	82,0
13	342	4	85,5
14	252	3	84,2
15	235	3	78,3
16	169	2	84,7
17	591	7	84,4
18	268	3	89,4
19	346	4	86,6
20	169	2	84,5

Average twist length (nm)	**83,9**
Standard deviation (nm)	**3,2**

Table III.2. Average twist length measured from a micrograph (presented in **Figure III.4**) of a library dominated by $\mathbf{1}_8$ stirred at 800 rpm.

III.6.g. Calculation of the Polydispersity index

The number average length L_n and weight average length L_w were calculated using respectively equations (1) and (2), where n is the number of measurements for each sample, N_i the number of fibres of length L_i.

$$L_n = \frac{\sum_{i=1}^{n} N_i L_i}{\sum_{i=1}^{n} N_i} \quad (1)$$

$$L_W = \frac{\sum_{i=1}^{n} N_i L_i^2}{\sum_{i=1}^{n} N_i L_i} \quad (2)$$

The polydispersity index of each sample is characterized by the ratio L_w/L_n.

III.7. Acknowledgements

Morteza Malakoutikhah is acknowledged for the preparation of libraries involving peptides **1** and **3** and their HPLC monitoring presented in Figure III.1.a and III.1.c.

III.8. References

[1] K. Soai, T. Shibata, H. Morioka, K. Choji, *Nature*, **1995**, 378-767.

[2] K. Soai, T. Kawasaki, *Top. Curr. Chem*., **2008**, 284, 1-33.

[3] H. Nishino, A. Kosaka, G. A. Hembury, F. Aoki, K. Miyauchi, H. Shitomi, H. Onuki, Y. Inoue, *J. Am. Chem. Soc.,* **2002**, 124, 11618-11627.

[4] (a) R. Pascal, L. Boiteau, *Wiley Encyclopedia of Chemical Biology*, **2009**, Vol. 3, 510-516; (b) R. Pascal, L. Boiteau, A. Commeyras, *Top Curr Chem*, **2005**, 259, 69-122 ; (c) I.G. Draganic, Z.D. Draganic, M.J. Shushtarian, *Radiation Research*, **1976**, 66, 54-65; (d) T. Takano, J.-I.Takahashi, T. Kaneko, K. Marumo, Katsumi, K. Kobayashi, *Earth and Planetary Science Letters*, **2007**, 254, 106-114.

[5] N.N. Nair, E. Schreiner, D, Marx, *J. Am. Chem. Soc.,* **2008**, *130*, 14148-14160.

[6] M. Paecht-Horowitz, Mella, K. Matsuno, K. Dose, K. Harada, *Mol. Evol. Protobiol.*, **1984**, 189-206.

[7] M. Ruiz-Bermejo, C. Menor-Salván, S. Osuna-Esteban, S. Veintemillas-Verdaguer, *Orig Life Evol Biosph*, **2007**, 37, 123-142.

[8] F. de Souza-Barros, A. Vieyra, *Comparative Biochemistry and Physiology, Part C*, **2007**, 146, 10-21.

[9] J. M. Ribo, J. Crusats, F. Sagues, J. Claret, R. Rubires, *Science*, **2001**, 292, 2063-2066.

[10] O. Arteaga, A. Canillas, J. Crusats, Z. El-Hachemi, J. Llorens, E. Sacristan, J. M. Ribo, *Chemphyschem*, **2010**, 11(16), 3511-3516.

[11] (a) P. J. Flory, *Statistical Mechanics of Chain Molecules, Interscience Publishers in New York*¸ **1969**; (b) J. G. Williams, Polym. *Eng. & Sci*., **1977**, 17 (3), 144-149; (c) B. Audoly, S. Neukirch, *Phys. Rev. Lett*., **2005**, 95 (9), 095505; (d) M. Shioya, A. Takaku, *Comp. Sci. and Tech*., **1995**, 55(1), 33-39; (e) F.G. Torres , M.L. Cubillas, *Polym. Test*., **2005**, 24 (6), 694-698.

[12] (a) H. D. Wagner, O. Lourie, Y. Feldman, R. Tenne, *Appl. Phys. Lett*., **1998**, 72, 188-190; (b) H. Qian, A. Bismarck, E. S. Greenhalgh, M. S.P. Shaffer, *Composites: Part A*, **2010**, 41, 1107-1114; (c) N. Melanitis, C. Galiotis, P.L. Tetlow, C.K.L. Davies, *J. of Comp. Mat*., **1992**, 26 (4), 574-610.

[13] (a) D. E. Dunstan, P. Hamilton-Brown, P. Asimakis, W. Ducker, J, Bertolini, *Protein Engineering Design & Selection*, **2009**, 22, 741–746; (b) J. E. Gillam, C. E. MacPhee, *J. Phys.: Condens. Matter*, **2013**, 25, 373101; (c) A. Buttstedt, T. Wostradowski, C. Ihling, G. Hause, A. Sinz, E. Schwarz, *Amyloid*, **2013**, 20(2), 86-92; (d) A.T. Petkova, R. D. Leapman, Z. Guo,W.-M. Yau, M. P. Mattson, R. Tycko, *Science*, **2005**, 307, 262-265; (e) C. L. Teoh, I. B. Bekard, P. Asimakis, M. D. W. Griffin, T. M. Ryan, D. E. Dunstan, G.J. Howlett, *Biochemistry*, **2011**, 50, 4046-4057; (f) M. Reches, E. Gazit, *Science*, 2003, 300, 625-627; (g) T. P. J. Knowles , M. J. Buehler, *Nature Nanotechnology*, **2011**, 6, 469-479;

[14] J. F. Smith, T. P. J. Knowles, C. M. Dobson , C. E. MacPhee, M. E. Welland, *PNAS*, **2006**, 103 (43), 15806-15811.

[15] W. F. Xue, A. L. Hellewell, E. W. Hewitt, S. E. Radford, *Prion*, **2010**, 4 (1), 20-25.

[16] J.M.A. Carnall, C.A. Waudby, A.M. Belenguer, M.C.A. Stuart, J.J.-P. Peyralans, S. Otto, *Science*, **2010**, 327, 1502-1506.

[17] M. Malakoutikhah, J. J-P. Peyralans, M. Colomb-Delsuc, H. Fanlo-Virgos, M.C.A. Stuart, S. Otto, *J. Am. Chem. Soc.,* **2013**, *135*, 18406-18417.

[18] O. D. Monera, T. J. Sereda, N. E. Zhou, C. M. Kay, R. S. Hodges, *J. Pept. Sci.*, **1995**, 1, 319-329.

Chapter IV
Control over fibre breakage using a rheological device

The breakage of fibres formed by self-replication in dynamic combinatorial libraries formed from different peptide building blocks is controlled through a device designed in our group, and the resulting fibre morphology and length are evaluated depending on the peptide sequence and the shear stress applied to the system.

IV.1. Introduction

The importance of controlling the shear stress in the peptide system developed in our group has been made clear in Chapter II of this Thesis, and studied further in Chapter III, in which it was demonstrated that, depending on the stress applied to the system through variations in the rate of stirring, a clear influence could be observed on the kinetics of replication, and the length of the assembled fibres resulting from the self-assembly of the system[1]. However, in the experiments discussed earlier, the stress applied to the system was induced by stirring the libraries with a stirring bar placed in a vial. Although this method allows an efficient breaking of the fibres present in the media, the shear stress is not homogeneous in the solution, since the shearing in the vicinity of the stirring bar is stronger than at other locations in the vial.

Moreover, the obtained results are solely qualitative, and a method allowing to estimate the energies involved in the fibre breaking process would be valuable to further the understanding of the system and get further insights into the process of fibre breakage.

For this reason, the stress applied to the system should be quantified, through rheological measurements. Among the several rheological methods and instruments existing to evaluate the stress induced by a flowing system[2,3], we chose to work with a device allowing to work in a closed system, capable of creating a Couette flow[4], referred to as a Couette cell, in which the shear applied can be controlled, having within certain experimental conditions a homogeneous stress applied to the whole sample. This apparatus, introduced as a rheometer by the physicist Maurice Couette in the late 19th century[5,6,7], has been widely used in fluidic mechanics, but also more recently in a biological context[8], and in the study of the behaviour silk fibrils formed from β-sheet interactions[9], and represents for this reason a tool of choice for the study of our system. It is composed of a cylinder fitting into a cell with a thin gap between both, in which the solution to be sheared is placed. A general overview of the principle of a Couette cell is given in Scheme IV.1.

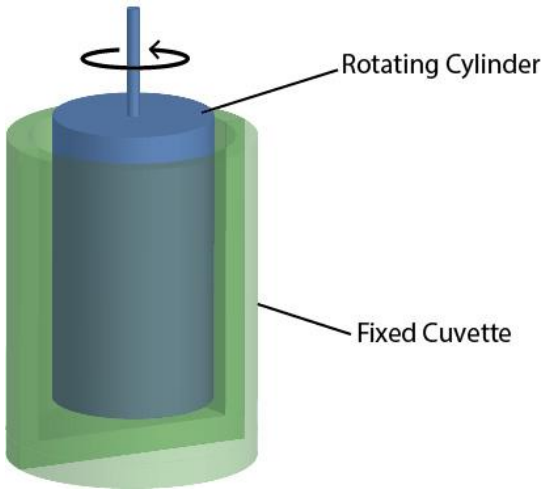

***Scheme IV.1**. General representation of a Couette cell.*

Upon an external input, the cylinder rotates, creating shear forces that are transmitted to the solution present in the cuvette. Regulating the speed of rotation of the cylinder allows control over the shear stress experienced by the sample.

IV.2. Design of the Couette Cell

The goal of the following study is to find an experimental approach to quantify the shear stress applied to dynamic combinatorial libraries containing fibres, in order to assess at which stress the fibre breakage is effective, and what the resulting fibre length averages are depending on the stress applied. In order to reach this goal, a Couette cell was designed according to previously described designs in different contexts[10,11,12].

Some rough estimation of the shear rates applied to the system in a library placed in a vial stirred with a small stirring bar, and in a library shaken on a rotating shaking plate have been reported earlier by our group[13]. It was estimated that a stirred sample undergoes a shear stress of about 300 $N.m^{-2}$, while a shaken sample undergoes a stress of approximately 2 $N.m^{-2}$.

The design of the Couette cell should therefore take in account those parameters, and a Couette cell was designed in a way to be able to provide shear stresses higher than those values.

The shear stress applied to a system placed in a Couette cell can be estimated through equation (1)[14]:

$$\tau = \gamma \times \mu \quad (1)$$

In which τ, expressed in $N.m^{-2}$, represents the shear stress of the system, γ the flow velocity (in s^{-1}), and μ is the dynamic viscosity of the solution (in Pa.s, or $kg.m^{-1}.s^{-1}$). In our case, the value of the viscosity of the system is considered to be the same as the one of water (1.002 Pa.s at 20 ^{o}C), since in the studied cases, the fibres formed in the libraries do not show any evidence of hydrogel formation, and no significant increase in the viscosity of the solution upon fibre formation was noticed.

The flow velocity γ depends on the distance between the liquid and the rotating cylinder. Its two extreme values, on the wall of the outer cylinder γ_o and on the wall of the inner cylinder γ_i are expressed respectively by equations (2) and (3):

$$\gamma_i = \frac{2\Omega r_i^2}{(r_o^2 - r_i^2)} \quad (2)$$

$$\gamma_o = \frac{2\Omega r_o^2}{(r_o^2 - r_i^2)} \quad (3)$$

Where r_o represents the outer radius (in m), r_i the inner radius (in m), and Ω is the angular velocity of the cylinder (in $rad.s^{-1}$). It can be expressed by equation (4), in which f represents the frequency of the rotation (in s^{-1}, or Hz).

$$\Omega = 2\pi f \quad (4)$$

Equations (2) and (3) can therefore be rewritten as two new equations, respectively (5) and (6):

$$\gamma_i = \frac{4\pi f r_i^2}{(r_o^2 - r_i^2)} \quad (5)$$

$$\gamma_o = \frac{4\pi f r_o^2}{(r_o^2 - r_i^2)} \quad (6)$$

Combining equations (5) and (6) with equation (1) leads to equations (7) and (8):

$$\tau_i = \frac{4\pi f r_i^2}{(r_o^2 - r_i^2)} \times \mu \quad (7)$$

$$\tau_o = \frac{4\pi f r_o^2}{(r_o^2 - r_i^2)} \times \mu \quad (8)$$

In which τ_i represents the shear stress applied to the system at the inner wall of the cell, and $\tau_o$the shear stress at the outer part of the cell, both expressed in N.m^{-2}.

In a Couette cell where the gap between the inner and outer walls is small, i.e. $r_0 - r_i \ll 1$, the difference in shear stress between the inner and outer wall can be neglected for practical purposes[17]. For this reason, the gap between the static cuvette and the rotating cylinder from the Couette cell was designed to be of 250 µm, the cuvette having a diameter of 40.00 mm and the diameter of the cylinder being of 39.50 mm.
Those parameters being constant, as well as the dynamic viscosity µ, the average shear rate $\tau = (\tau_i + \tau_0)/2$, experienced by peptide fibres placed in the Couette cell can therefore be estimated according to equations (7) and (8), and is proportional (within a certain frequency range) to the frequency of rotation of the cylinder.

For this study, the samples were sheared at frequencies ranging from 3.33 Hz to 83.33 Hz, corresponding to shear rates comprised between 1.6 x 10^3 N.m^{-2} and 41,6 x 10^3 N.m^{-2}.
These relatively high shear rates ensures a strong shearing of the fibres. Indeed, above certain shearing rates, the flow in the Couette cell is not laminar anymore, and tends to undergo Taylor-Couette instabilities and become turbulent.

The Taylor number, *Ta*, is a dimensionless value introduced by G. Taylor[15] in order to assess the state of the flow in a system. Above a certain threshold (Ta_{crit} ≈ 1700), Taylor instabilities are occurring in the system. *Ta* can be evaluated with equation (9)[16]:

$$Ta = \frac{\Omega^2 r \Delta r^3}{v^2} \quad (9)$$

In which Ω is the angular velocity, r the average radius, Δr the gap between the inner and the outer cylinder, and v the kinematic viscosity (1.004 x 10^{-6} $m^2.s^{-1}$ in the present case).

With the rotating frequencies used in the present study, $Ta > Ta_{crit}$ (for the values see Table IV.3 in the experimental section). The flow in the Couette cell under these conditions is turbulent, preventing direct quantification of shear stress.

The ideal material from which the Couette cell was made was then chosen. Due to the small distance between the inner and outer walls of the device, and the relatively high speeds, metals are preferred over plastics, due to their resistance to deformations. Glass or quartz were not used because of their potential fragility.

Among metals, several were tried under library conditions, in order to be certain that they will not be interacting with the libraries. In order to test this, a library prepared from peptide **1** (see Scheme IV.3) was divided into 5 samples, in which a piece of metal was placed. The libraries were stirred at 1200 rpm, and the evolution of their absorbance was monitored by UV-vis. λ_{max} was determined to be 412 nm. The absorbance at λ_{max} was monitored for the different libraries, and the resulting plot is shown in Figure IV.1.

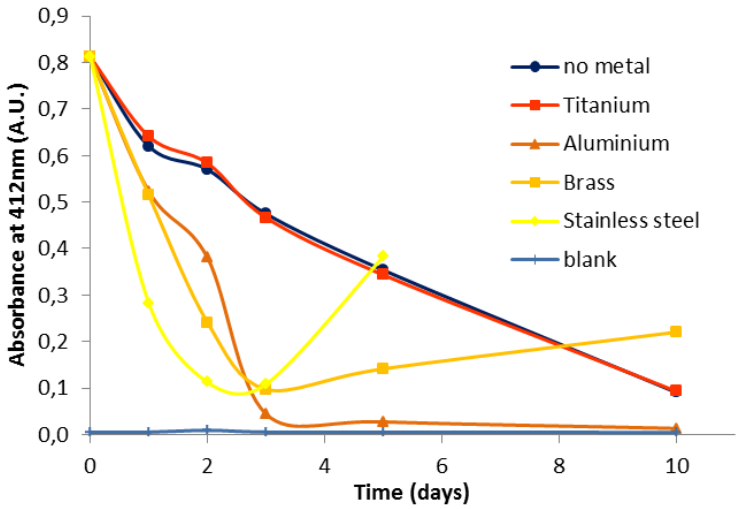

Figure IV.1. *Evolution with time of the UV absorbance measured at 412 nm for different libraries exposed to different metals.*

Titanium has the least interaction with the library, since the changes in UV absorbance in the presence of this material follow that of the library in which no metal was placed. The other metals tested proved to interact with the libraries. In the case of stainless steel and brass, the library started to become cloudy after some days, which explains the increase in absorbance in the case of stainless steel.

Therefore, titanium was chosen as a material of choice for constructing the Couette cell, due to its inert behaviour towards the library.

The different specifications of the Couette cell were then discussed together with Elio Mattia and the workshop from the University of Groningen. The rotation of the cylinder is induced by an electric motor, connected to it with a belt to reduce the vibrations. The motor itself is connected to a computer, and its rotating frequency is controlled and monitored via software developed by the University workshop, with a rotation speed ranging from 0 rpm to 5000 rpm with an increment of 1 rpm. The device was designed and manufactured by the workshop, as depicted in scheme IV.2.

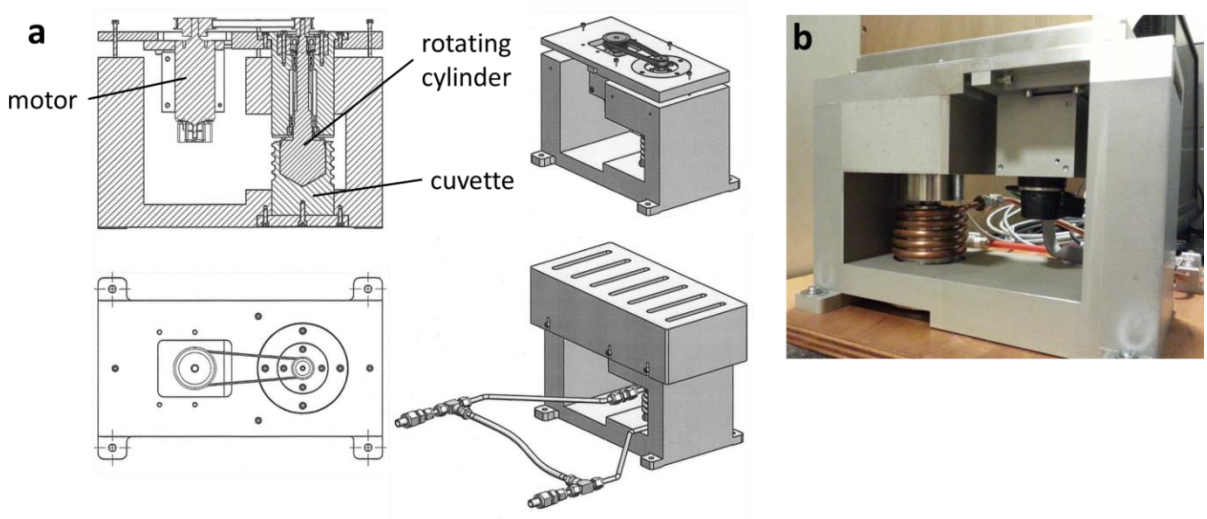

Scheme IV.2*. a: General design of the Couette cell used for the following study, b: Picture of the Couette cell. The copper spiral seen on the design and picture is a cooling system, which has not been actively used in the present study.*

IV.3. Peptide fibres under Couette flow

IV.3.a. Description of the building blocks used in this study

In order to broaden the scope of the study and reach a better understanding of the behaviour of the peptide fibres and test the capacities of the Couette cell, a series of peptide libraries differing in peptide sequence was studied. The building blocks used for this study, displayed in Scheme IV.3, were already studied in a different context by Morteza Malakoutikhah[17,18] under different shearing conditions (non-agitated, shaken on a shaking plate, and stirred with a stir bar at 1200 rpm). These peptide building blocks represent therefore good candidates for the study of the effect of the Couette cell, since their behaviour is already know in other shearing conditions.

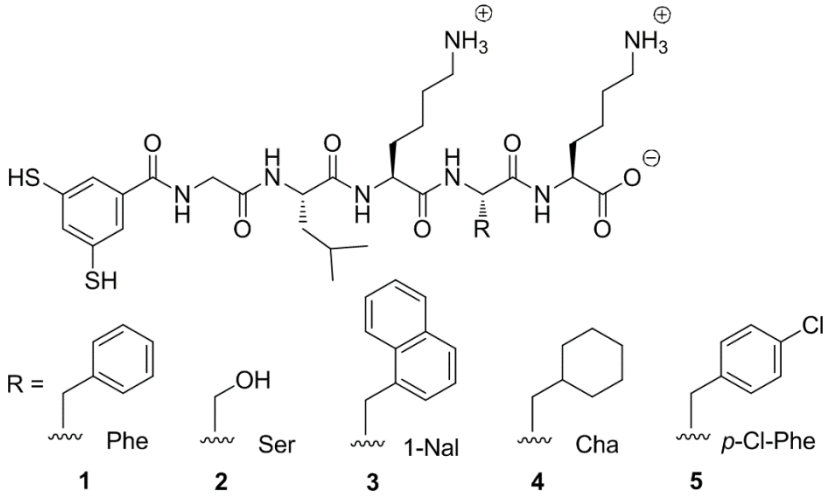

Scheme IV.3. *Different peptide sequences studied*

The building blocks used in this study share the same scaffold, but differ in the second amino acid starting from the C-terminus of the peptide chain. The set includes natural and non-natural amino acids with different hydrophobicities (see Chapter V, table V.1).Libraries made from these building blocks lead to the emergence of replicating species, following the pathway described earlier in this thesis (section II.2), which are able to stack on top of each other, resulting in the formation of fibres[13]. Depending on the sequence, the replicating species are not the same. Indeed, the replicating species emerging from the oxidation of the most hydrophobic peptide building blocks are the hexameric macrocycles, $\mathbf{1}_6$, $\mathbf{4}_6$, and $\mathbf{5}_6$, while octameric macrocycles $\mathbf{2}_8$ are observed in the case of **2**, more hydrophilic than the others[17], and a mixture of trimers $\mathbf{3}_3$ and tetramers $\mathbf{3}_4$ is obtained in the case of **3**, the most hydrophobic peptide used in this study.

IV.3.b. Estimation of fibre breakage

A first series of experiments using the Couette cell was performed on a library made from peptide **1** fully oxidized, at a stage where the sample contains long fibres made from the hexameric $\mathbf{1}_6$ species, whose TEM micrograph is depicted in Figure IV.2.

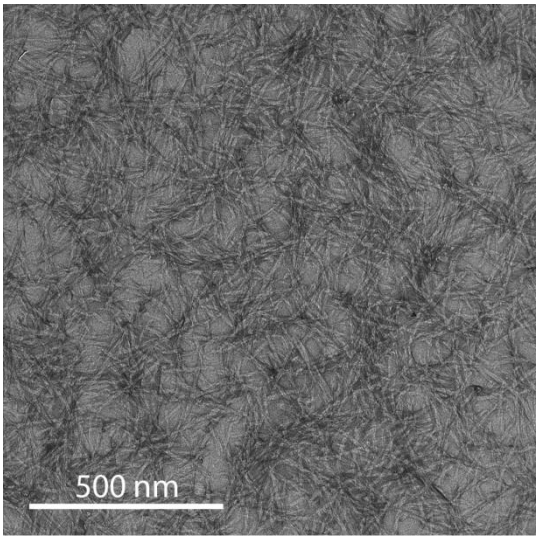

Figure IV.2. *Micrograph of a peptide library made from **1**, before shearing with the Couette cell.*

The high fibre density does not allow a systematic fibre length measurement on this sample, but relatively long fibres, reaching lengths exceeding 1 µm, can be observed.

A first set of experiments done on the library depicted in Figure IV.2 was to assess the efficiency of the shear rate on the fibre breakage. Therefore, the library was sheared at different rates for a total time of 10 min for each experiment, with rotation frequencies of 16.67 Hz, 93.33 Hz and 166.67 Hz. Immediately after shearing, an aliquot of the sheared library was diluted 40 times and deposited on a TEM grid, in order for the fibres to be observed, and for the average fibre length to be determined. The resulting micrographs are presented in Figure IV.3, in which it can be observed that the fibre length distributions and morphologies vary depending on the shear stress applied to the system.

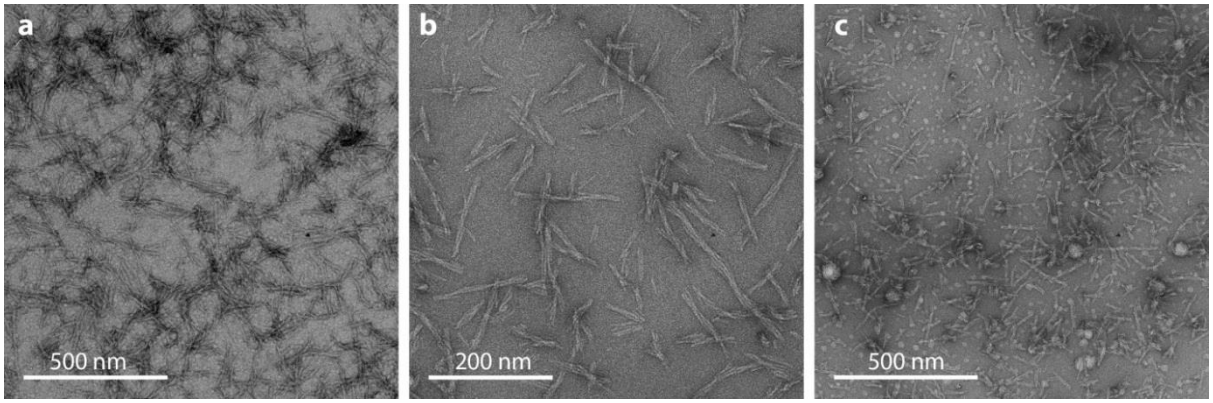

Figure IV.3. *Micrographs of peptide libraries made from **1**, sheared with a Couette cell for 10 min at rates of a: 16.67 Hz, b: 83.33 Hz, c: 166.67 Hz.*

Indeed, although the fibres were too long and overlapped for accurate measurements at a rate of 16.67 Hz, they were clearly shorter for the other samples, and their fibre length average is reported in Table IV.1. However, as can be observed in Figure IV.3.c, when applying higher shear rates, new objects other than fibres are present in the micrograph. These round-shaped objects may correspond to aggregates. It is however difficult to account for their nature, one possibility being that they are aggregates made from $\mathbf{1}_6$, resulting from the destruction of fibres.
The results of the measurements depicted in Table IV.1 confirm that the peptide fibres are sensitive to the shear stress applied to the system, and provide insights on the range of fibre lengths obtained after shearing for 10 min, and on the range of shear stresses compatible with fibres made from $\mathbf{1}_6$. At low shear rates they are not efficiently broken, but at higher rates, they potentially break down into other objects. Indeed, it is important to notice that the length measurements performed on the sample sheared at 166.67 Hz included only the observable fibres, and did not take in account the round-shaped objects, which may explain the longer fibre average observed for a higher shearing rate.

Rotatory frequency (Hz)	Fibre length average (nm)	Measurements
16.67	n.d.	0
83.33	56.4	50
166.67	92.4	58

Table IV.1. *Fibre length averages measured from micrographs depending on the frequency of rotation of the Couette cell cylinder. Samples were sheared for 10 min.*

A second set of experiments was performed with a library containing long fibres made from $\mathbf{1}_6$, to which a shear stress was applied using the Couette cell at a constant shearing rate of 83.33 Hz, and sampling was performed at different points in time in order to assess the rate at which the Couette cell can break the fibres, and to test the resistance of the fibres to the mechanical stress provided by the Couette cell. The average fibre length of each sample was determined after different times of shearing. The obtained micrographs, depicted in Figure IV.4 show that the fibres are clearly shorter than the ones present in the original sample (Figure IV.2), demonstrating the efficiency of the Couette cell. Moreover, it can be observed that, even after a relatively short time of 1 min, the fibres are already broken by shear stress.

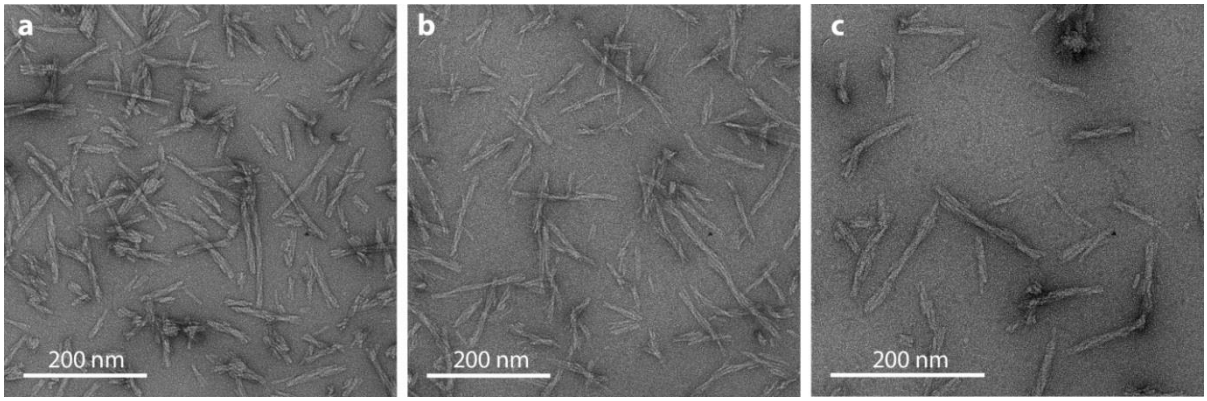

Figure IV.4. *Micrographs of peptide libraries made from* ***1****, sheared with a Couette cell at a shearing rate of 83.33 Hz for a time of a: 1 min, b: 10 min, c: 60 min.*

The average fibre lengths of these samples are depicted in Table IV.2, in which it can be seen that, as suggested by a direct observation of the micrographs, the fibres are relatively short, even after a short period of shearing. It is interesting to notice that fibres appear to be slightly longer when sheared for a longer time. This could be explained by the error on the data, or by fibre recombination.
These small fibre length averages suggest that the energy provided by the system at 83.33 Hz is sufficient to efficiently break the fibres even after a short period of shearing.

Shearing time (min)	Fibre length average (nm)	Measurements
1	60.6	61
10	56.4	50
60	76.4	58

Table IV.2. *Fibre length averages measured from micrographs depending on the shearing time. Samples were sheared at 83.33 Hz.*

This first set of experiments demonstrates the efficiency of the Couette cell to break fibres. Depending on the rates applied to the system, different fibres morphologies can be observed: at lower rates the fibres are still long, while high shearing rates result in disintegration of the fibres to create new objects. Fibre breakage seems efficient even after shearing for a short time, demonstrating therefore that the fibres are breaking rapidly when sheared.
Further experiments with other peptide sequences and intermediate shearing rates were done in order to lead to new insights.

IV.3.c. Comparison between the different peptide sequences

After those preliminary studies aimed at finding the right shearing conditions for a given peptide sequence, we probed further intermediate shearing rates for a set of other peptide building-blocks in order to broaden the scope of the study.

A library of each of the building blocks previously introduced in Scheme IV.3 was prepared by dissolving the different monomers individually to a concentration of 3.8 mM in a 50 mM solution of borate buffer at pH 8.2. The vial was then equipped with a stirring bar, and the libraries were continuously stirred at 80 rpm until complete oxidation of the libraries. This low value in stirring is meant to provide a good mixing of the libraries without providing too much mechanical energy to the system, in order to obtain long fibres and avoid extensive fibre breakage.

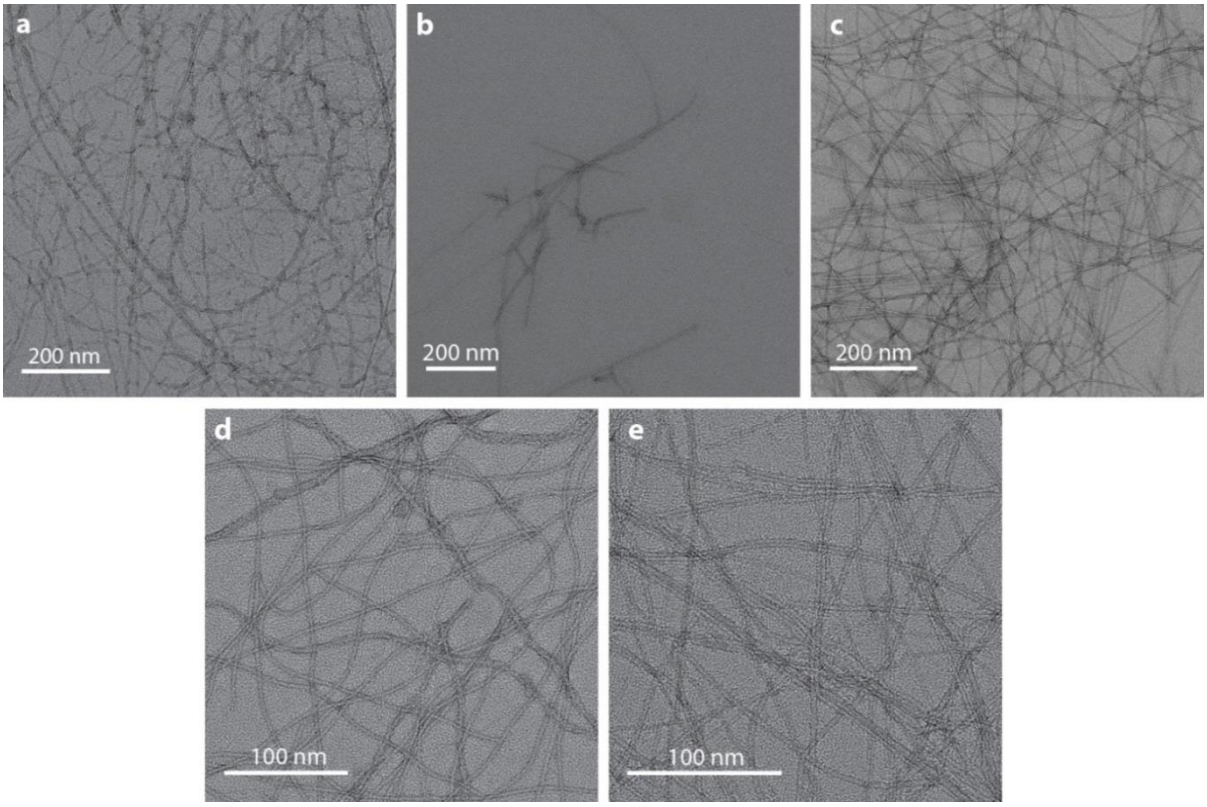

Figure IV.5. *Micrographs of peptide fibres from libraries stirred for 10 days at 80 rpm on a stirring plate, prepared from building blocks a:* ***1****, b:* ***2****, c:* ***3****, d:* ***4****, e:* ***5****.*

After 10 days, the libraries were monitored by TEM in order to assess the presence of fibres. The micrographs depicted in Figure IV.5 show that fibres are obtained for all the libraries studied. Although most of them feature long overlapping fibres with lengths reaching over 2 µm, it can be observed that the fibres formed from building block **2** are less concentrated, and shorter in length. This might be due to the fact that not all the material present in the library has been formed as fibres, or that a part of the sample was drained out during the blotting of the TEM grid.

The oxidised libraries containing long fibres were then split in two parts. The first half was put in a vial with a stirring bar, and stirred at 1200 rpm during 8 hours. The second half was sheared with the Couette cell, in order to estimate the resistance of the fibres present in the sample to the mechanical stress imposed on the system. Different shearing frequencies, ranging from 3.33 Hz to 83.33 Hz,

corresponding to shear stresses comprised between 1.69 x 10^3 $N.m^{-2}$ and 42.23 x 10^4 $N.m^{-2}$, calculated from equation (7), were performed. The resulting fibre population from those libraries were observed by sampling each library on a copper grid, immediately after shear and observing it with TEM.

The results for the first library, containing fibres consisting of $\mathbf{1}_6$ are presented in Figure IV.6. Upon visual inspection of the micrographs, it can be seen that all the samples except for the highly sheared one (Figure IV.5.e) contain long fibres, meaning that the fibres are relatively resistant to shear forces. However, from a shearing rate of 16.67 Hz (Figure IV.6.c), shorter fibres can be observed, and their amount with respect to longer fibres increases along with the shearing rate, to eventually represent the majority of the sample when sheared at 83.33 Hz. Although the technique of TEM does not allow any accurate quantification of the ratio between long and short fibres, due to difficulties in estimating the length of the longer fibres, it is clear that the concentration of the shorter fibres is increasing along with the shear rate, confirming that, above a given threshold, the fibres are able to break apart upon shear stress. When comparing the fibres sheared through the Couette cell with the ones stirred on a stirring plate (Figure IV.6.f), it can be observed that the latter contains a high amount of long fibres, confirming that for this sequence the stress provided by stirring is less efficient than the one provided to the highly sheared samples with the Couette cell.

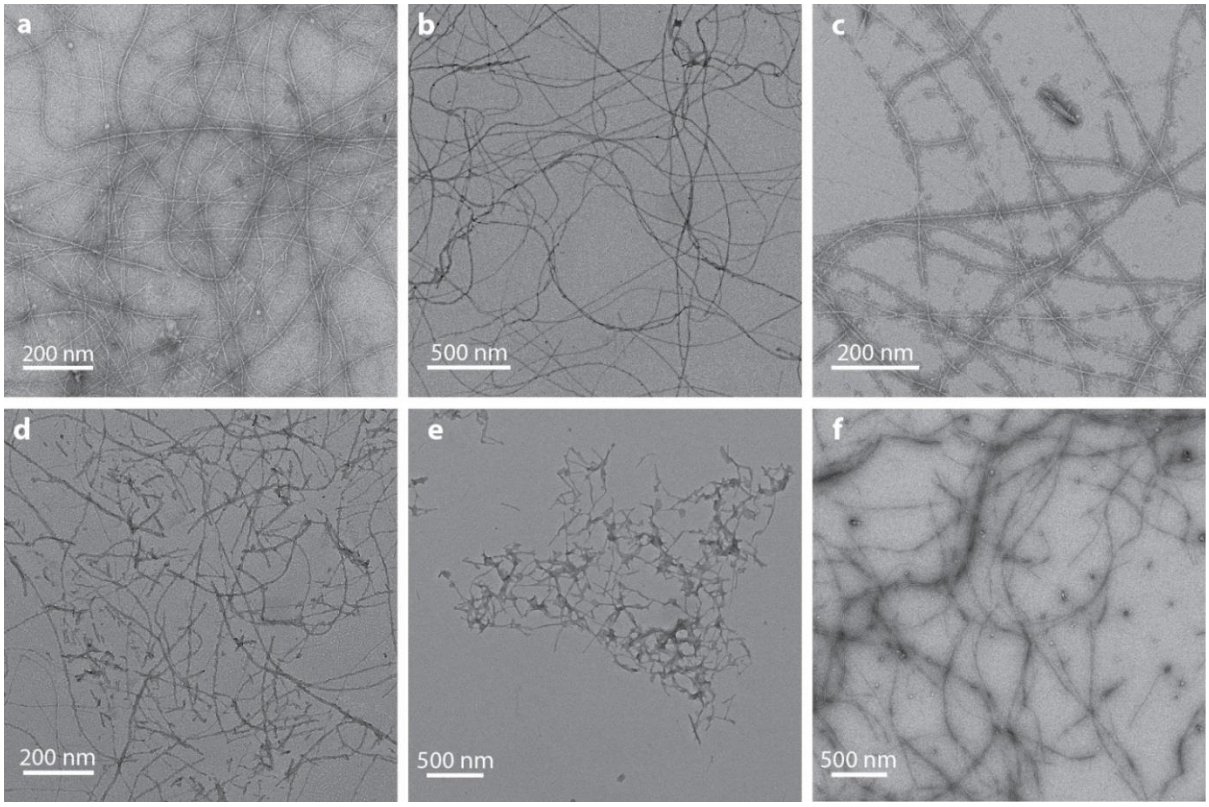

Figure IV.6. *Micrographs of peptide fibres from* ***1***$_6$ *sheared at shearing rates of a: 3.33 Hz, b: 8.33 Hz, c:* 16.67 Hz*, d: 33.33 Hz, e: 83.33 Hz, f: stirred on a stirring plate at 1200 rpm.*

The observations of the micrographs coming from experiments done with the peptide sequence **2** are giving some new insights on the effect of the shear stress on the system. Despite a low concentration of fibres in this library, Figure IV.7 shows that the fibres morphology is changing, starting from relatively straight fibres at a low shearing rate (Figure IV.7.a), to change in shape and eventually reach a state where mainly aggregates of organic matter can be observed. These results show that not only the mechanical forces applied to the system were here able to break the fibres into shorter ones, but also to destroy their very nature, creating a new kind of objects. It is however hard to assess the nature of these aggregates, and to know if they are composed of short fibres being laterally associated, or of octameric macrocycles linked to each other in a disordered manner.

The stirred library, depicted in Figure IV.7.f, shows to some extent that the fibres are affected by the magnetic stirring, since among the fibres some aggregates are already present.
The reason for this propensity to break apart more easily than the other peptide sequences observed may come from weaker interactions between the macrocycles, since, despite forming larger replicating macrocyclic rings (octamers) than the other sequences, due to its higher hydrophobicity, the interactions between adjacent peptide chains are weaker.

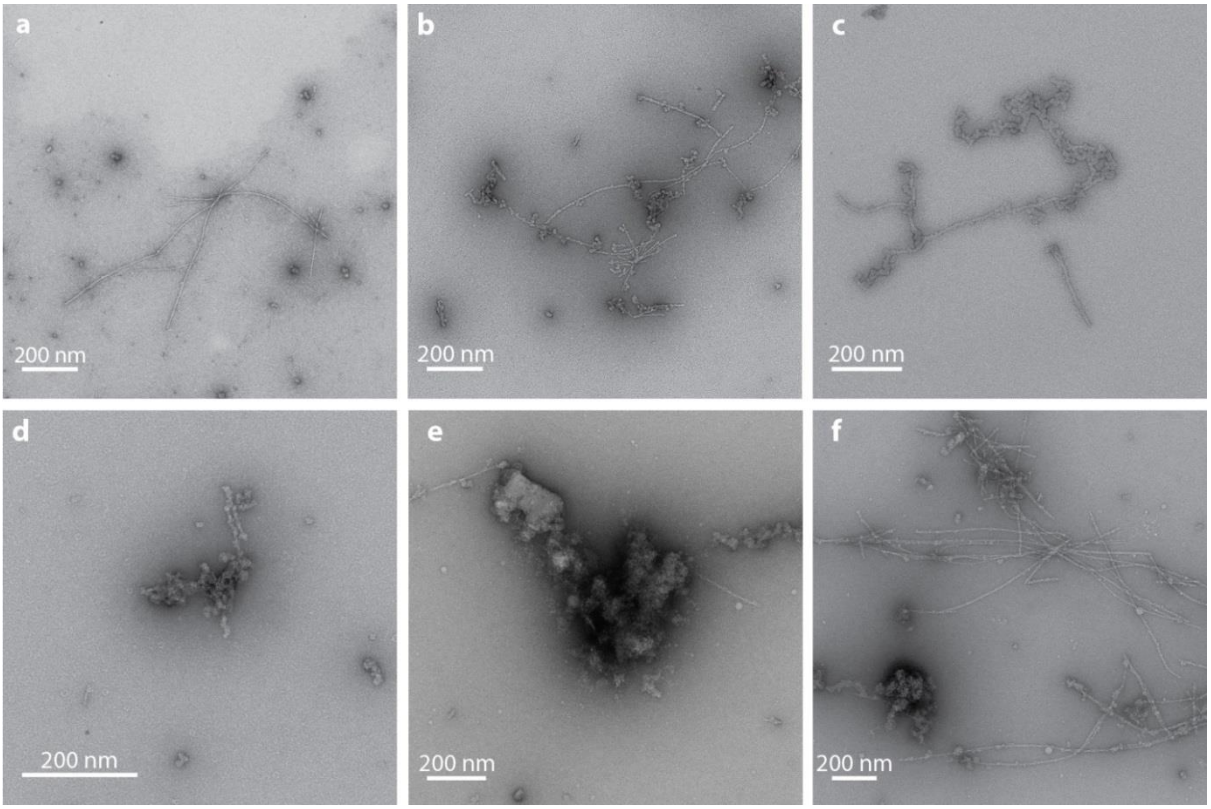

Figure IV.7. *Micrographs of peptide fibres from* $\mathbf{2}_8$ *sheared at shearing rates of a: 3.33 Hz, b: 8.33 Hz, c:* 16.67 Hz*, d: 33.33 Hz, e: 83.33 Hz, f: stirred on a stirring plate at 1200 rpm.*

The outcome of the experiments performed on fibres formed from $\mathbf{3}_3$ and $\mathbf{3}_4$, depicted in Figure IV.8 resemble more the results and observation made on the libraries made from the peptide building block **1**, in that long fibres are obtained at low shearing rates, but get smaller with increasing the stress applied to the system. However, the fibres from this library seem to be more prone to breakage, since short fibres can already be observed at rates of 3.33 Hz (Figure IV.8.a), and only a few fibres are reaching 1 µm in length when the library is sheared at 33.33 Hz, whereas long fibres were still observable in the case of fibres made from $\mathbf{1}_6$. This observation suggests that the fibres originating from peptide building block **3** are more sensitive to the shear stress than the fibres made from building block **1**, and therefore less resistant, implying that at a molecular level the interactions between the staked macrocycles composing the fibres are weaker, consistent with a smaller macrocycle size. When the library is sheared at 83.33 Hz, short fibres are observed, but interestingly, these short fibres have a tendency to associate with each other, keeping however their fibre nature, compared to what was observed with peptide **2** at high shearing rates. This aggregation could be an artefact induced by the drying of the sample on the TEM grid, but since is not observed for the other libraries, it may very well be representative of the interactions occurring in solution. The stirred sample (Figure IV.8.f) is mainly composed of long fibres, but short ones can be noticed, making it comparable with the sample sheared with a Couette cell at rates 8.33 Hz or 16.67 Hz.

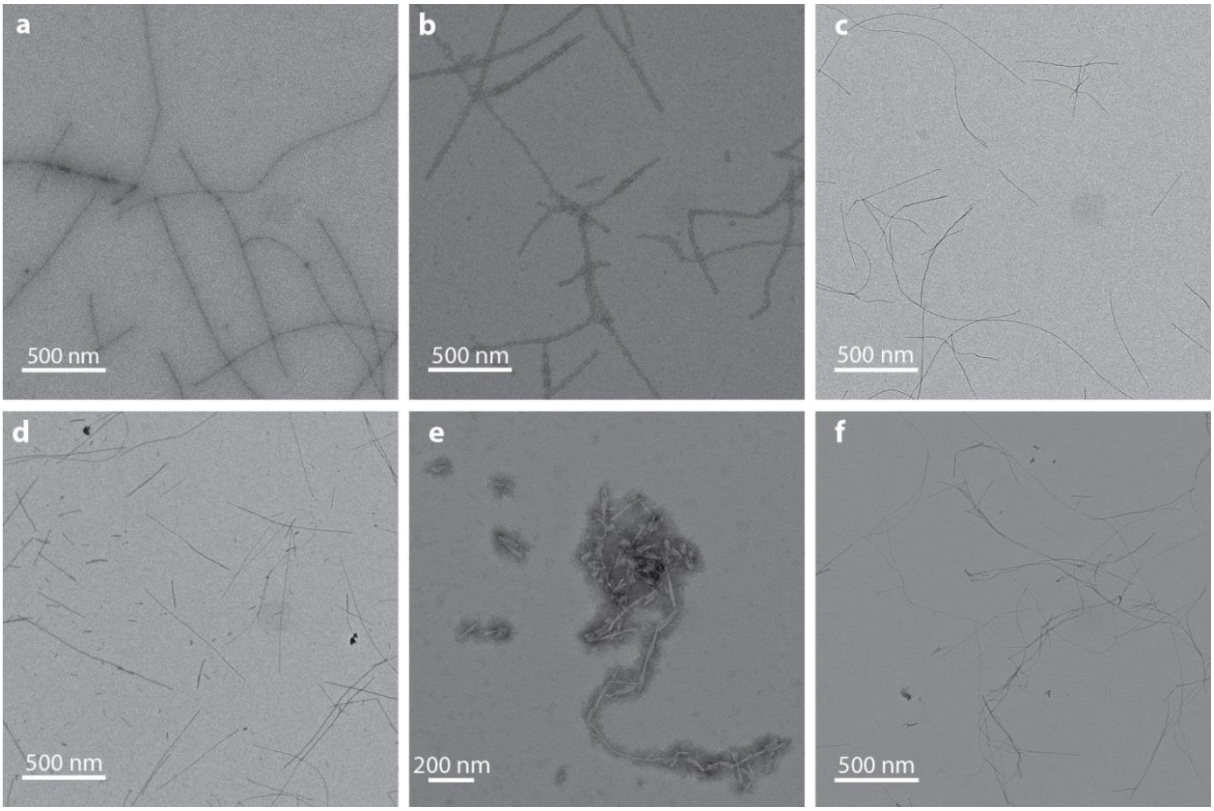

Figure IV.8. *Micrographs of peptide fibres from* $\mathbf{3}_3$ *and* $\mathbf{3}_4$ *sheared at shearing rates of a: 3.33 Hz, b: 8.33 Hz, c:* 16.67 Hz*, d: 33.33 Hz, e: 83.33 Hz, f: stirred on a stirring plate at 1200 rpm.*

The micrographs from experiments performed on fibres coming from libraries made of building block **4**, presented in Figure IV.9, gave similar results to the ones observed with peptide building block **1**, in that the library initially contains long fibres which are getting shorter upon shearing. However, it is interesting to notice that, as in the case of peptide **3**, shorter fibres are already present even at lower shearing rate, although their amount is not as significant as what was observed with peptide **3**. The ratio between short and long fibres at higher rates is anyhow high enough to confirm that fibres were broken upon mechanical stress applied to the system. The micrograph of the stirred library of this peptide, presented in Figure IV.9.f, shows that the fibres in this library are relatively long, and can be compared to the sample sheared using the Couette cell with shearing frequencies between 8.33 Hz and 16.67 Hz.

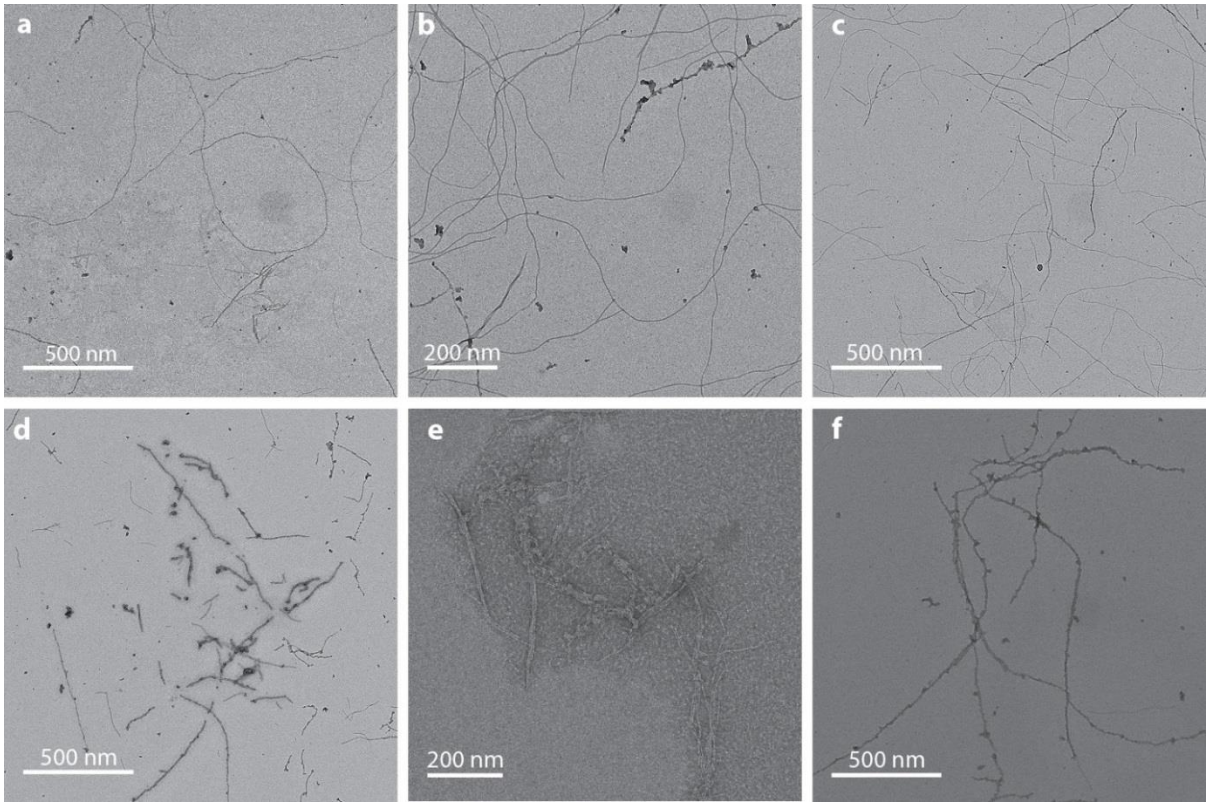

Figure IV.9. *Micrographs of peptide fibres from* ***4***$_6$ *sheared at shearing rates of a: 3.33 Hz, b: 8.33 Hz, c:* 16.67 Hz*, d: 33.33 Hz, e: 83.33 Hz, f: stirred on a stirring plate at 1200 rpm.*

The last peptide sequence studied produces fibres made from **5**$_6$, whose micrographs are depicted in Figure IV.10. As for the previous samples, longer fibres can be observed when lower shearing forces are applied to the system. However, it seems that this peptide is able to form the longest fibres observed of all peptides, with many fibres reaching above 2 µm in length, and even longer than 4 µm in case of the long curly fibre observable in Figure IV.10.a. The samples sheared at stronger rates may give some insights into this observation, for it can be seen that, although the fibres are getting shorter when applying stronger shearing forces, long fibres of above 1 µm are always present with shearing speeds up to 33.33 Hz, similarly to what was observed in the case of peptide **1**, except for the fact that in the present case few really short fibres are present, and the shorter ones seems to be predominant in the system only at the highest shearing rate (Figure IV.10.e).

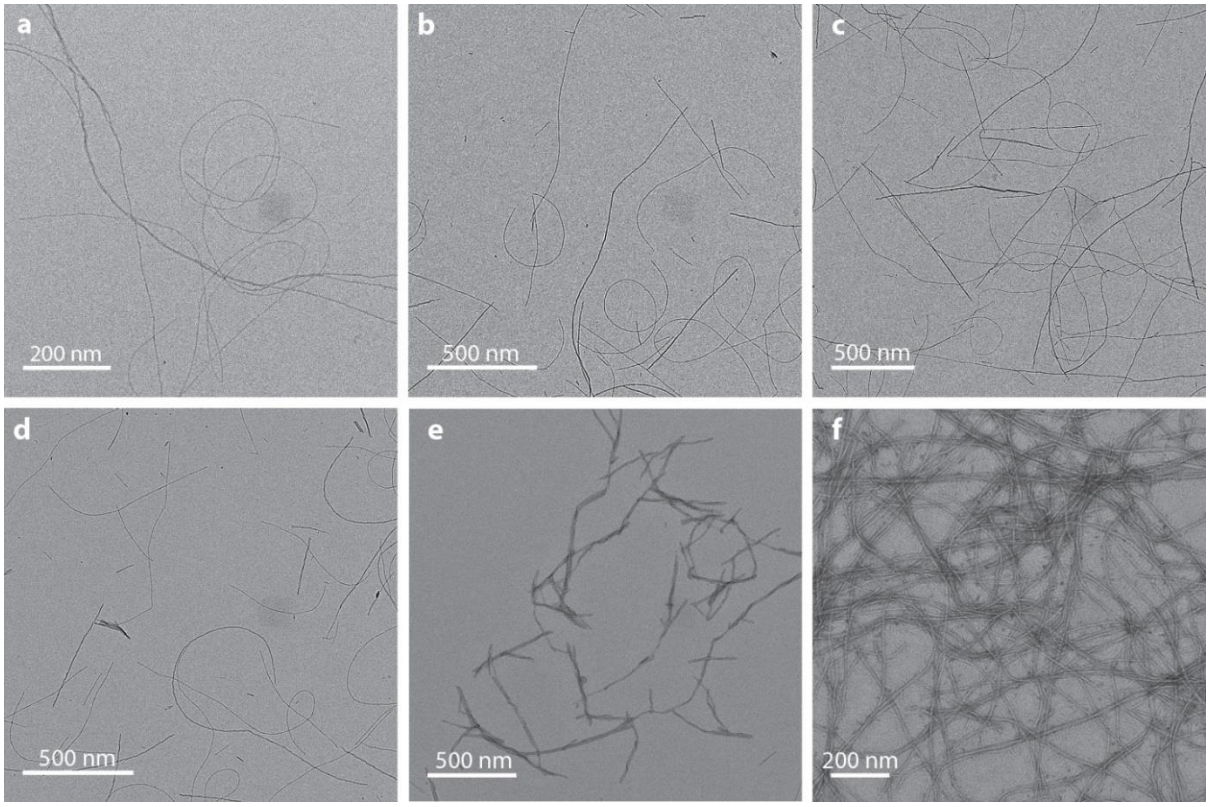

Figure IV.10. *Micrographs of peptide fibres from* ***5***$_6$ *sheared at shearing rates of a: 3.33 Hz, b: 8.33 Hz, c:* 16.67 Hz*, d: 33.33 Hz, e: 83.33 Hz, f: stirred on a stirring plate at 1200 rpm.*

This phenomenon, certainly due to a better resistance of the fibres to shear stress, is coming from stronger interaction within the fibres between the macrocycles forming them, influencing their tertiary structure and explaining therefore their longer length observed.

The library seems to be strongly resistant to the stress provided by stirring the library, since no short fibre is observed, even after stirring the library at 1200 rpm for 8 hours.

In conclusion, shearing fibres through a Couette cell has revealed different breakage efficiencies, depending on the shear rate and the peptide sequence. Overall, the morphology and length of fibres coming from libraries stirred with a stirring bar at 1200 rpm can be compared to samples sheared with the Couette cell at frequencies between 8.33 Hz and 16.67 Hz.

IV.3.d. Comparison of the fibre lengths at higher shearing rates between the different peptide sequences

After comparing the evolution of the libraries profiles while increasing the shear stress, measurements were done in order to determine the average length and length distributions of the different peptide fibres. These measurements were done for the libraries sheared at a rates ranging from 16.67 Hz to 83.33 Hz, since overlapping fibres and long lengths made measurements for the other shearing rates impossible. The results, presented in Figure IV.11 show that, although all of the libraries share a similar profile, differences can be observed depending on the peptide sequence.

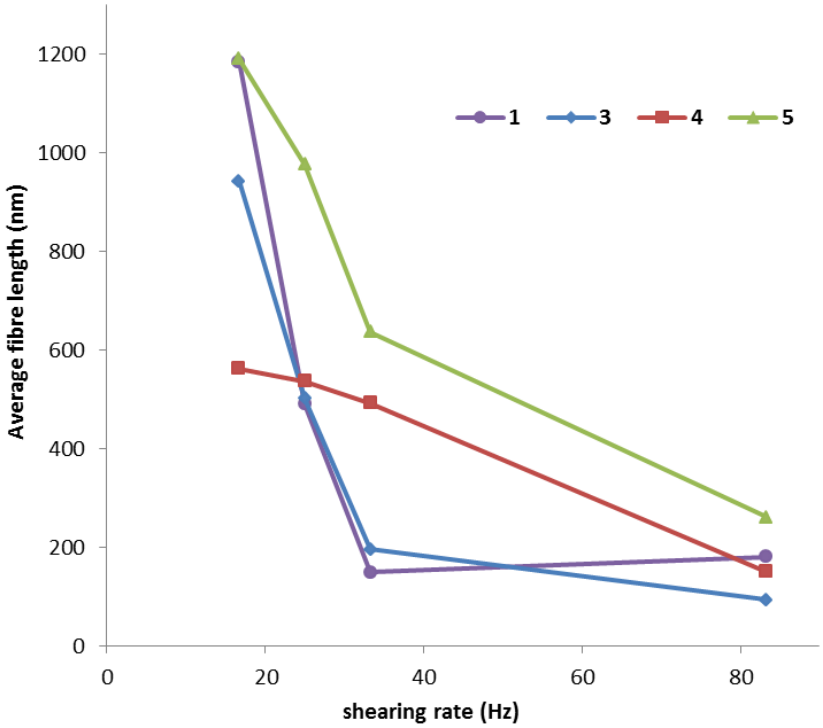

Figure IV.11. *Fibre length averages determined from TEM micrographs for the different peptide sequences studied at different shearing rates.*

The first point that should be discussed her is the fact that the fibre length average of peptide **1** is in the present case of 181 nm, when it was of 56 nm for similar conditions in the results presented in Table IV.2. This significant difference may come from differences in the age and history of the libraries, since in the present case the library used has been stirred at 80 rpm for 10 days, when in the library used for the preliminary study, the library had been left without agitation during several weeks prior to Couette cell measurements.

However, making comparisons between the different libraries in the results presented in Figure IV.10 is considered justified, since all the libraries from this table share the same history and the same methodology.

The results show that all of the sequences studied are strongly sensitive to the shear stress, since the average fibre length average is significantly shorter at higher shearing rates. However, the different peptide building blocks do not respond all the same way to the shear stress applied to the system. Fibres made from peptide **1**, for example, are undergoing a very dramatic change in average fibre length. Fibres made from peptide **3** follows a similar pathway as **1**. In contrast, peptide **4** seems to undergo a relatively linear response in breaking to the stress applied to the system, unlike all the other sequences.
Peptide **5** has relatively long fibres compared to the other sequences, but they seem fragile.
These observations are suggesting that the peptide sequence plays an important role in the strength of the peptide fibres. The hydrophobicity or the size of the macrocycles appear to be important parameters for controlling strength.
When considering only the higher shearing rates, the results show that depending on the sequence, the fibre lengths averages differ significantly, ranging from fibres of 93 nm in the case of libraries

made from peptide building block **3** up to 261 nm for libraries made from peptide **5**. These observations are in accordance with the results discussed in the previous paragraph, in which a direct observation of the micrographs showed a tendency of the fibres formed from species $\mathbf{5}_6$ to be longer than the others.
Fibre length measurements were not done for peptide **2**, as fibres showed lateral association.

From the same data series, histograms representing the fibre length distribution at the highest shearing rates of the different libraries were plotted. The results, presented in Figure IV.12, show that the fibre length profiles of the libraries are substantially different. The library made from peptide **5**, depicted in Figure IV.12.d results in a broad distribution. This broad range of fibre lengths reflects an inhomogeneous breakage, showing that the shear stress applied was not sufficient to efficiently break the fibres.

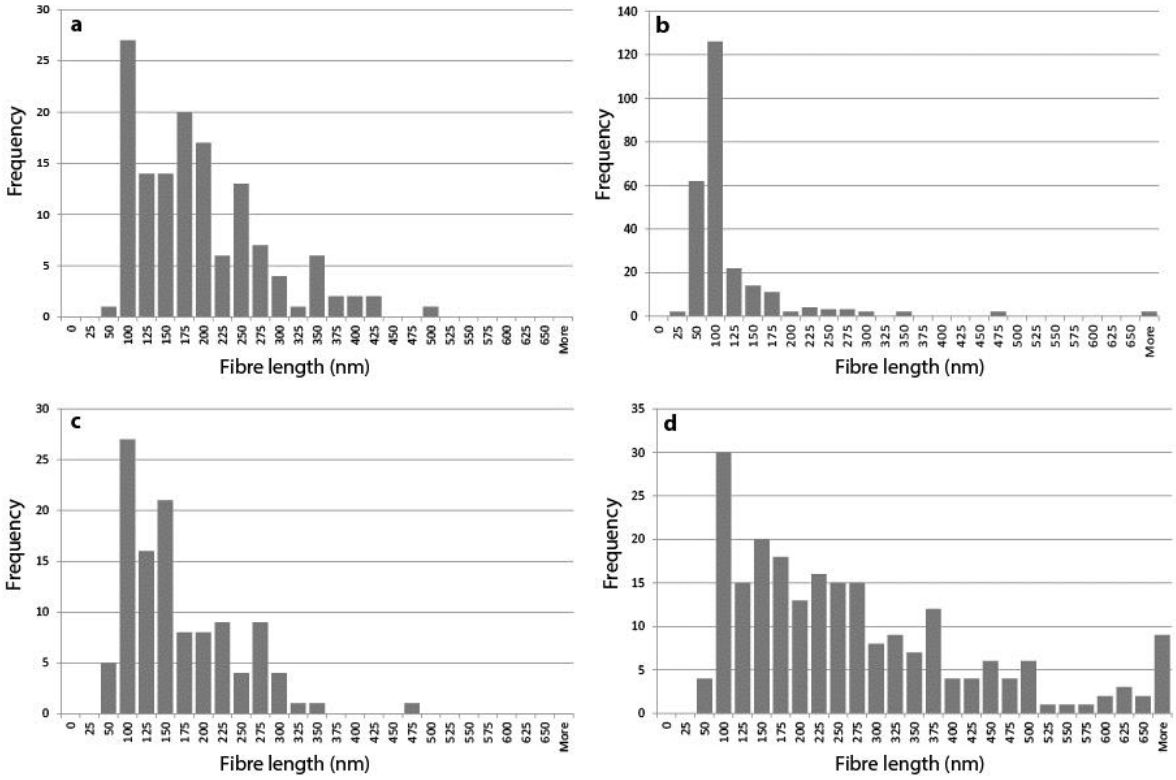

Figure IV.12. *Fibre length distributions obtained from measurements on micrographs of libraries made from a:* ***1****, b:* ***3****, c:* ***4****, d:* ***5****. Samples were sheared at 83.33 Hz.*

Another interesting library to observe is the one composed of $\mathbf{3}_3$ and $\mathbf{3}_4$, presented in Figure IV.12.b which displays a relatively narrow distribution, and has a polydispersity index of 1.45, reflecting its propensity to break more homogeneously upon shearing compared to the other peptide sequences.

The other peptide sequences are giving intermediate results, with relatively broad fibre length distributions.

IV.4. Conclusions and perspectives

The results presented in this section proved that the breakage of the fibres originating from the self-assembly of peptide macrocycles can be controlled through a Couette cell. However, their behaviour differs depending on the sequence of the peptide building block. It has been previously demonstrated that the peptide building block has an influence on the nature of the replicator emerging from the library, and it now shows that for a given pool of same replicator sizes, differences can be observed in terms of breakage, and therefore in terms of fibre resistance to mechanical stress, and to molecular interactions within the fibres. These differences in behaviour may come from the different strengths of interactions between the peptides in the fibres.

The replication process is happening at the fibre ends. A peptide sequence which is more prone to breakage will have a higher concentration of short fibres when under mechanical stress, and therefore more replication sites. For this reason, in case of competition with other replicators, the one more prone to breakage may have an advantage over the others, which is relevant in the case of self-replicating system, and more specifically in the case of possible Darwinian evolution of such systems.
Moreover, the shearing rates performed through the Couette cell have shown to be stronger than the ones provided by stirring the sample with a stirring bar at the maximum stir rate of 1200 rpm. Samples sheared with this device may therefore represent good seeds for performing seeding experiments similar to the ones presented in Chapter II of this Thesis.

IV.5. Experimental section

IV.5.a. Materials and methods

Peptide building blocks **1**, **2**, **3**, **4** and **5** were synthesized by Cambridge Peptides Ltd (Birmingham, UK) from 3,5-bis(tritylthio)benzoic acid, which was prepared via a previously reported procedure[13]. Doubly distilled water, boron oxide and potassium hydroxide utilized for the preparation of buffers were obtained from in-house double distillation facilities, Aldrich and Merck Chemicals, respectively.
Libraries were prepared in clear HPLC glass vials (12 × 32 mm) closed with Teflon-lined snap caps purchased from Jaytee. Magnetic stir bars were Teflon coated (2 × 2 × 5 mm) and obtained from VWR. An IKA RCT basic magnetic stirrer was used for the stirred libraries.

IV.5.b. Couette cell specifications

$D_{cylinder}$: 39.50 mm
$h_{cylinder}$: 50 mm
$D_{cuvette}$: 40.00 mm
Gap at the bottom of the cuvette between the cylinder and the cuvette: 0.25 mm
f_{min}: 0.17 Hz
f_{max}: 166.67 Hz

IV.5.c. Evaluation of the shear rates and Taylor number in this study

f (s^{-1})	Ω (s^{-1})	γ ($N.m^{-2}$)	Ta
3,3	20,7	1648	2119
8,3	52,1	4146	13405
16,3	102,4	8142	51700
33,3	209,2	16633	215776
83,3	523,4	41608	1350218

Table IV.3. Angular velocities, shear rates, and Taylor number for the different rotating frequencies used in this study. Ω was calculated from equation (4), γ from equations (7) and (8), and Ta from equation (9).

IV.5.d. UV-vis measurements

UV-vis measurements were performed using a Varian Caryo Bio UV-visible spectrophotometer. A quartz cuvette with 1 cm path length was used for all measurements. The absorption spectra were recorded from 350 nm to 600 nm.

IV.5.e. Negative staining TEM measurements

An aliquot of a sample taken from a peptide library was diluted 40 times in doubly distilled water. Shortly thereafter, a small drop of the diluted sample was deposited on a 400 mesh copper grid covered with a thin carbon film. After 30 seconds, the droplet was blotted on filter paper. The sample was then stained with a solution of uranyl acetate deposited on the grid and blotted on filter paper after 30 seconds. The staining process was repeated in order to have an enhanced contrast. The grids were observed in a Philips CM12 electron microscope operating at 120 kV. Images were recorded on a slow scan CCD camera. During the measurements, a relatively strong defocus, around -2500 nm, was applied in order to enhance the contrast on the micrographs and facilitate the length measurements.

IV.5.f. Fibre length measurements

TEM micrographs were analysed using imageJ. When needed, the contrast of the micrograph was enhanced using the “Brightness/Contrast” tool. A scale was set on each micrograph according to its magnification, and an average length of each sample was determined by measuring fibres from the micrograph, using the measuring tool of ImageJ. The data was then transferred to MS Excel, and analyzed.

IV.6. References

[1] M. Colomb-Delsuc, E. Mattia, J. Sadownik, S. Otto, *manuscript submitted*. See Chapter II of this Thesis.

[2] H. A. Barnes, J. F. Hutton, K. Walters, *An Introduction to Rheology, 3rd Edition, Elsevier*, **1993**.

[3] A. Y. Malkin, A. I. Isayev, *Rheology: Concepts, Methods, and applications, 2nd Edition, Elsevier*, **2011**.

[4] G.I. Taylor, Phil. Trans. Royal Society, **1923**, A223, 289-343.

[5] M. Couette, *Compt. Rend. Acad. Sci. Paris*, **1888**, 107, 388-390.

[6] J.-M. Piau, M. Piau, *Rhéologie*, **2005**, 8, 1-4.

[7] J.-M. Piau, M. Piau, M. Bremond, J.-M. Couette, *Les Cahiers de la Rhéologie*, **1994**, XII, 47-69.

[8] G. J. Zwartz, A. Chigaev, T. D. Foutz, B. Edwards, L. A. Sklar, *Cytometry Part A*, **2011**, 79A, 233-240.

[9] M. Rössle, P. Panine, V. S. Urban, C. Riekel, *Biopolymers*, **2004**, 74, 316-327.

[10] L. Porcar, W.A. Hamilton, P.D. Butler, G.G Warr, *Rev. Sci. Instrum.*, **2002**, 73, 2345-2354.

[11] P. W. Fontana, M. Kearney-Fischer, S. Rogers, J. V. Ulmen and S. Windell, *Rev. Sci. Instrum.*, **2007**, 78, 033907.

[12] R. Marrington, T. R. Dafforn, D. J. Halsall, J. I. MacDonald, M. Hicks, A. Rodger, *Analyst*, **2005**, 130, 1608-1616.

[13] J.M.A. Carnall, C.A. Waudby, A.M. Belenguer, M.C.A. Stuart, J.J.-P. Peyralans, S. Otto, *Science*, **2010**, 327, 1502-1506.

[14] C. Kleinstreuer, *Modern Fluid Dynamics, Springer*, **2010**.

[15] G. I. Taylor, Philos. Trans. Roy. Soc. London Ser. A, **1923**, 223, 289-343.

[16] F. M. White, Fluid Mechanics, 4rd edition, McGraw Hill, **1998**.

[17] M. Malakoutikhah, J. J-P. Peyralans, M. Colomb-Delsuc, H. Fanlo-Virgos, M.C.A. Stuart, S. Otto, *J. Am. Chem. Soc.*, **2013**, 135, 18406–18417.

[18] See part V.1 of this Thesis.

Chapter V
Electron Microscopy as a tool for observation of self-assembling and self-replicating systems

Several collaborations involving the use of Electron Microscopy for the observation of supramolecular structures emerging from self-assembling systems took place during the course of this thesis. This chapter describes three examples in which electron microscopy proved to be a useful tool for the characterization of the obtained supramolecular objects in different fields of chemistry and biochemistry.

Parts of this chapter have been published:

M. Malakoutikhah, J. J-P. Peyralans, M. Colomb-Delsuc, H. Fanlo-Virgos, M.C.A. Stuart, S. Otto, *Journal of the American Chemical Society*, **2013**, *135*, 18406-18417

W. H. Rombouts, M. Colomb-Delsuc, M. W. T. Werten, S. Otto, F. A. d. Wolf, J. van der Gucht, *Soft Matter*, **2013**, 9, 6936-6942

J. Wang, M.A.C. Stuart, A.T.M. Marcelis, M. Colomb-Delsuc, S. Otto, J. van der Gucht, *Macromolecules*, **2012**, 45(17), 7179-7185

V.1. Transmission Electron Microscopy: a powerful tool in modern research

Electron Microscopy was developed in the early 1930's by Max Knoll and the 1987 Nobel Prize winner Ernst Ruska.[1,2] It was introduced in order to overcome the resolution limitations of light microscopy and allows the observation of objects too small to be observed using a classical light microscope.
This was achieved by using electrons for the observation of specimens instead of visible light. The resolution depends on the wavelength of the electrons used for the observations, which allows surpassing the resolution that would be achieved with a light microscope, and permits the observation of object with a size smaller than visible wavelengths.

Scheme V.1 shows the main parts of a Transmission Electron Microscope. The source of electrons comes from an electron gun on which a tungsten filament with a highly negative potential, up to 300kV in modern microscopes, emits an electron beam, which is then passing through a series of magnetic lenses, each of them individually controlled by an electrical input, which allows the user to tune the beam passing through them. The electrons are then passing through the loaded specimen to be observed. Depending on the material and on the interactions, a part of the electrons from the beam are absorbed by the object present on the specimen, while others are passing through, and reach an imaging plate or a CCD camera. The magnification and the focus can be tuned by varying the electric current given to the different lenses. The resulting micrograph can be either directly observed by the user on a fluorescent screen, or recorded as an image and observed on a computer.

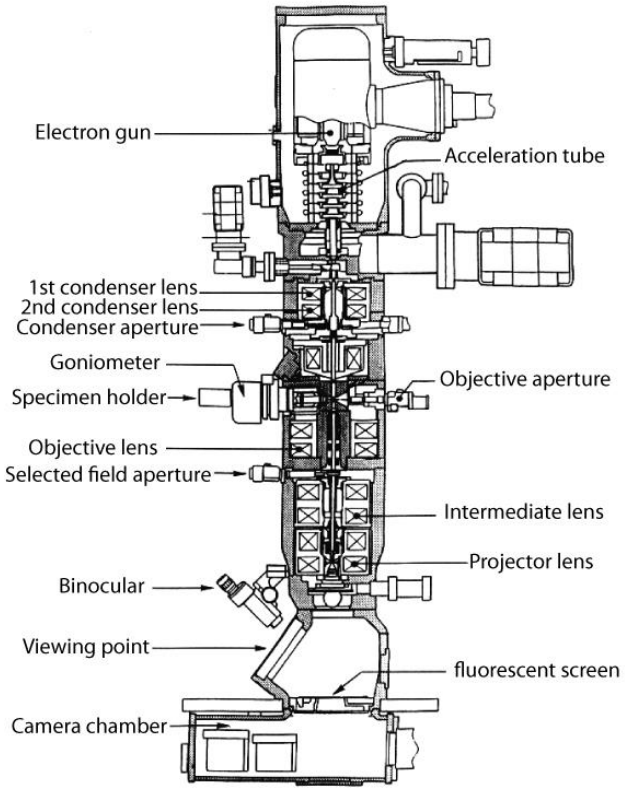

***Scheme V.1**. General scheme representing the cross section of a Transmission Electron Microscope. (reproduced from ref 3).*

With increased resolution, and the development of new techniques, Transmission Electron Microscopy (TEM) became a more and more predominant tool and finds nowadays numerous applications in a broad range of domains not only in life sciences such as biology [4,5] and pharmaceutics[6,7], or in nanotechnology, material sciences[8,9,10,11], and supramolecular chemistry[12], but also in other sciences like archaeology, or geology [13,14,15]. This series of examples is not exhaustive, for the use of electron microscopy is limited only by the person who wants to observe sub-angstrom objects.

In this chapter, three collaborations in which TEM proved to be a useful tool to serve different purposes are described. The first part describes a study in which TEM helped confirming that the assembly of self-replicating peptides resulted in fibre formation, and allowed the study of their morphology depending on the conditions of the experiment. In a second study, the presence of polymer micelles formed by metal coordination was investigated by TEM measurements, which also allowed a comparison of their observed size with the ones obtained by other techniques. Finally, in a third example TEM was used to show the bundling of two types of proteins from which the association enhances the mechanical resistance of the system.

V.2. Uncovering the selection rules for the emergence of multi-building-block replicators from dynamic combinatorial libraries.

V.2.a. Introduction

As previously described in this thesis, Dynamic Combinatorial Chemistry is a relevant tool in the context of the understanding of the emergence of life, and the study of the mechanisms that led to the formation of the first prebiotic systems. A study was done in order to understand the selection rules that govern the emergence of replicators from a complex mixture. To uncover these rules from a system based on peptide building blocks similar to the ones described in Chapters II, III and IV of this thesis, it was necessary to study the interactions needed for the macrocycles to efficiently stack on top of each other and therefore replicate. To serve this purpose, a new series of peptide building blocks was synthesized, in which the peptide sequence was modified by changing the hydrophobicity of the peptide chain. This change in hydrophobicity may be able to change the minimum size of the macrocycle necessary for two of them to stack on top of each other. It was chosen to make these peptides differ in only one residue. Therefore, all of the peptides in the following study differ only in the second residue of the chain, starting from the C-terminus. A broad variety of amino acids, including natural and non-natural amino acids, ranging from the hydrophilic serine to the strongly hydrophobic naphthylalanine were chosen. The latter non-natural amino acid was chosen in order to have peptides more hydrophobic than phenylalanine, which is the most hydrophobic natural amino acid. The structures of the peptide building blocks used for this study are depicted in Scheme V.2.

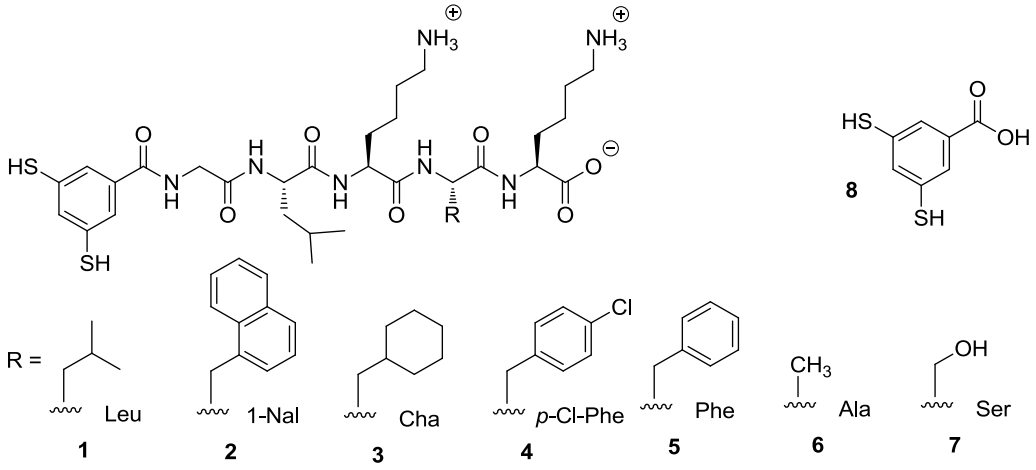

Scheme V.2. *Different peptide sequences studied.*

It has been reported previously that the ranking of peptide hydrophobicity sometimes does not follow the same order as the residues constituting the peptide.[16] Therefore, the relative hydrophobicity of the peptides used for this study was determined by Morteza Malakoutikhah by injecting the building blocks in reversed phase HPLC, and comparing their retention time. The results shown in **Table V.1** allow us to rank them by hydrophobicity.

Peptide	Sequence	Retention Time (min)
2	X-Gly-Leu-Lys-*1*-***Nal***-Lys-COOH	12.4
3	X-Gly-Leu-Lys-***Cha***-Lys-COOH	12.3
4	X-Gly-Leu-Lys-***p-Cl-Phe***-Lys-COOH	12.2
5	X-Gly-Leu-Lys-***Phe***-Lys-COOH	11.1
1	X-Gly-Leu-Lys-***Leu***-Lys-COOH	10.7
6	X-Gly-Leu-Lys-***Ala***-Lys-COOH	9.5
7	X-Gly-Leu-Lys-***Ser***-Lys-COOH	9.4

Table V.1. *Peptide sequences and their retention time in reversed-phase HPLC, with a gradient from 5 to 95% CH_3CN in water in 30 min using a Phenomenex phenylhexyl C18 column 4.6 × 75 mm, 3 µm. X: 3,5-dimercaptobenzoic acid.*

V.2.b. Results

The libraries discussed in this section were prepared and analysed by Morteza Malakoutikhah. For each peptide sequence, the kinetics of evolution were monitored over time, for a series of three libraries in which the effect of the shear forces was studied by modifying the stress applied to the system through not agitating, shaking on a shaking plate, or stirring with a stirring bar on a magnetic stirring plate.

The resulting graphs showing the changes in product distributions over time of these libraries are depicted in Figure V.1. It can be observed that for all the libraries, the monomer is quickly oxidized to form a pool of larger oligomers which are changing in relative abundance in a dynamic fashion. Depending on the sequence and the shear stress applied, the main species emerging from the libraries differ in macrocycle size.

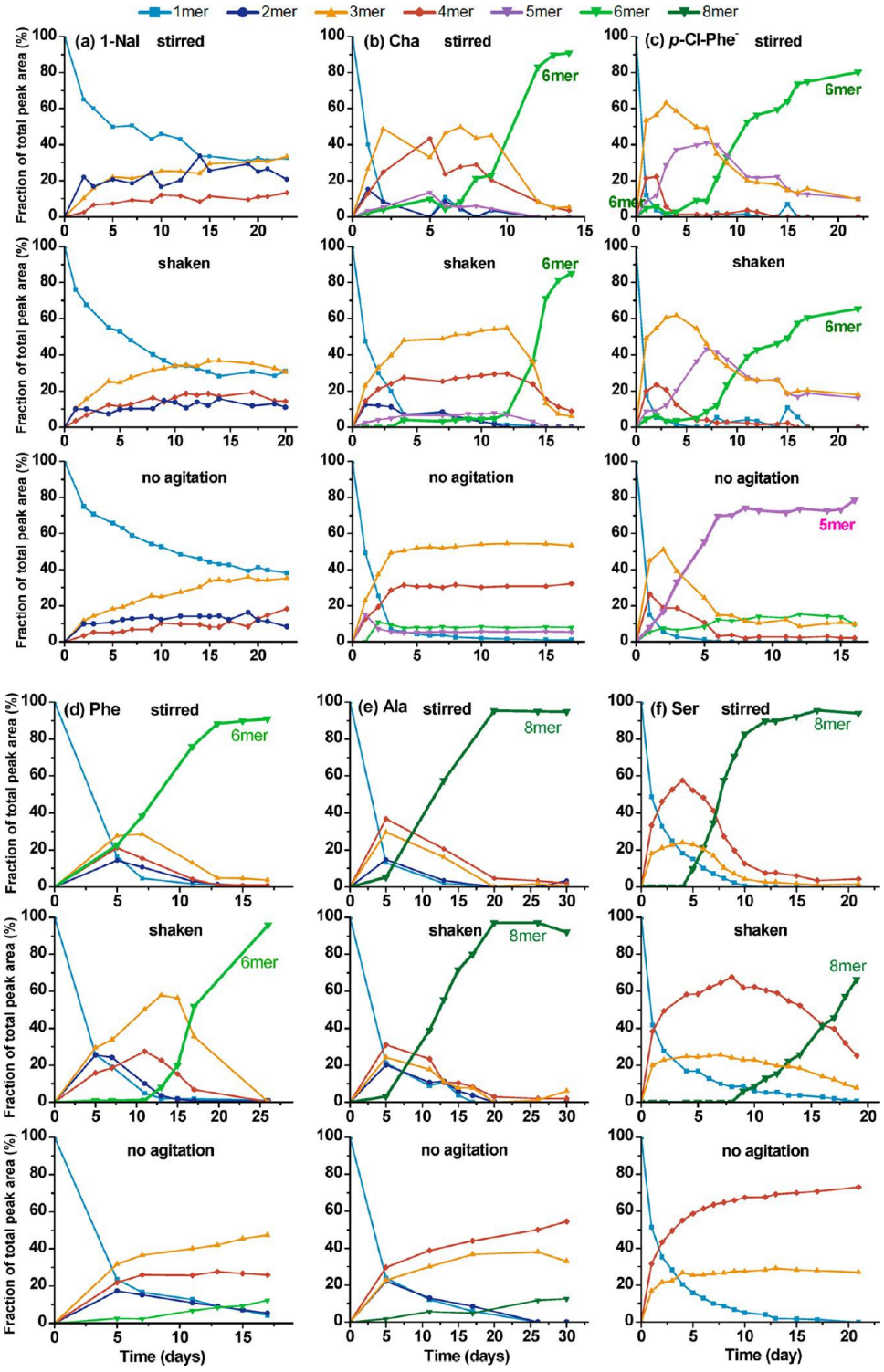

Figure V.1. *Evolution of the product distribution of small DCLs (3.8 mM dithiol building block in 50 mM borate buffer pH 8.2) made from libraries containing (a) 1- naphthylalanine, (b) cyclohexylalanine, (c) p-chlorophenylalanine, (d) phenylalanine, (e) alanine, and (f) serine while stirred at 1200 rpm; shaken at 1200 rpm or not agitated. To maintain disulfide exchange in the samples made from* ***3****, 5–30 mol % of monomer* ***3*** *was added to the stirred sample at t = 2, 5, and 9 days and 15 mol % of monomer* ***3*** *was added to the shaken sample at t = 6 days. Similarly, to the DCLs made from p-Cl-Phe was added 10–20 mol % of monomer to the stirred and shaken samples at t = 7, 9, and 14 days.*

For most of the agitated libraries, a larger macrocycle appears and becomes predominant after a lag time ranging from 5 to 15 days. The replicator nature of these macrocycles was verified through a set of seeding experiments,[17] in which an aliquot of the larger species was added to a young library, and its change in composition was monitored over time. It could be concluded from this that most of the larger oligomers (larger than tetramer) are indeed replicators, except for ClPhe pentamers.

When relating the macrocycle size of the replicator to the peptides sequence, there is a clear trend: the more hydrophobic the peptide, the smaller the replicator size. This behaviour can be explained by the fact that there is a critical number of interactions that should be reached for the macrocycles to start stacking on one another, and for less hydrophilic residues, more of them are needed in order to reach sufficient interactions for the macrocycle to form β-sheets. This leads to the first selection rule: in order to replicate, macrocycles need to reach a critical size from which they will start stacking on top of each other, and this critical size is determined by the peptide sequence of the building-block used.

Since these peptides are designed to form a β-sheet like structure, CD and fluorescence analyses were performed in order to understand and confirm the mode of assembly.[17]

V.2.c. Transmission Electron Microscopy measurements

While doing investigations on the system, it was important to assess the presence of fibres, and study their morphology depending on the conditions of the library, and on the peptide sequence. To achieve this, TEM was a good method, and some negatively stained measurements were made on libraries after they reached the stage where the replicator is present in major amounts.
The first goal of these studies was to verify the presence of fibres, in order to confirm the self-assembly of the replicating macrocycles.

As shown in Figure V.2, the presence of fibres for the building block XGLK(Nal)K for all of the shearing conditions tested can be observed. Although the fibre concentration is very high for the standing sample, it can nevertheless be observed qualitatively that the fibres are longer in the case of the standing sample than for the samples that were subjected to stronger shear forces.

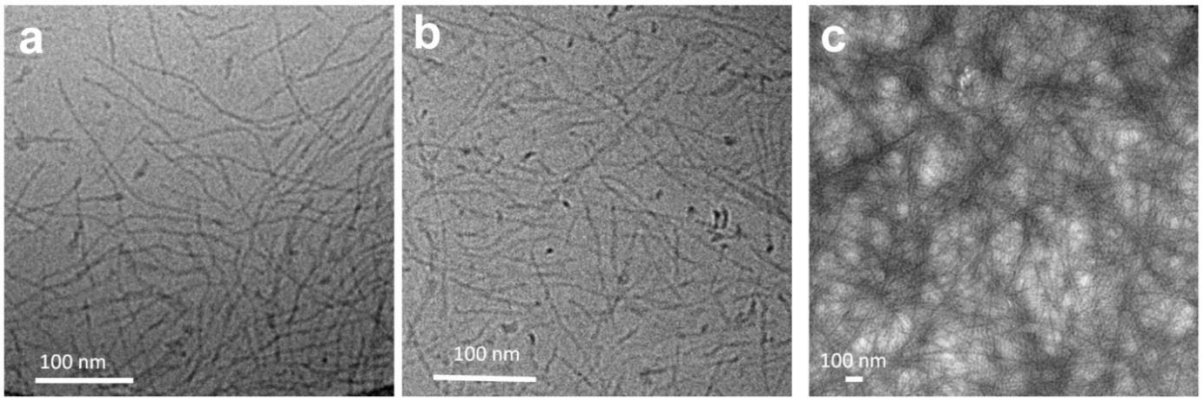

***Figure* V.2.** *Electron micrographs for the peptide sequence XGLK(Nal)K of a (a) stirred sample, (b) shaken sample, (c) standing sample. The micrographs (a) and (b) were obtained by cryo-TEM while (c) was obtained by negative staining TEM.*

Figure V.3 shows the electron micrographs obtained for the peptide XGLK(Cha)K. Relatively long fibres can be observed for all the samples.

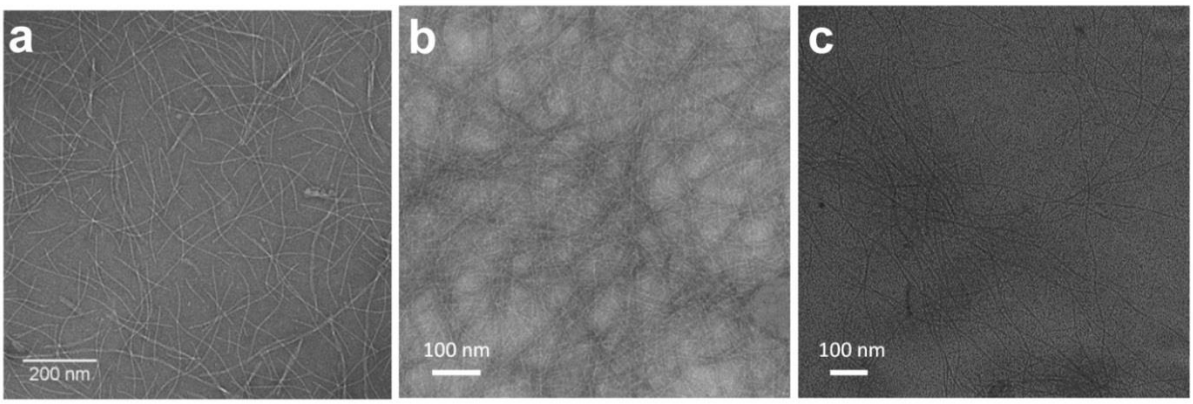

***Figure* V.3.** *Electron micrographs for the peptide sequence XGLK(Cha)K of a (a) stirred sample, (b) shaken sample, (c) standing sample. The micrograph (c) was obtained by cryo-TEM while (a) and (b) were obtained by negative staining TEM.*

In Figure V.4 we can see the micrographs for the sequence XGLK(*p*-ClPhe)K. We can observe twisted fibres, some of which appear to form bundles (in the standing sample), while the stirred samples seem to consist of single fibres twisting onto themselves.

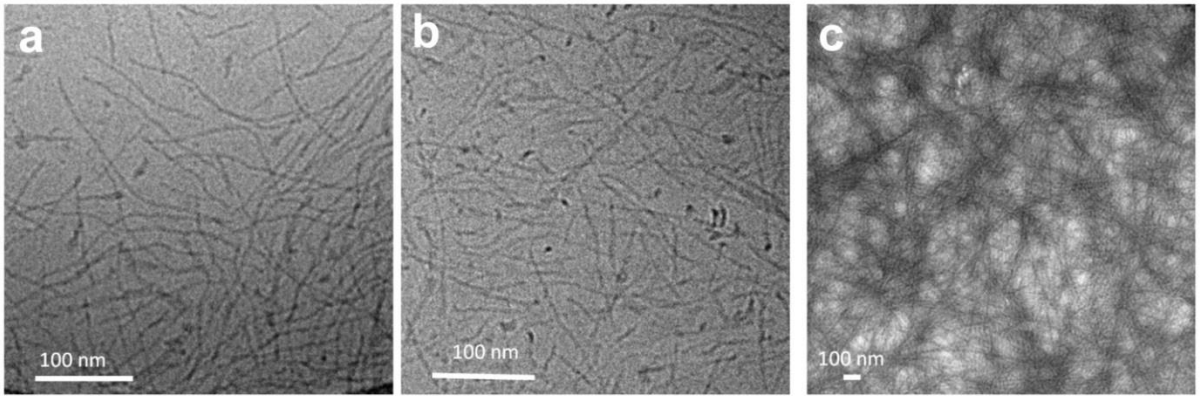

***Figure* V.4.** *Electron micrographs for the peptide sequence XGLK(p-Cl-Phe)K of a (a) stirred sample, (b) shaken sample, (c) standing sample. Micrographs (a) and (c) were obtained by cryo-TEM while (b) was obtained by negative staining TEM.*

The XGLKSK sequence was then investigated, and the obtained micrographs are shown in Figure V.5. It can be observed that the fibres for this peptide sequence are short for the stirred, and longer for the shaken sample. This can be explained by the difference in shear stress applied to those samples.

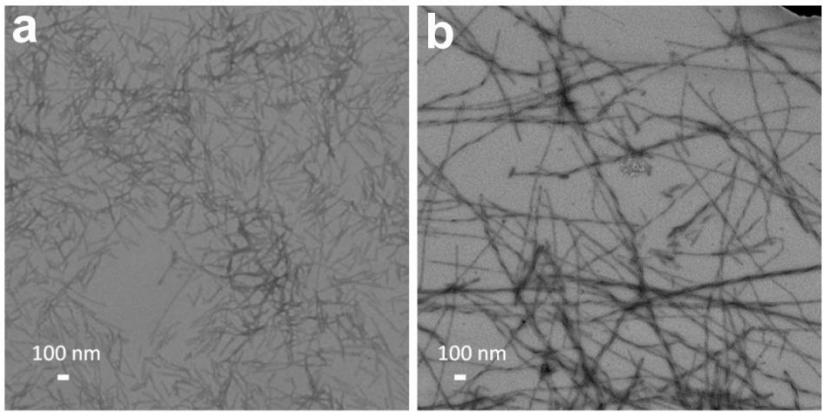

***Figure* V.5.** *Negatively stained electron micrographs for the peptide sequence XGLKSK of a (a) stirred sample, (b) shaken sample.*

Finally, some stirred samples of XGLKAK and XGLKFK were observed. The obtained micrographs, depicted in Figure V.6, show the presence of fibres for these samples, confirming that self-assembly took place also for these samples. It is interesting to notice the presence of ribbon like structures made by the bundling of several fibres in the case of peptide XGLKAK.

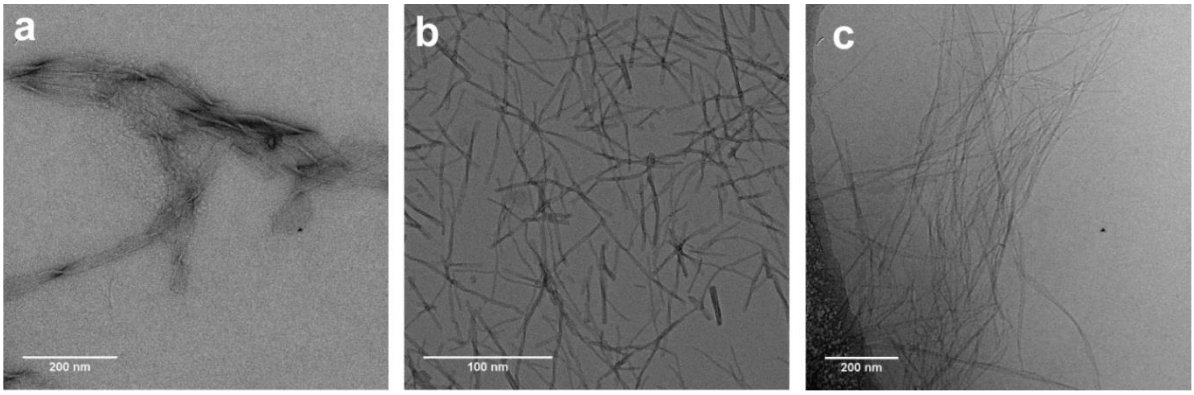

***Figure* V.6.** *Electron micrographs obtained from (a) a stirred library of the peptide sequence XGLKAK (b) a stirred library of the peptide sequence XGLKFK and (c) a standing library of the peptide sequence XGLKFK. Micrographs (a) and (b) were obtained by negatively staining, and (c) by cryo-TEM.*

Interestingly, the standing libraries are composed mainly of the thermodynamic products: trimers in the case of NaI, a mixture of trimers and tetramers for Cha, and pentamers for Cl-Phe. However, fibres can be observed for those libraries (Figures V.2.c, V.3.c and V.4.c) while seeding experiments with those species did not accelerate fibre growth, meaning that for these macrocycles self-assembly occurred without following an autocatalytic pathway. This suggests that for a self-replication process to be sustainable, the replicating species should be only be a minor product under conditions where an autocatalytic pathway is not possible in the system. In other words, the spontaneous formation of the replicator should be inefficient compared to its autocatalytic formation.

V.2.d. Studying the morphology of the fibres

Further analyses were done on several micrographs for each peptide sequence in order to study the different morphologies that can be observed depending on the parameters of the system. Those observations are summed-up in Table V.2, and allow some empirical rules to be drawn up that govern fibre morphology.

	Sequence	observed length			stiffness			association		
		< 200 nm	200 nm <length< 800 nm	> 800 nm	straight	curved	twists	single	bundle of 2-3 fibres	ribbons
Standing	XGLK(Nal)K			+++		+++		+++		
	XGLK(Cha)K			+++		+++		+++		
	XGLK(4-ClPhe)K			+++	++	+		+++		
	XGLKFK		+	++	+	++		++		
	XGLKLK			+++	+	++		+++		
Shaken	XGLK(Nal)K		++	+	++	+		+++		
	XGLK(Cha)K		++	+	+	++		+++		
	XGLK(4-ClPhe)K	+	++		++		+	++	++	
Stirred	XGLK(Nal)K	+++			+++			+++		
	XGLK(Cha)K	+	++		++	++		+++		
	XGLK(4-ClPhe)K	+++			+++					+++
	XGLKFK	+++	+		+++	+		+++		
	XGLKLK	+++			+++			+++		
	XGLKAK	+++	+		+++					+++
	XGLKSK	++	+		+++	+	+++		+++	

***Table* V.2.** *Observation of the fibres, according to different parameters, and for peptide sequences varying in hydrophobicity. The colours and number of crosses of the in the table represent the relative quantities observed in the micrographs. Blank: no presence observed; +: presence observed in small quantities; ++: presence observed in several parts of the sample, but not representative of it; +++: presence observed throughout the sample.*

First, stirred libraries give mainly short and straight fibres, while with less shear stress the fibres are longer. Although these observations are here just qualitative, they are in accordance with the results discussed in chapter III of this thesis, and confirm the fact that the fibres are sensitive to shear stress and break when subjected to high shear stress.

By looking at the organization of the fibres, we can see that some of them are prone to form bundles that are twisting. Some, like XGLKAK even form ribbon-like structures. The nature of the forces leading to these tertiary structures only for some specific sequences is not entirely clear, although it seems that only the less hydrophobic sequences XGLKAK and XGLKSK that form the largest macrocycles display such structures. Therefore, the macrocycle size from which the fibres are made may play a role in this organisation, since those two building blocks are the only ones having fibres made of octamer macrocycles.

V.2.e. Conclusions

By studying the effect of the peptide hydrophobicity on the behaviour of the libraries and on the emerging macrocyclic replicator, this work suggests two rules that govern the self-replication process. First, a critical macrocycle size is needed for the interactions to be strong enough for the macrocycles to stack on top of each other and initiate the self-replication process. Second, the spontaneous formation of the replicating macrocycle should be inefficient compared to its autocatalytic formation.
Investigations on the fibre morphologies proved that the fibre's shape and size depend on the conditions in which the libraries are made, confirming the observations from Chapter III of this thesis, but also depend on the peptide sequence used and the macrocycle constituting the fibres.
These new insights may provide some useful information for the people working in the field of self-replicating systems, and may help understanding other systems.

V.3. Stable Polymer micelles formed by metal coordination

V.3.a. Introduction

The use of metal-ligand coordination bonds for building supramolecular structures is an emerging field that could find promising applications in various domains, including the development of functionalised inorganic-organic hybrid materials.[18,19,20]
Several methods have been developed in order to reach stable supramolecular complexes, most of them involving a hydrophobic inner core, and a hydrophilic outer shell that can coordinate to metals ions. The formed micelles are stabilized by ionic interactions between the metal and the ligand and are therefore highly sensitive to the addition of salt. [21,22,23,24,25,26]
An alternative to this method has been developed by using the electrostatic interactions between a polycationic, neutral diblock copolymer and an anionic reversible coordination polymer consisting of metal ions coordinated by a ditopic ligand[27], in order to form self-assembled metal-containing micelles. Such a system shows a better resistance to the addition of salts than the system described previously, but the electrostatic driving force limits their stability when the ionic strength becomes high.[28,29]
All these systems use hydrophobic or ionic interactions as the driving forces for the self-assembly process, their limited stability to the addition of salts being due mainly to the ionic interactions. In order to be able to work with efficient self-assembling systems independently of the salt concentration of the media, non-salt dependent interactions should be involved in the mechanism of self-assembly. To reach this, a new system was developed in which coordination bonds are used as the driving force for self-assembly.A building block with a terdendate ligand was used, in order to give it a strong affinity for metal ions.
The building block used in the following study is a diblock copolymer featuring a polypyridine chain linked to a PEG chain.[30] A 4-ethoxypyridine-2,6-dicarboxylic acid group is linked to the pyridinium group, as depicted in Scheme V.3.

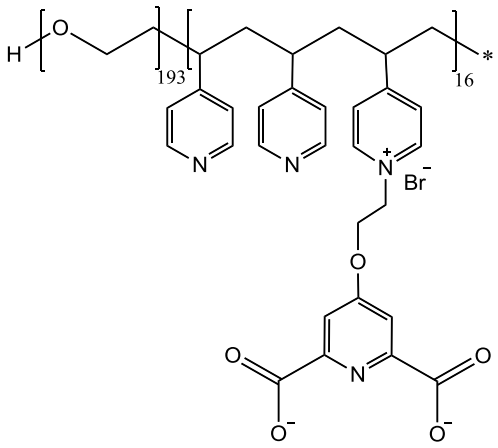

1

Scheme* V.*3. *Diblock copolymer building block **1**, to which a ligand is attached.*

The studies were performed at pH 6, which is in the range of solubility for this compound. Upon addition of $Zn(NO_3)_2$, both light scattering studies and TEM measurements suggest the emergence of micelles. Those are formed as a result of a coordination bonding between one Zn^{2+} ion, and two of the terdendate ligands from the building block. This linkage can be either intramolecular or intermolecular. Scheme V.4 depicts a schematic representation of the formed micelles.

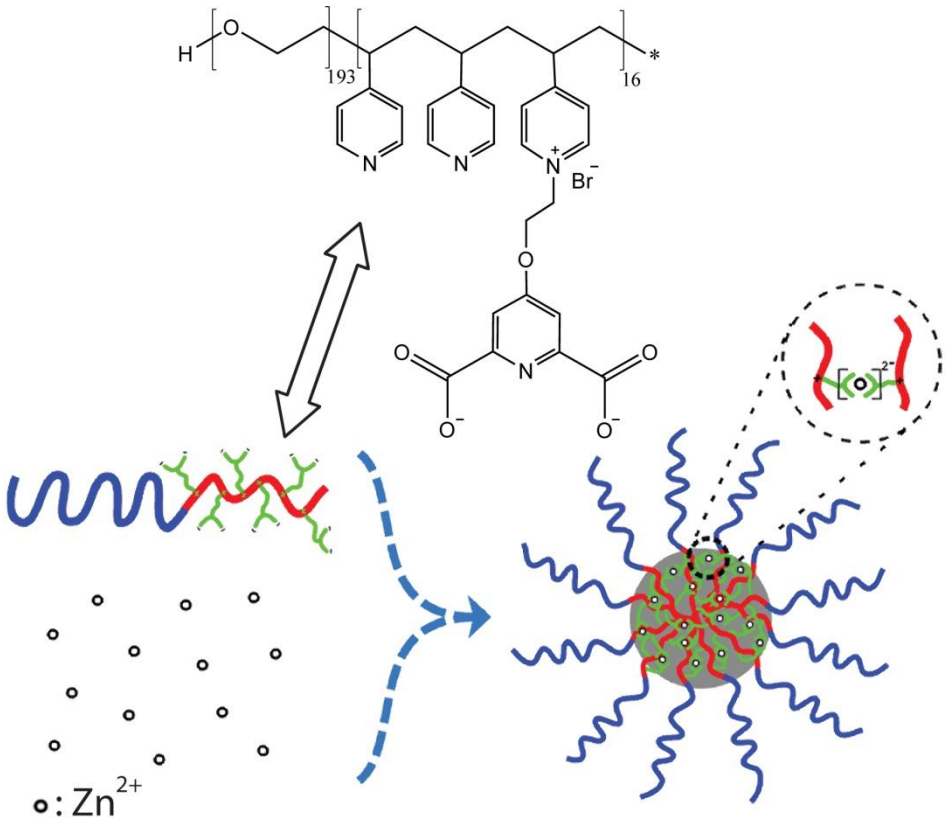

***Scheme* V.4.** *Schematic representation of micelle formation.*

In the following study, light scattering experiments prove the existence of aggregates, and TEM measurements prove their nature as being round shaped micelles.

V.3.b. Cryo-TEM measurements

The measurements other than cryo-TEM displayed in the following part were performed by Junyou Wang, from the University of Wageningen, and the set of results presented in this paragraph is part of a more complete study done on this system.[31]

Cryo-TEM was chosen as the method of choice for direct observation of the objects, since this technique allows overcoming the limitations of some other techniques. The small size of the objects to be observed is not suitable for optical microscopy techniques or SEM, and since the micelles should preferably be observed in solution, especially when investigating their resistance to different salt concentrations, negatively stained TEM and AFM also had to be discarded.

As shown on Figure V.7.a, cryo-TEM measurements suggest the presence of micelles. For this sample the molar ratio between the metal and the ligand M/L=0,25, and the concentration of NaCl = 0,1 M. When comparing the size of the micelles to the sizes observed by light scattering (Figure V.7.b), a difference can be noticed: the micelles observed by TEM have a 10 nm diameter, while light scattering experiments indicates a diameter of 20 nm. This can be explained by the fact that the TEM micrographs show only the metal-ion containing inner core of the micelles, while the outer shell cannot be observed due to a lack of contrast.

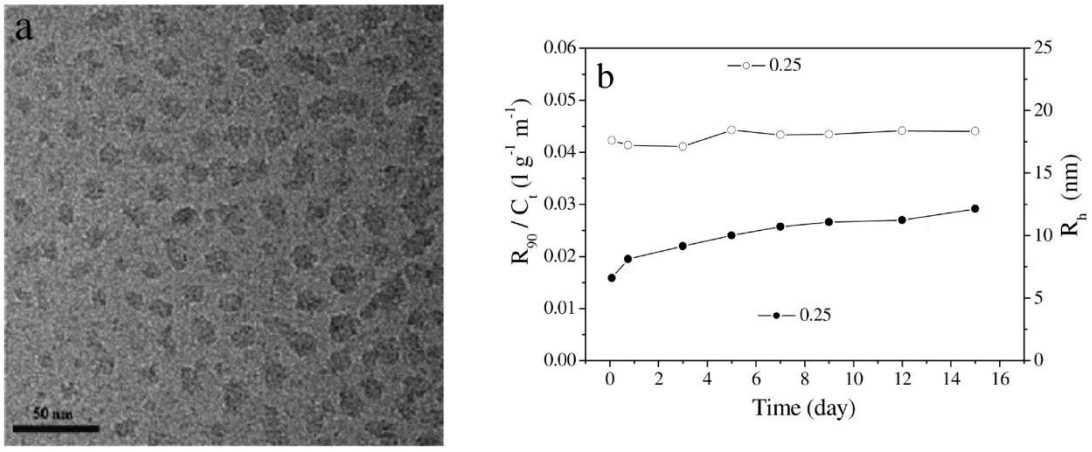

***Figure* V.7.** *(a) Cryo-TEM image of the micelles formed from **1** and Zn^{2+} at 0.25 M/L. (b) Variations of light scattering intensity and hydrodynamic radius of micelles formed at 0.25 M/L.*

A set of experiments was then performed in order to investigate the influence of the M/L ratio on the kinetics of formation and size of the micelles. Once again, light scattering measurements were performed together with cryo-TEM. The results shown in Figure V.9 demonstrate that the size of the particles decreases when the M/L ratio increases. This phenomenon is depicted with more accuracy in Figure V.8, in which it can be observed that, after increasing rapidly from a M/L ratio of 0 to 0.3, the size of the micelles start to decrease to finally reach a constant size around M/L=0.5.

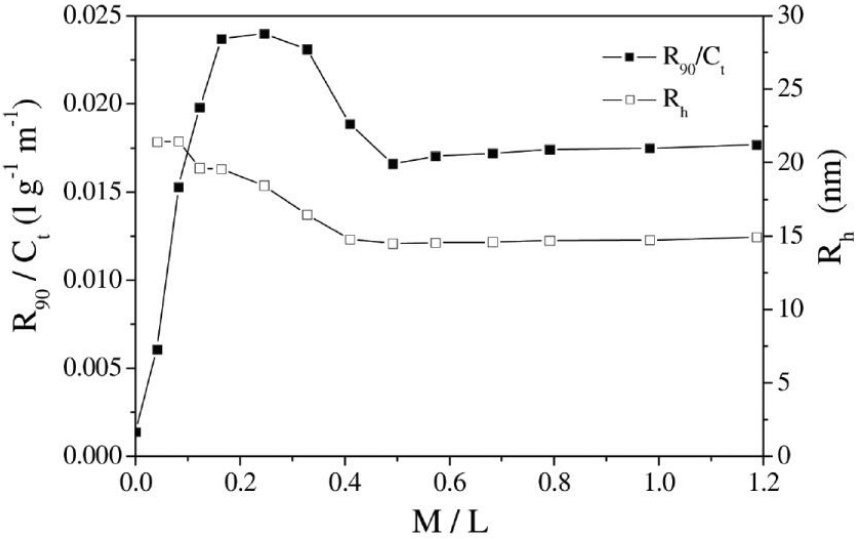

***Figure* V.8.** *Light scattering intensity and hydrodynamic radius as a function of the M/L ratio.*

The TEM micrographs are in accordance with those observations, since at M/L=0.25, the micelles have a diameter of 10-20 nm (Figure 9a), while for the higher M/L ratios of 0.5 and 1.0, the diameter of the observed objects diminishes to 6-12nm (Figures 9b and 9c). One explanation for this phenomenon can come from the differences in global charges in the system upon changes in the M/L ratio. Indeed, at M/L ratios below 0.5, all the Zn^{2+} ions are coordinated, but some of the carboxylate ligands are still free, giving an overall negative charge to the system. This may lead to repulsive forces which result in a swelling of the micelles. On the other hand, from M/L ratios of 0.5, all the carboxylate ligands are coordinated with a Zn^{2+} ion, and therefore, the overall charge of the whole structure is zero, since the two negative charges resulting from the complex formed by a Zn^{2+} ion with four carboxylates are compensated by the two pyridinium ions present in the vicinity of the complex. Without repulsive forces, the aggregates are smaller.

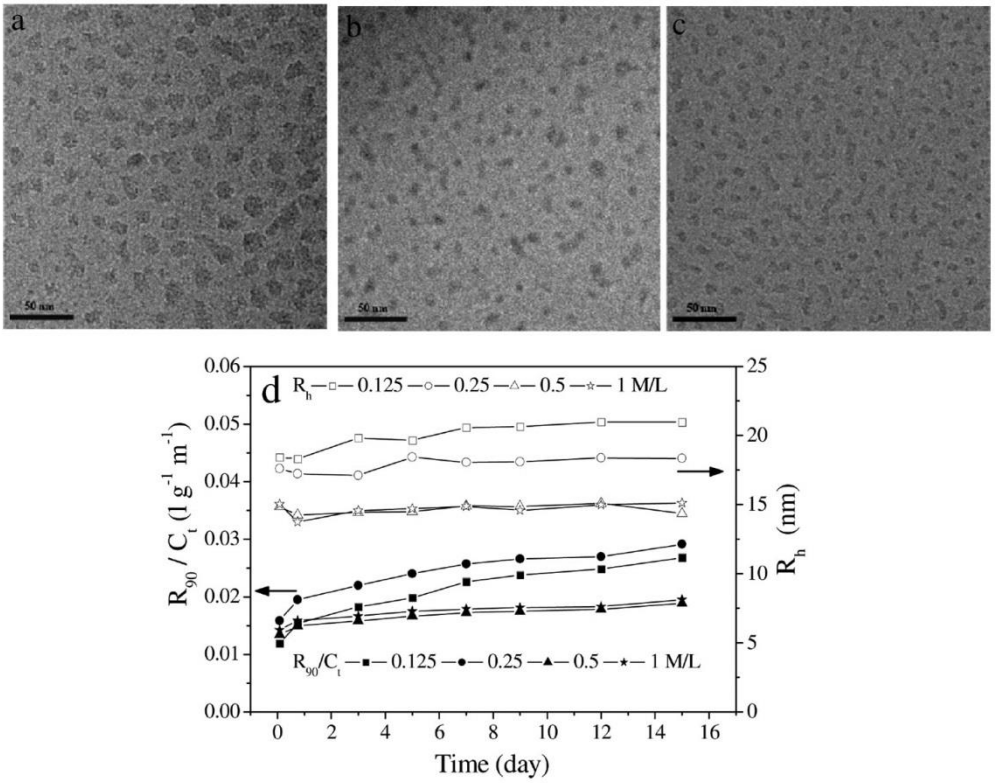

***Figure* V.9.** *Cryo-TEM images of Zn-L-P4VP48-b-PEO193 micelles at different M/L: (a) 0.25, (b) 0.5, and (c) 1 (polymer concentration is fixed at 2.53 g/L, MES buffer, pH 6, 0.1 M NaCl, measured after 5 days) d. Variations of light scattering intensity and hydrodynamic radius of Zn-L-P4VP48-b-PEO193 micelles formed at different M/L ratios.*

After determining the formation mechanism and the behaviour of the system depending on the M/L ratio, the stability of the system to added salt solutions was tested. As shown in Figure V.10, an increase in the concentration of salts hardly affects the micelles. Their size is even significantly larger at higher salt concentrations. This peculiar phenomenon can be explained by considering the screening effect of the salt ions, increasing with their concentration, which weakens the interactions in the core of the micelles between the positively charged pyridines and the negatively charged metal complexes, resulting therefore to an increase in the core size. However, those screening interactions are not sufficient to break the micelles apart, even at relatively high concentration of salts, confirming therefore the relative stability of those structures to the salinity of the media.

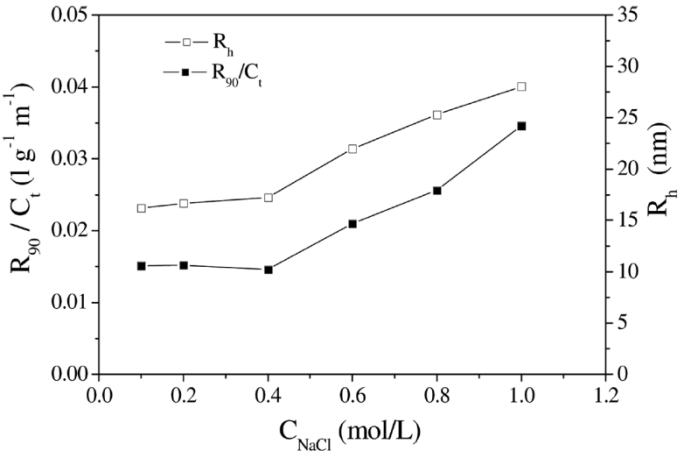

***Figure* V.10.** *Effect of salt on the scattering intensity and hydrodynamic radius of Zn-L-P4VP48-b-PEO193 micelles.*

V.3.c. Conclusions

In conclusion, this study introduces a new type of self-assembled micelles stable to the presence of salts in solution, thanks to a self-assembling process due to coordination forces, in contrast to most of the systems described today that rely on hydrophobic and ionic forces for self-assembly. The TEM measurements support the results, providing further details on the shape of the obtained objects, and confirm their micellar nature.

V.4. Enhanced rigidity and rupture strength of composite hydrogel networks of bio-inspired block copolymers

V.4.a. Introduction

Hydrogels are a class of materials that has been intensively studied in the past decades. Such an interest is due to some of their properties that can find numerous applications in different fields. Indeed, biocompatible [32,33] hydrogels can find use in several biomedical applications, such as contact lenses, scaffolds, biosensors, and drug delivery systems.[34,35,36]
Most of the hydrogels described feature some chemical crosslinks, making them strong, but giving them limitations in terms of remodelling. Physical crosslinks through non-covalent interactions between the components of the hydrogel brings more flexibility to the system since such hydrogels can be designed to respond to external parameters (pH, temperature, salt concentration). However, those weak crosslinking interactions usually give a limited mechanical strength to the systems.[37]
In order to overcome those limitations, composite networks, as found in Nature, can be considered as a good inspiration for synthetic systems, as they can give some crosslinks with reinforced mechanical strength. Since most of the composite networks described to date feature chemical crosslinks,[38,39,40,41,42,43] it would be interesting to test some composite networks systems in which the crosslinks are due to physical interactions.

The rheology experiments described in this section were performed by Wolf Rombouts, from the University of Wageningen. These focussed on the study of composite networks consisting of two

recombinant self-assembling protein polymers. The first one, CSSC, is composed of two hydrophilic blocks (C) consisting each of a 198 amino acids long extremely hydrophilic glutamine, asparagine, and serine-rich collagen-like polypeptide developed in Waganingen[44], surrounding two pH-responsive silk-like blocks (S) corresponding to the sequence $[(Gly\text{-}Ala)_3\text{-}Gly\text{-}Glu]_{48}$. When protonated at low pH, the glutamic acid residues of the S block allow an assembly through β-sheet like interactions. The blocks are then stacking on top of each other, leading to the formation of long, semiflexible fibrils.[44,45] The C block stays in a random coil that forms a corona around the fibrils.
The second block-copolymer usedin the following study, TR4T, consists of two collagen inspired blocks (T) composed of the sequence $(Pro\text{-}Gly\text{-}Pro)_9$ linked through an hydrophilic R block, featuring the same amino acid composition as the C block, but with the amino acids arranged in a different sequence. Three of the (T) blocks are able to assemble into a triple helix at low temperature.[46,47]
More information and the complete amino acid sequence of TR4T can be found in GenBank under the number ACF33479.
Table V.3 gives an overview over the individual properties of the composite networks CSSC and TR4T.

Protein Polymer	Composition	Molar mass ($kg.mol^{-1}$)	Properties
CSSC	C block: ~ 200 amino acids S block: $[(Gly\text{-}Ala)_3\text{-}Gly\text{-}Glu]_{48}$	65.8	Fibrillar networks at low pH
TR4T	T block: $(Pro\text{-}Gly\text{-}Pro)_9$ R block: ~400 amino acids	41.7	Flexible polymer networks at low T

Table* V.*3. *Overview of the protein block copolymers used in this research.*

The following study describes the mechanical properties of the composite networks formed by mixing CSSC and TR4T, obtained through different analytical methods. Cryo-TEM measurements were done in order to provide further insights into the system.

V.4.b. Rheology measurements

A first set of experiments was done in order to study the rheological properties of the CSSC and TR4T building blocks individually. The obtained results, depicted in Figure V.11, show that CSSC at pH 2 forms a gel within hours, reaching a modulus of around 2500 Pa. At pH 5, the sixteen glutamic acid residues composing the TR4T building block are mostly deprotonated. However, no increase in modulus above the detection limit of the rheometer is reached, meaning that the negatively charged glutamic acid residues prevent self-assembly of the system. The TR4T polymer reaches a modulus close to 50 Pa within hours, independently of the pH of the system, meaning that its assembly does not depend on the protonation state of its residues.

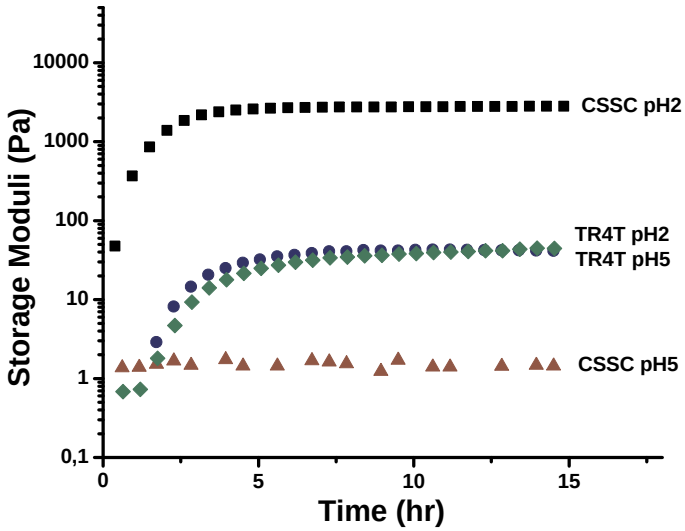

***Figure* V.11.** *Storage moduli (G')of single networks of 0.14 mM CSSC and 1.0 mM TR4T (at pH 2 and 5) as a function of time (f=1Hz, γ= 0.1% and T=20°C).*

After determining the behaviour of the individual block-copolymers, another study was done by mixing them. The results presented in Figure V.12.a show a clear increase in the storage moduli of the mixed systems compared to the ones observed in the single network studies. By increasing the concentration of TR4T, the modulus also increases. At 2.2 mM of TR4T, the storage modulus reaches 25 kPa, which is an order of magnitude higher than the storage modulus of the single network of CSSC.

Figure V.12.b depicts the increase in modulus depending on the protein polymer concentration. The results obtained here are in accordance with the observations from Figure V.12.a, and confirm the fact that an increase in the TR4T concentration leads above 0.2 mM to a linear increase in the modulus of the system.

Finally, a study was done with those systems by varying the angular frequency, in order to check their stability to shear stress. As shown in Figure V.12.c, all the different composite networks stay stable while increasing the shear stress applied to the system, confirming their strength and stability, even when under mechanically stressed conditions.

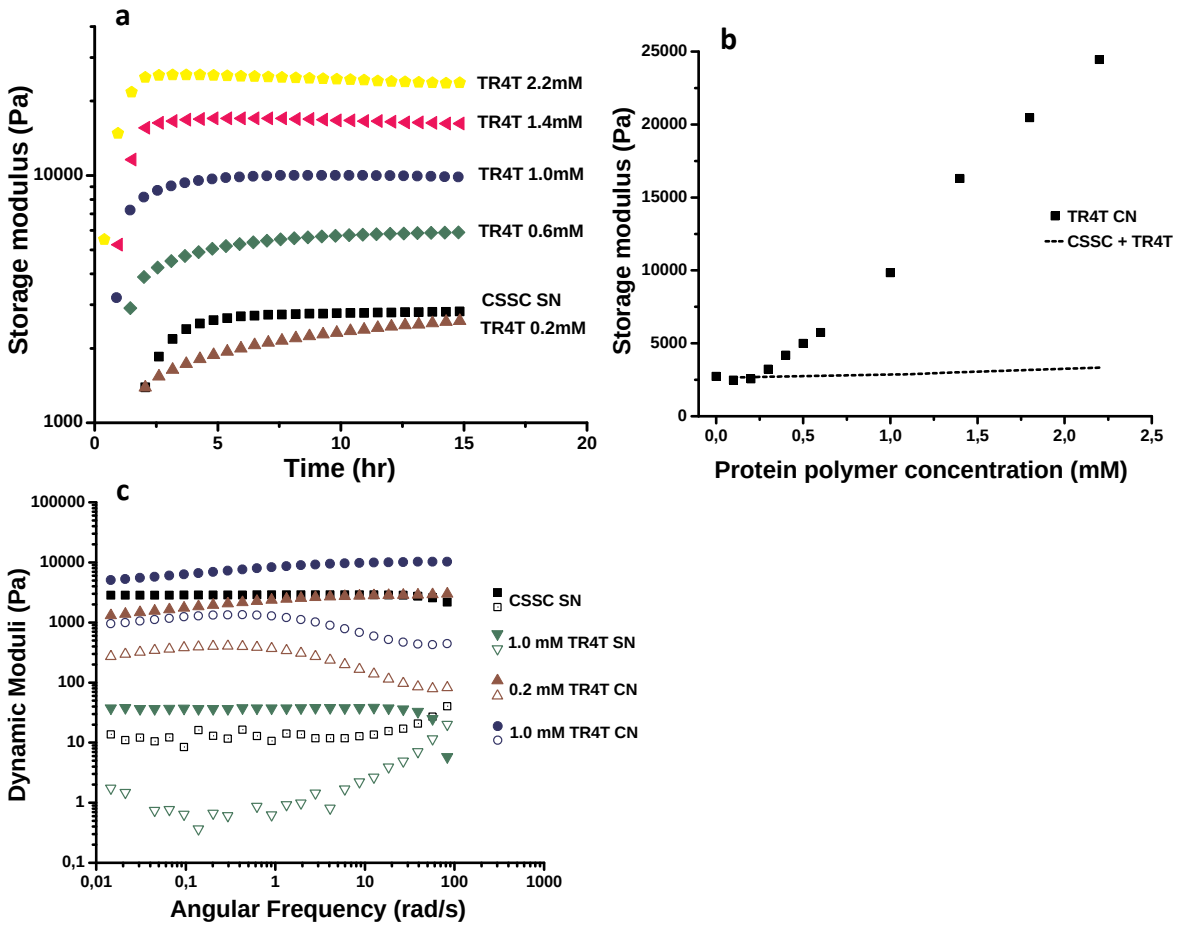

***Figure* V.12.** *(a) Storage moduli (G') of single networks (SNs) and composite networks (CNs) as a function of time (f = 1 Hz, γ = 0.1%, pH = 2 and T = 20 °C). [CSSC]=0.14 mM for all experiments. [TR4T] vary as indicated. (b) Average plateau storage moduli (G') of CSSC/TR4T composite networks as a function of TR4T concentration (closed squares). The dashed line represents the sum of the moduli of the separate CSSC and TR4T networks. (c) Frequency sweeps of CSSC and TR4T SNs and CSSC/TR4T CNs. Storage moduli (G', closed symbols) and loss moduli (G'', open symbols) are shown. [CSSC]=0.14 mM for all experiments; [TR4T] is varied as indicated.*

Further non-linear rheological measurements[48] were performed at a constant shear rate on the system, in order to assess whether the composite structure nature of the networks has some influence on their morphological features. This led to interesting results showing that the composite networks have stronger resistance to stress, due to a combination of the parameters of the individual components.

V.4.c. Cryo-TEM measurements

Cryo-TEM measurements were done in order to understand the results observed with the light scattering measurements, and give more insights into the structure and interactions between the networks composing the system. This method was chosen for the observation and understanding of such a system, since it gives a direct observation on the sample as it is in solution.

The first attempts done with samples at the same concentrations as the ones used for the rheological measurements were unsuccessful. The samples proved to be difficult to prepare and

their observation did not lead to any satisfying result, because of a too high concentration, that was leading to overcrowded samples, and difficulties in finding single objects to observe. Therefore, samples were diluted, in order to reach concentrations at which objects could be observed more easily. The concentrations of CSSC used for the above measurements are 1.4 µM, which is an order of magnitude lower than the concentrations used for the rheological measurements. Nevertheless, the observation of these diluted samples is still considered to be relevant, since the effect of TR4T addition to the system is assumed to be at least qualitatively the same as at the one at the higher concentration, used for the rheology experiments. Even if the structure of the composite network may differ when compared to the one at higher concentrations, the effects of addition of TR4T should be qualitatively similar to the ones done at 0,14 mM in the rheological experiments.
First, the single CSSC networks were observed. As shown in Figure V.13, these polymers are able to self-organise into long fibres that were measured to have an average diameter of 10.4 nm ±2.0 nm. These measurements are in agreement with the X-ray scattering experiments and the model predictions done at Wageningen University.[49] It can be observed on the micrographs that the fibres obtained are rather long and curly.

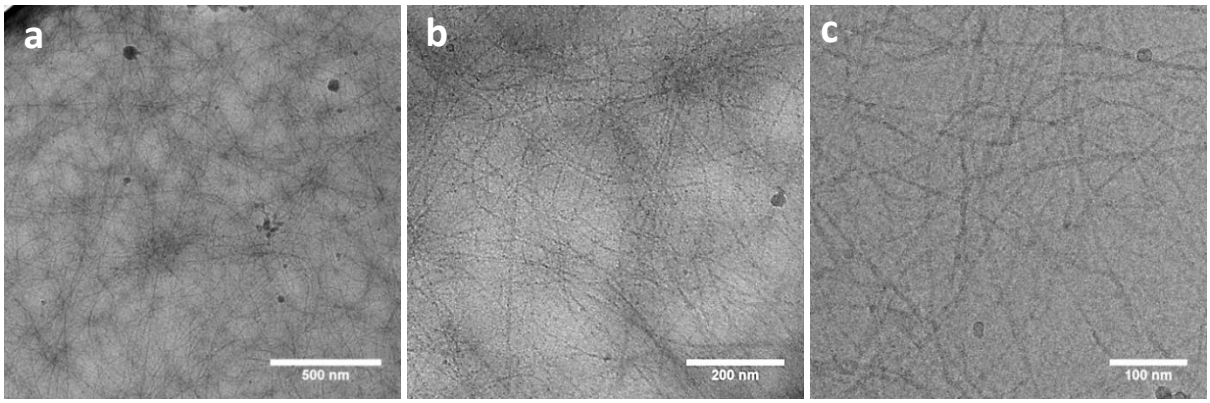

***Figure* V.13**. *Cryo-TEM images of CSSC single networks (0.1 g/L) at magnifications of 14000x (a), 30800x (b) and 49000x (c).*

Subsequently, the composite networks made from CSSC and TR4T were observed. The micrographs depicted in Figure V.14 indicate the presence of fibres, but their size is much larger than the ones obtained with single networks, with an average diameter of 27.5 nm ±4.7 nm. They are likely to be bundles of CSSC fibres that associate with each other through depletion, a physical process in which the macromolecules present in a solution are attracted to each other and eventually aggregate[50,51]. The strength of this attraction is determined by the osmotic pressure of the solution and the diameter of the macromolecules. In the present case, the observed diameter of the networks would correspond to bundles of two to three fibres.

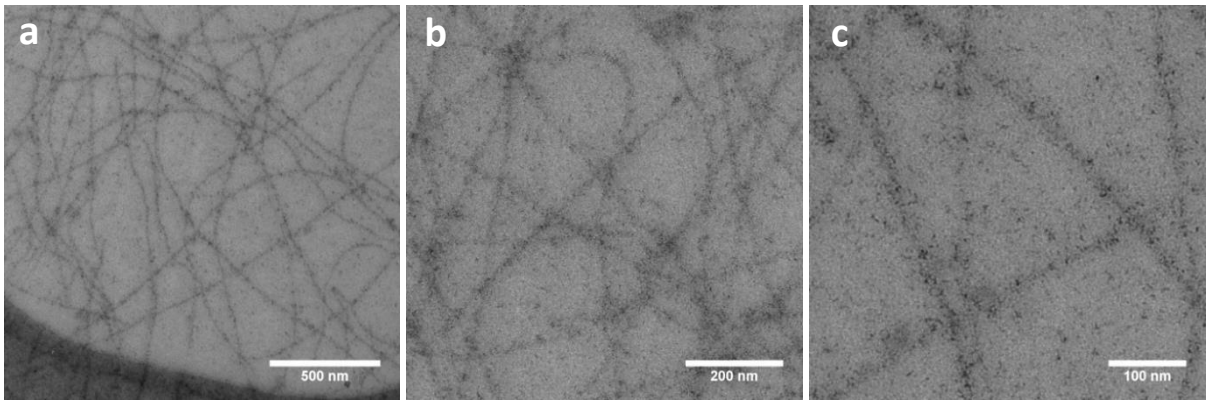

***Figure* V.14.** *Cryo-TEM images of CSSC/TR4T composite networks (0.1 g/L CSSC and 1.0mM TR4T) at magnifications of 14000x (a), 30800x (b) and 49000x (c).*

From the micrographs, it can be observed that, even though the fibres are curly, they are clearly stiffer than the single network ones, due to their increased thickness, which explains the higher modulus observed during the rheological measurements of the composite networks. This can be especially seen when comparing them at higher magnifications (Figures V.13.c and V.14.c).
Another observation made from the rheological measurements was that the non-gelling control molecules show a larger modulus than the fibres formed from TR4T. This phenomenon can be explained by considering the fact that a depletion-induced bundling may be more efficient in a polymer solution than in a gel, this phenomenon being the consequence of two parameters. First, the osmotic pressure, which is lower in a gel, is actually the main driving force of depletion bundling. Second, the gel itself may prevent bundling formation due to kinetic hindrance. Therefore, the fibres made from the non-gelling control molecules are more prone to depletion than the TR4T fibres, resulting in a lower modulus for the latter.

V.4.d. Conclusions

The study presented here shows an interesting system consisting of two block-copolymers from which the composite networks feature enhanced mechanical resistance to shear stress, illustrated by an increase in modulus, relative to the individual networks. Cryo-TEM measurements gave insights into the reason of this increase by proving the existence of bundled fibres, most likely caused by a depletion mechanism between the polymers. This system represents therefore an interesting non-chemically linked network with interesting properties.

V.5. Outlook

An overview of the different possibilities of using TEM as a useful technique for the understanding of systems was given in this chapter, through a series of three examples.
First, it helped giving some insights into the formation of peptide fibres during a self-replication process in dynamic combinatorial libraries. The micrographs of the fibres obtained during this study gave some interesting insights into the morphology of the fibres. These insights could be used in order to predict the morphology of the fibres that can be expected depending on the building block used for making libraries.

Then, in a different field, TEM helped in the observation of organic aggregates stabilized by metal-ligand interactions. This led to the confirmation of the micellar structure of the aggregates. Their size was determined from the micrographs, and confirmed by light scattering measurements.
TEM was also useful for the understanding and observation of silk-like protein fibres. The existence of bundled fibres, observed from the TEM images, demonstrated their organisation that most likely originated from a mechanism of depletion between the polymers, and which may account for the increase in modulus relative to the individual polymers.
In conclusion, this chapter demonstrates the usefulness of TEM by giving some examples in which the technique proved to be useful in different ways and in different domains, by confirming the theories proposed and supporting the other analytical techniques used, giving therefore a better understanding of the systems studied.

V.6. Experimental section

V.6.a. Grids preparation for negatively stained TEM

A thin layer of carbon was deposited onto a mica sheet by evaporating carbon from graphite in an evaporation chamber by applying current under reduced pressure. The obtained carbon film was then stored in a petri dish.
Bare copper grids 400 mesh, obtained from Ted Pella Inc., were placed on a glass slide dipped in a water bath, and the thin carbon film was laid on the top of the water. The water was then removed by pumping it out, and the carbon film got deposited on the copper grids.
The carbon coated grids were then dried under an infrared lamp for 30 min, and then stored in a petri dish.

V.6.b. Microscope and sample holders

The microscope used for the studies described in this part is a Philips CM 12 electron microscope. The electron beam is emitted at a voltage of 120 kV from a tungsten filament. For negatively stained samples, the grid was loaded on a TEM holder. For the cryo-TEM samples, the grid was loaded at -180°C on a Gatan model 626 cryo-stage, and immediately inserted in the microscope. The images were recorded on a slow-scan CCD camera.

V.6.c. Negatively stained TEM

A small drop of sample was deposited on a 400 mesh copper grid covered with a thin carbon film. After 30 seconds, the droplet was blotted on filter paper. The sample was then stained twice with a solution of 2% uranyl acetate deposited on the grid and blotted on filter paper after 30 seconds. The grids were then loaded on a TEM holder and inserted in a Philips CM12 Cryo-electron microscope. They were observed at 120 kV. Images were recorded on a slow scan CCD camera.

V.6.d Cryo-TEM

A few microliters of a solution of sample were deposited on holey carbon-coated grids (Quantifoil 3.5/1, Quantifoil Micro Tools, Jena, Germany). After blotting the excess liquid, the grids were vitrified in liquid ethane on a vitrobot (FEI, Eindhoven, The Netherlands) and transferred to a Philips

CM 120 electron microscope equipped with a Gatan model 626 cryo-stage, operating at 12 kV. Micrographs were recorded under low-dose conditions with a slow-scan CCD camera.

V.7. Acknowledgements

As this chapter describes how electron microscopy was used as complementary analysis to further the insights on the projects involves, all the principal investigators of the studies presented herein are acknowledged. Morteza Malakoutikhah prepared and monitored by HPLC the peptide libraries described in section V.2. Junyou Wang performed all the light scattering experiments discussed in section V.3. Wolf Rombouts performed all the rheological measurements presented in section V.4.

V.8. References

[1] E. Ruska, D.B. Dahlem, W. Germany, D.M. Planck-Gesellschaft, *Reviews of Modern Physics*, **1987**, *59*, 627-637.

[2] F. Haguenau, P.W. Hawkes, J.L. Hutchison, B.S. Jeunemaître, G.T. Simon, *Microscopy and Microanalysis*, **2003**, 9, 96-138.

[3] B. Fultz, J. Howe, *Transmission Electron Microscopy and diffractometry of materials, 3rd edition, Springer,* **2005**, 61.

[4] E.M. Belavtseva, Y.A. Klyachko, A.G. Filatova, *Bulletin of the Russian Academy of Sciences: Physics*, **2011**, *75*, 1254-1259.

[5] L.F. Kourkoutis, J.M. Plitzko, W. Baumeister, *Annual Review of Materials Research*, **2012**, 42, 33-58.

[6] E. Eskelinen, F. Reggiori, M. Baba, P.O. Seglen, *Autophagy*, **2011**, 7:9, 935-956.

[7] V. Klang, C. Valenta, N.B. Matsko, *Micron*, **2013**, 44, 45-74.

[8] Y. Ding, Z.L. Wang, *Handbook of Nanoscopy, 1st Edition, Wiley-VCH Verlag GmbH & Co. KGaA.,* **2012**, 961-993.

[9] N. Kawamoto, D.M. Tang, X. Wei, X. Wang, M. Mitome, Y. Bando, D. Golberg, *Microscopy*, **2013**, 62, 157-75.

[10] G. van Tendeloo, S. Bals, S. van Aert, J. Verbeeck, D. van Dyck, *Advanced materials*, **2012**, 24, 5655-5675.

[11] Y. Yan, *Handbook of Nanoscopy, 1st Edition, Wiley-VCH Verlag GmbH & Co. KGaA.,* **2012**, 1212-1246.

[12] S.I. Stupp, V. LeBonheur, K. Walker, L. S. Li, K. E. Huggins, M. Keser, A. Amstutz, *Science*, **1997**, 276, 384-389.

[13] K. Janssens, *Electron Microscopy. Modern Methods for Analysing Archaeological and Historical Glass, 1st Edition, Jon Wiley & Sons Ltd.*, **2013**, 129-154.

[14] I. Reiche, C. Vignaud, M. Menu, *Archaeometry*, **2002**, 44, 447-459.

[15] C. Viti and M.L. Frezzotti, *Lithos*, **2001**, 55, 125-138.

[16] C.J. Bowerman, W. Liyanage, A.J. Federation, A. J.; B.L., *Biomacromolecules*, **2011**, 12, 2735-2745.

[17] M. Malakoutikhah, J. J-P. Peyralans, M. Colomb-Delsuc, H. Fanlo-Virgos, M.C.A. Stuart, S. Otto, *J. Am. Chem. Soc.*, **2013**, 135*,* 18406-18417.

[18] X. Wang, R. McHale, *Macromol. Rapid Commun*., **2010**, 31, 331-350.

[19] F.A.A. Paz, J. Klinowski, S.M.F. Vilela, J.P.C Tome, J.A.S Cavaleiro, J. Rocha, *J. Chem. Soc. Rev.*, **2012**, 41, 1088-1110.

[20] Winter, A.; Hager, M. D.; Newkome, G. R.; Schubert, U. S. *Adv. Mater.*, **2011**, 23, 5728-5748

[21] K. Kimpe, T.N. Parac-Vogt, S. Laurent, C. Pierart, L.V. Elst, R.N. Muller, K. Binnemans, *Eur. J. Inorg. Chem*., **2003**, 3021-3027.

[22] E. Gianolio, G.B. Giovenzana, D. Longo, I. Longo, I. Menegotto, S. Aime, *Chem. Eur. J.* , **2007**, 13, 5785-5797.

[23] T. Owen, A. Butler, *Chem. Rev.*, **2011**, 255, 678-687.

[24] J.F. Gohy, B.G.G Lohmeijer, U.S. Schubert, *Macromolecules*, **2002**, 35, 4560-4563.

[25] J.F. Gohy, B.G.G Lohmeijer, U.S. Schubert, *Macromol. Rapid Commun.*, **2002**, 23, 555-560.

[26] C. Ott, R. Hoogenhoom, S. Hoeppener, D. Wouters, J.F. Gohy, U.S. Schubert, *Soft Matter*, **2009**, 5, 84-91.

[27] Y. Yan, N.A.M. Besseling, A. de Keizer, A.T.M. Marcelis, M. Drechsler, M.A. Cohen Stuart, *Angew. Chem., Int. Ed.*, **2007**, 46, 1807-1809.

[28] Y. Yan, A. de Keizer, M.A. Cohen Stuart, M. Drenchsler N.A.M. Besseling, *Phys. Chem. B*, **2008**, 112, 10908-10914.

[29] J.Y. Wang, A. de Keizer, R. Fokkink, Y. Yan, M.A. Cohen Stuart, J.J. van der Gucht, *Phys. Chem. B*, **2010**, 114, 8313-8319.

[30] Y. Yan, A. de Keizer, M.A. Cohen Stuart, N.A.M. Besseling, *Adv. Polym. Sci.* **2011**, 242, 91−115.

[31] J. Wang, M.A.C. Stuart, A.T.M. Marcelis, M. Colomb-Delsuc, S. Otto, J. van der Gucht, *Macromolecules*, **2012**, 45(17), 7179-7185.

[32] J. Kopecek and J. Yang, *Polym. Int.,* **2007**, 56, 1078-1098.

[33] R. E. Sallach, W. Cui, F. Balderrama, A. W. Martinez, J. Wen, C. A. Haller, J. V. Taylor, E. R. Wright, R. C. Long and E. L. Chaikof, *Biomaterials*, **2010**, 31, 779-791.

[34] A. S. Hoffman, *Adv. Drug Delivery Rev.*, **2002**, 54, 3-12.

[35] R. Langer, D. A. Tirrell, *Nature*, **2004**, 428, 487-492.

[36] N. A. Peppas, J. Z. Hilt, A. Khademhosseini, R. Langer, *Adv. Mater.,* **2006**, 18, 1345-1360.

[37] J. P. Gong, *Soft Matter*, **2010**, 6, 2583-2590.

[38] W.-C. Lin, W. Fan, A. Marcellan, D. Hourdet, C. Creton, *Macromolecules*, **2010**, 43, 2554-2563.

[39] M. Lemmers, E. Spruijt, S. Akerboom, I. K. Voets, A. C. v. Aelst, M. A. C. Stuart, J. van der Gucht, *Langmuir*, **2012**, 28, 12311-12318.

[40] K. Haraguchi and H.-J. Li, *Macromolecules*, **2006**, 39, 1898-1905.

[41] C. Zhou, Q. Wu and Q. Zhang, *Colloid Polym. Sci.,* **2011**, 289, 247-255.

[42] J. R. Capadona, K. Shanmuganathan, D. J. Tyler, S. J. Rowan, C. Weder, *Science*, **2008**, 319, 1370-1374.

[43] Y. Jiao, J. M. Stark, P. Akcora, P. Nair, R. T. Tran and J. Yang, *Soft Matter*, **2012**, 8, 1499–1507.

[44] A.A. Martens, G. Portale, M.W.T. Werten, R.J. de Vries, G. Eggink, M.A. Cohen Stuart, F.A. de Wolf, *Macromolecules*, **2009**, 42, 1002-1009.

[45] M. T. Krejchi, S. J. Cooper, Y. Deguchi, E. D. T. Atkins, M. J. Fournier, T. L. Mason and D. A. Tirrell, *Macromolecules.*, **1997**, 30, 5012-5024.

[46] P. J. Skrzeszewska, F. A. de Wolf, M. W. T. Werten, A. P. H. A. Moers, M. A. C. Stuart and J. van der Gucht, *Soft Matter*, **2009**, 5, 2057-2062.

[47] P. J. Skrzeszewska, F. A. de Wolf, M. A. C. Stuart and J. van der Gucht, *Soft Matter*, **2010**, 6, 416-422.

[48] W. H. Rombouts, M. Colomb-Delsuc, M. W. T. Werten, S. Otto, F. A. de Wolf and J. van der Gucht, *Soft Matter*, **2013**, 9, 6936-6942.

[49] A. A. Martens, G. Portale, M. W. T. Werten, R. J. d. Vries, G. Eggink, M. A. C. Stuart and F. A. de Wolf, *Macromolecules*, **2009**, 42, 1002-1009.

[50] S. Asakura and F. Oosawa, *J. Polym. Sci.,* **1958**, 33, 183-192.

[51] D. Marenduzzo, K. Finan and P. R. Cook, *J. Cell Biol.,* **2006**, 175, 681-686.

Summary

The creation of artificial life has been inspiring humans' imagination since the early ages of mankind. Science is nowadays trying to give a rational approach to reach this goal by studying independently the parameters that may one day lead to the creation of a system capable to self-sustain its species. The different parameters currently studied include (i) compartmentalisation, as a living system needs to be contained in a defined space, (ii) metabolism, as to keep being alive a system needs to gather energy from the outside world, and (iii) exponential self-replication, to sustain the species and take over potential other species capable of less efficient self-replication.

Exponential self-replication is therefore a process of prime importance for the early emergence of life, and an efficient system considered for the creation of *de-novo* life should include that feature. Up to date, the observation of exponential self-replication is reported in few synthetic systems, and a complete experimental description of the full process is lacking. The work described in this thesis is using Dynamic Combinatorial Chemistry as a tool for the description of a self-replicating system based on the self-assembling peptide building block. Placed in a favourable aqueous environment, the peptide building block is capable of self-assembly, giving rise to a pool of multimeric assemblies. Among this pool, one of the multimeric assemblies revealed to be capable of self-replication through the formation of long fibres. Chapter II proposes a demonstration of the exponential self-replication nature of that peptide system, and describes the different steps and essential parameters of the process that lead to an exponential self-replication.

During that study, the length of fibres resulting from the self-assembly of the peptide building-blocks has shown to be a parameter of prime importance during the self-replication process. The peptide length is directly influenced by the shear stress applied to the system, as strong shearing forces result in efficient breakage and therefore shortening of fibres. Chapter III gives insights on the role played by the fibre length in the self-replication cycle by reporting studies done on peptide libraries with varying peptide sequences that have been undergoing different amounts of shear stresses. The evolution of the peptide libraries was monitored together with the peptide length in those libraries. Those parameters were correlated with the kinetics of growth of the libraries, highlighting the influence of the peptide length, by demonstrating that the self-replicating cycle was enhanced by the presence of higher shear rates and therefore shorter fibres.

The shear stress applied to the system through these studies was varied by changing the speed of stirring. As this parameter is not easily tuneable and an accurate estimation of the energy given to the system through this process is tedious, a Couette Cell, a rheological device allowing accurate control of the shear forces, was designed rendering possible a full control of the stress applied to the system through the whole process of self-assembly and self-replication of the peptide libraries. Chapter IV describes the design of the Couette cell, and presents a first set of experiments that was performed on a peptide library using that device.

Transmission electron microscopy (TEM) has been widely used over the course of this thesis and became a useful tool for a direct observation of the fibres resulting from the self-assembly of the

peptide system developed in the group. Moreover, TEM revealed a usefool tool for other projects and has been used for collaborations within the group but was also the opportunity to initiate collaborations with other universities. Chapter V describes three projects where TEM was used to serve a broad scope of research. The first part of the chapter describes the observation of fibres resulting from self-assembly of peptides with new building block features that showed novel fibres structures and assemblies, giving new insights into the morphology of the fibres depending on the peptide sequence, rendering possible the prediction of the morphology of the fibres that can be expected depending on the building block used for making libraries. The second part of the chapter focuses on the observation and description of organic aggregates stabilized by metal-ligand interactions. Their micellar nature was confirmed thanks to the TEM observations, and their morphology and size could be determined from the obtained images. Finally the last part of that chapter describes the observation of silk-like protein fibres by TEM, during which the existence of bundled fibres was demonstrated, giving insights on their mode of organisation and on the rigidity of the material formed.

Samenvatting

De oprichting van artificial life heeft de mens al sinds het begin van de mensheid geinspireerd. De wetenschap tegenwoordig doet een poging met een rationele benadering om dit doel te bereiken door onderzoek van onafhankelijke parameters die kunnen uitmonden in de oprichting van een systeem dat zichzelf onderhoudt. De verschillende parameters die momenteel bestudeerd worden omvatten (i) compartimentering, omdat een levend systeem nou eenmaal moet worden geborgen in een gedefinieerde ruimte, (ii) metabolisme, om het systeem in leven te houden zal het energie moeten verzamelen uit de buitenwereld, en (iii) exponentiële zelfreplicatie, opdat de soort zich zelf kan handhaven en andere potentiële soorten die minder instaat zijn tot efficiënte zelfreplicatie kan overnemen.

Exponentiële zelfreplicatie is dus een proces dat van doorslaggevend belang kan zijn voor de vroege opkomst van leven, en een efficiënt systeem voor het creëren van nieuw leven moet dus minstens die functie omvatten. Up-to-date, de waarneming van exponentiële zelfreplicatie is gerapporteerd in paar synthetische systemen en een complete experimentele beschrijving van het volledige proces ontbreekt. De werkzaamheden beschreven in dit proefschrift is het gebruik van dynamische Combinatorische Scheikunde als instrument voor de beschrijving van een zelf-replicerende systeem gebaseerd op het zelfgeassemblerende peptide bouwblok. Geplaatst in een gunstig waterig milieu, de peptide-bouwsteen is geschikt als zelfbouwpakket, die aanleiding geeft tot een groep van multimeriche samenstellingen. In deze groep bleek, één van de multimeriche samenstellingen zich te kunnen kopieren door de vorming van lange vezels. Hoofdstuk II stelt een demonstratie van de exponentiële zelfreplicatie; beschtijft het karakter van dit peptide system en beschrijft de verschillende stappen en essentiële parameters van het proces dat leidt tot een exponentiële zelfreplicatie.

Tijdens deze studie is gebleken dat de lengte van de vezels die voortkomen uit de zelfgeassemblerende peptide bouwblokken een parameter is die van het grootste belang is tijdens het zelfreplicatie proces. De peptide lengte wordt rechtstreeks beïnvloed door de schuifspanning op het systeem, zoals sterke afschuifkrachten die resulteren in een efficiënte breuk en dus een verkorting van de vezels veroorzaken. Hoofdstuk 3 geeft inzicht in de rol van de vezellengte in de zelfreplicatie cyclus door studies over peptide groepen met wisselende peptide sequenties die ondergaan verschillende hoeveelheden schuifspanningen. De evolutie van de peptide groepen werd bewaakt samen met de peptide lengte in de groepen. Deze parameters zijn gecorreleerd met de kinetiek van groei van de peptidegroepen, met de nadruk op de invloed van de peptide lengte, door te laten zien dat de zelf-replicerende cyclus werd versterkt door de aanwezigheid van een hogere graad en dus kortere vezels.

De schuifspanning op het systeem toegepast door deze studies werd gevarieerd door het veranderen van de snelheid van roeren. Deze parameter bleek niet gemakkelijk in te stellen en een nauwkeurige raming van de energie van het systeem bleek tijdrovend, een Couette cel, een reologische apparaat die een nauwkeurige regeling van de afschuifkrachten mogelijk maakt, werd ontworpen waardoor het mogelijk werd een volledige controle van de spanning op het systeem te

hebben. tijdens het hele proces van montage en zelfreplicatie van de peptide-groepen. Hoofdstuk IV beschrijft het ontwerp van de Couette cel en presenteert een eerste reeks experimenten die werd uitgevoerd op een peptide groep met dat apparaat.

Transmissie Elektronen Microscopie (TEM) is veelvuldig gebruikt tijden dit proefschrift en werd een nuttig hulpmiddel voor een directe observatie van de vezels van het zelfgeassemblerende peptide-systeem ontwikkeld in de groep. Bovendien, TEM bleek een nuttige tool voor andere projecten en is tevens gebruikt bij andere projecten en samenwerkingsverbanden binnen de groep, maar er was ook de gelegenheid om samenwerkingsverbanden te vormen met andere universiteiten. Hoofdstuk V beschrijft drie projecten waar TEM werd gebruikt met het doel een ruime reikwijdte van het onderzoek te verkrijgen. In het eerste deel van het hoofdstuk worden de waarneming beschreven van de vezels die afkomen van de zelfgeassemblerende peptiden met de nieuwe bouwsteen functies die de nieuwe vezels structuren en constructies lieten zien, waardoor er nieuwe inzichten in de morfologie van de vezels zijn gekomen afhankelijk van de peptide sequentie, waardoor het mogelijk is geworden een voorspelling te doen van de morfologie van de vezels die verwacht kunnen worden afhankelijk van het bouwblok dat gebruikt is voor het maken van de peptidegroepen. Het tweede deel van dit hoofdstuk richt zich op de waarneming en beschrijving van organische toeslagstoffen gestabiliseerd door metaal-ligand interactie. De aard van het micellar hydrolisaat werd bevestigd dankzij de TEM observaties De morfologie en omvang konden worden bepaald aan de hand van de verkregen beelden. Tenslotte het laatste deel van dit hoofdstuk beschrijft de waarneming van zijde-achtige eiwitvezels door TEM, gedurende welk het bestaan van gebundelde vezels werd aangetoond, waarbij inzichten over de wijze van organisatie en de stijfheid van het materiaal wordt gevormd.

Acknowledgements

Sijbren, thank you for having given me the opportunity to work in your group. I will always remember when I came for the interview, very stressed and tensed, with a poor English, but you trusted me and gladly welcomed me in your group freshly moved to Groningen. I have learned a lot through these years thanks to you, not only in the field of Dynamic Combinatorial Chemistry, but also, and mainly in the way research is done. I now know that if I had been doing my thesis in France I would not have had such freedom when working in the lab that I had here, which took me a long time to understand but I am grateful that you gave me this freedom.
During the course of this thesis, I learnt how to use TEM, and discovered a new whole field of Science. I immediately liked it, and started analyzing samples from the group, and never stopped since then, as I am now working in the field. Thank you Sijbren for having given me the opportunity to learn it, and thank you Marc for your teaching and your patience, as you were always available to help me whenever I started experiencing difficulties.

I would like to thank the members of the reading committee, Prof. dr J.G. Roelfes, Prof. van der Gucht and Prof. G. Ashkenasy for the time they dedicated reading this thesis, as well as for their useful suggestions and corrections.

Jan and Boris, many thanks to you for having accepted to support me as paranimfs for my defense. Thank you Musa for your help with translating the summary.

When I freshly arrive in Groningen, I first met with Jérôme, Hugo and Saleh. Many thanks to you for having been there to take care of me during the first weeks, introducing me the lab and the city.

Guys from the Otto group, spending those years with such great minds and personalities was an amazing experience. I came to believe that everybody in the group is really crazy in its own way. One would believe that such heteroclite personalities would normally result in conflictual situations, but for some obscure reason it created a strong synergy, giving rise to a really stimulating atmosphere, working with all of you was a great pleasure. Jérôme, Hugo, Saleh, Yang, Manuel, Jianwei, Elio, Piotr, Andras, Vittorio, Jan, Andrea, Ashish, Shuo, Ivica, Giulia, Boris, Gaël, Meniz, Yigit, David, many thanks to all of you for all this time spent together, and for all of those unforgettable moments, in the lab.

Jérôme, when I just started you introduced me to the project, the lab and all the methodology of the group. Since that day you were here for me, supporting me and always available whenever I had questions or doubts. Thank you for that, as well as for all the time spent with you out the lab, as you have also been of great support whenever needed.

Nop, I'm really glad that I had the opportunity to meet you, I learnt a lot from you, and having the chance to welcome you in my place and visit yours was great. I hope to see you again soon.

Besides the lab, we of course had many opportunities to spend some time together with the labmates. All the evenings spent together, and the film/food marathons were for sure some of the most unique experiences of my life. Thanks a lot Vittorio for sharing all those talks about videogames, let's hope our project of study about it will one day lead to something. Andrea, your

passion for the literature, cinema and comics has always been the occasion of nice discussions and unexpected discoveries for me. Thanks also for those evening spent playing board games.

Pat and Céline, thank you for your enthusiasm in welcoming me in the great Pelsterstraat apartment. Spending a year with you was great, I have many nice memories from those moments and will long remember all of those great parties and nice dinners, but also of the winter evenings spent in the living room with jackets to watch TV.

My thanks also go to all the friends with whom I shared some nice moments during the course of this thesis. Felix, Julia, Ugo, Tizi, Seb, Claudia, Nop, Miriam, Pat, Massimo, Krzys, Matea, Francesca, Adi, Ashoka, Milon, Suresh many thanks to you for all the time spent together, you made these years really special, and spending time with you in evenings, parties, week-ends, concerts, travels, cricket matches and all other activities was a true pleasure. Thank you to all of the "Dr A and the minions" team members for all those pubquiz evenings, even though we never managed to finish first I always nice having a beer with you whilst trying to answer questions. To the "Cheap Hoodies", our jam sessions will not stay in the history of music, but they are engraved in my memory for a long time.

Tizi and Ugo, it was comforting to have you as neighbors and know that anytime we would miss anything we could just go upstairs and ring. Sorry also for all the discordant piano notes you may have heard during this period. Julia and Felix, I remember well the first time I really spoke to you, during this concert in the Stadspark. Since that time I am grateful for having had the opportunity to spend some time with you, you both are two really special persons, all the short trips we did to Germany with you were always the occasion for me to discover new german traditions, and I cannot imagine my life today without bratwurst, Sunday morning pumpkin soup, or Flunkyball. Many thanks for all of this. Claudia, Seb and Moka, thanks to the three of you for having welcoming me during my last month in Groningen, it was a good opportunity for me to practice a bit of Italian and learn how to live with a cat. Now that you are in Lyon, I'm sure that we will anyway have plenty of other opportunities to meet each other.

Merci à tous mes amis français, vous avez toujours été là pour moi, et avez sans hésité franchi les frontières pour venir me rendre visite dans le grand nord (plusieurs fois même pour certains). Je tiens énormément à vous et suis fier de savoir que je peux compter sur vous. Merci aussi à mes parents, ma sœur, ainsi qu'à toute ma famille pour votre support tout au long de ces années, chaque retour au pays me fait du bien, et chaque fois que vous avez pu venir me voir était pour moi l'occasion de me ressourcer un peu.

Je tiens enfin à remercier Céline pour tout le support que tu as su m'apporter au long de ces années. T'avoir à mes côtés durant tout ce temps a été d'un grand réconfort et tu as toujours su être là. Merci à toi.

Mathieu

"All grown-ups were once children, but only few of them remember it." - Antoine de Saint Exupéry